DECOMPOSITION OF ESTERS ON ALUMINOSILICATES

DECOMPOSITION OF n- AND sec-BUTYL ACETATE ON SYNTHETIC ZEOLITES AND SILICA-ALUMINA

By

TAMOTSU IMAI, M.Sc.

A Thesis

Submitted to the School of Graduate Studies

in Partial Fulfilment of the Requirements

for the Degree

Doctor of Philosophy

McMaster University

May 1971

DOCTOR OF PHILOSOPHY (1971) McMASTER UNIVERSITY
(Chemical Engineering) Hamilton, Ontario

TITLE: Decomposition of n- and sec-Butyl Acetate on Synthetic Zeolites and Silica-Alumina

AUTHOR: Tamotsu Imai, B.Eng. (Tokyo Institute of Technology)
M.Sc. (University of Alberta)

SUPERVISOR: Professor R. B. Anderson

NUMBER OF PAGES: xiii, 205

SCOPE AND CONTENTS:

A kinetic and mechanistic study on catalytic decomposition of n- and sec-butyl acetate was carried out. The catalysts were silica-alumina and synthetic zeolites including type A, X, Y and mordenite. The reactions were performed in the temperature region of 140° to 290°C at atmospheric pressure using a fixed-bed flow reactor.

The esters decomposed to acetic acid and n-butenes. The isomerization of butenes occurred consecutively. The mechanism of ester decomposition was different from that of pyrolysis. The catalytic activity was effected by acidity, cations and pore size. The Langmuir-Hinshelwood rate equation corresponding to the surface reaction on dual-sites correlated data satisfactorily. Strong adsorption of acetic acid, crystal collapse and the blocking of pores with organic deposit caused aging of catalysts.

ACKNOWLEDGEMENTS

The author expresses his sincerest thanks to Dr. R. B. Anderson for his supervision and help during the course of this study.

The helpful discussions and suggestions of Drs. T. W. Hoffman and P. T. Dawson as members of his supervisory committee are greatly appreciated.

The financial support received from the Petroleum Research Fund, administered by the American Chemical Society, and McMaster University is gratefully acknowledged.

The author thanks his wife, Johanna, for her help, patience and love.

TABLE OF CONTENTS

LIST OF FIGURES

LIST OF TABLES

Chapter 1

INTRODUCTION

The purposes of this study are to investigate catalytic behavior of synthetic zeolites and reaction kinetics and mechanism for the decomposition of n- and sec-butyl acetate. The decomposition of n- and sec-butyl acetate on synthetic zeolites has several interesting features. The gas-phase pyrolysis of the esters has been studied (23, 27, 30, 39, 72). The structure and chemical nature of the synthetic zeolites have been determined (12). This information should be useful in interpreting experimental results. The butenes produced may help in interpreting the mechanism of the primary and subsequent reactions. The results of this study are described in Chapters 4 to 7. The present chapter introduces the main problems associated with this research.

In heterogeneous catalysis reactions occur at interfaces. Generally, activated intermediates form through the interaction of reacting substances with the catalyst surface often on active sites. The rate of reaction and the type of products depend on the reactivity and nature of the intermediate. The nature of the intermediate is determined by chemical and physical properties of both reacting substance and catalyst. Therefore, a catalytic reaction often differs from a similar

homogeneous reaction with respect to selectivity and reaction rate.

The gas-phase decomposition of esters is a well known reaction and extensive work has been done on n- and sec-butyl acetate (27, 72). The pyrolysis is first-order and an intramolecular mechanism involving a six-center ring intermediate has been postulated. For the pyrolysis of sec-butyl acetate, the ratio of 2- to 1-butene is 0.75 compared with 0.67 calculated on the basis of the number of β-hydrogens available for forming the cyclic intermediate (27, 72). Only 1-butene forms from the gas-phase decomposition of n-butyl acetate (27, 30, 72). The isomerization of butenes does not occur under the experimental condition used for the pyrolysis (27). Pettit and Anderson (58) decomposed sec-butyl acetate on charcoal at 300° to 400°C. The decomposition was faster on charcoal than in the gas-phase; however, the butenes produced on charcoal had nearly the same composition as from the pyrolysis and the butenes did not isomerize.

In many reactions, the catalytic action of zeolitic catalysts is attributed to the acidity which arises from Lewis acids (tricoordinated aluminum atoms) and/or Brönsted acids (acidic hydroxyl groups) and reactions involve ionic mechanisms (89). Therefore, the decomposition of the esters on zeolitic catalysts is possibly different from the gas-phase pyrolysis and the decomposition on charcoal.

Molecular sieving is a characteristic property of some zeolites. The effects of this property on activity and selectivity were first described as molecular-shape-selective catalysis by Weisz and co-workers (99). For the decomposition of the esters on zeolites with a small aperture diameter such as A zeolites and mordenites, the molecular sieving effect may be an important factor.(Chapter 4 and 5)

The surface of zeolites is ionic and/or polar and will have strong affinities for the esters and acetic acid (89). Therefore, it is expected that the concentrations of ester and acetic acid adsorbed on the surface are large. In heterogeneous catalysis, the retarding effect of a reactant and/or products adsorbed strongly on the catalyst surface is often an important factor in determining rate and selectivity. For such cases, the Langmuir-Hinshelwood rate equation has been used most widely and has good adaptability.

The application of the Langmuir-Hinshelwood rate equations to the catalytic decomposition of esters has been studied previously. Sashihara and Syverson (70) studied the decomposition of n-hexyl acetate on activated bauxite and metal oxide-bauxite catalysts. They found that the semi-empirical rate equation based on a dual-site surface reaction gave a satisfactory correlation with conversion-space time data. Pettit and Anderson (58) suggested a rate expression based on

the Langmuir-type adsorption of ester for the decomposition of sec-butyl acetate on charcoal. The rate expression corresponded to the first-order surface reaction of ester chemisorbed on a single site or adsorbed physically on the surface. (Chapter 6)

The aging of zeolites has been found in many organic reactions (89). The aging results from blocking or obliteration of an active site by polymeric organic compounds. The coking occurs through the dehydrogenation of such compounds. The crystal structure and the pore size and shape may affect aging. Venuto and co-workers found fast aging of mordenite for the alkylation of benzene with ethylene (87). The fast aging was suggested to be due to the narrow tubular pore structure of mordenite.

The resistance of zeolites to acids increases with the increase of Si/Al ratio. Crystallinity of mordenite, of which Si/Al ratio is high, is not destroyed by aqueous mineral acids. However, the crystallinity of NaX was lost markedly during the dehydrochlorination of ethyl chloride (85). The aging of NaX was attributed to the lattice collapse. In the decomposition of acetates, acetic acid may cause the collapse of the crystal structure of some zeolites. (Chapter 7)

Chapter 2

LITERATURE REVIEW

2.1 Synthetic Zeolites

2.1.1. Structures and Compositions

Zeolites are crystalline aluminosilicates composed of SiO_4 and AlO_4 tetrahedra arranged in various geometric patterns. At least 30 naturally occurring zeolite minerals, and several synthetic zeolites (12) are known. For synthetic zeolites, type A, X, Y and mordenite are well known and utilized widely in chemical and separation processes.

In typical synthesis of sodium zeolites, amorphous hydrous sodium-aluminosilicate mixtures, prepared from aqueous solutions of sodium aluminate, sodium silicate, and sodium hydroxide, are crystallized at temperatures ranging from room temperature to 150°C at atmospheric or autogenous pressure (12). Most of Linde zeolite particles are in the range of 0.5 to 5 microns (34, 83, 101).

The first structural analysis of synthetic zeolite A was reported in 1956 (64). A zeolites are members of the sodalite group which have cubic symmetry and a framework based on simple combinations of truncated octahedra (sodalite unit). The octahedra (Fig. 2-1-(a)) is composed of 24 (Al, Si) ions interconnected with 36 oxygen anions, and contains eight

hexagonal and six square faces. For A zeolites, the sodalite unit is linked to its neighbor by four bridging oxygen ions (Fig. 2-1-(b)). This arrangement produces a roughly spherical internal cavity, 11.4 Å in diameter (α-cage), that is entered through six circular apertures formed by a nearly regular ring of eight oxygen atoms with a free diameter of 4.2 Å. The sodalite units themselves enclose a second set of small cavities (β-cages) of 6.6 Å internal diameter. The β -cages interconnect with the large cavities by a distorted six-membered ring of oxygen atoms 2.2 Å in diameter. The unit cell composition of NaA (Linde 4A) is given in Table 2-1. Eight of 12 sodium ions are situated in the center of the six-membered rings in the hexagonal faces and four occupy positions adjacent to the eight-membered ring. When the zeolite is hydrated these four cations are probably completely hydrated and float in the center of a weakly coordinated sphere of water molecules (12). The three dimensional Fourier analysis of hydrated NaA located eight sodium ions, but gave no indication of the positions of the other four (14). The eight sodium ions in the six-membered rings are referred to as Type I and the remaining four are Type II. The sodium ions (Type I) in or near eight-membered rings in the A zeolite reduce the effective diameter of the aperture to less than 3.5 Å (91). CaA (Linde 5A) is made from NaA by ion-exchanging the blocking sodium cations with calcium.

Since each calcium cation replaces two sodium cations, the number of cations in the structure becomes six and most of the eight-membered rings are not blocked by cations. Thus, CaA has the aperture diameter of 4.2 Å. If sodium ions in NaA are exchanged for the larger potassium ion, a single potassium cation replaces a single sodium; the number of cations in the structure does not change. The free diameter of the 4.2 Å apertures of KA (Linde 3A) is reduced to about 3.2 Å by the potassium ions (91). However, the diameter of pore openings is apparently dependent on the particular diffusing species passing through the aperture as seen in Table 2-2.

The arrangement of the tetrahedra in the type X and Y zeolite is basically the same. Differences between these two zeolites are due to composition (Table 2-1) and other physical properties brought about by the compositional difference (12). The framework consists of a tetrahedral arrangement of sodalite units linked by hexagonal faces with six bridge oxygen ions (Fig. 2-1-(c)). This results in a series of wide, nearly spherical cavities (supercages), each of which opens by common windows (distorted 12-membered rings of 8 to 9 Å diameter) into four, identical, tetrahedrally distributed

cavities (Fig. 2-1-(d)) (7, 14). The cations in the structure of X and Y zeolites occupy three types of positions (Fig. 2-2).

These are:

Type S_I, in the centers of the hexagonal prism, 16 sites per unit cell;

Type S_{II}, on the six-membered rings, the unjoined hexagonal faces, 32 sites per unit cell; and

Type S_{III}, on the walls of the channels, 48 sites per unit cell.

The sodium ions of NaX and NaY are distributed as follows (12).

Site	S_I	S_{II}	S_{III}
Type X	16	32	38
Type Y	16	32	8

A major difference between NaX and NaY is the occupancy of the S_{III} sites.

In contrast to type A, X and Y zeolites with a three-dimensional pore structure that contains cages, mordenite has a one-dimensional tubular pore structure consisting of parallel nonintersecting pores (21, 49).

The crystal structure consists of chains of four- and five-membered rings of SiO_4 and AlO_4 tetrahedra linked so that a system of large, elliptical, parallel channels interconnected by smaller cross channels is created (Fig. 2-3). It has channels with a free diameter of 6.6 Å in one direction which are interconnected by smaller channels of 2.8 Å free diameter, whereas the effective pore openings had been determined to be about 4 Å by adsorption studies (5, 6). Meier suggested that mordenite was sensitive to stacking faults that could result in the reduction of the channel diameter from 6.6 Å to 4 Å (Fig. 2-3). However, another interpretation discounted the stacking fault hypothesis. The alternate explanation was that the cations in the pore of mordenite could reduce the effective pore diameter or block the pores (8, 22, 25).

The thermal stability and acid resistance of zeolites increases with increasing Si/Al ratio (53). Thus, the order of stability is A < X < Y < mordenite.

Depending on the size of apertures, molecules can be readily adsorbed, slowly adsorbed or completely excluded by zeolites (80). This is called molecular sieve effect . NaA has the effective pore diameter of about 4 Å and can readily adsorb materials such as H_2O, CO_2,

H_2S, SO_2 and all hydrocarbons containing one or two carbon atoms. Propane and higher hydrocarbons are physically excluded with the exception of propylene. CaA adsorbs straight paraffins, olefins and alcohols up to at least C_{14}. With the exception of cyclopropane, all branched chain, naphthenic, and aromatic molecules are excluded. NaX adsorbs molecules with diameters up to about 10 Å, but CaX can adsorb molecules of 9 Å. Table 2-3 shows the molecular sieve effects of A and X zeolites. Besides the size and shape of molecules, the polarity plays an important role in adsorption. The cations on the zeolite surface have strong localized positive charge and electrostatically attract the negative end of polar and polarizable molecules. The more polar or the more unsaturated the molecule, the more tightly it is held within the crystal.

The cations in zeolites exchange with other cations in aqueous solutions under suitable conditions. The hydrogen form of zeolites can be prepared by first exchanging the alkali metal ions with an ammonium ion and subsequently heating the ammonium form at 400°C to decompose the ammonium ions (13). In most cases complete exchange destroys the crystal structure of zeolites on heating. The sodium ions of NaA can be exchanged up to

35%. In Y zeolite and mordenite, a greater portion replacement is possible (12). The silver ions have great affinity with zeolites. For the ion-exchange of X zeolites, the decreasing order of affinity is: $Ag^{+} > Cu^{++} > H^{+} > Ba^{++} > Sr^{++} > Hg^{++} > Ca^{++} > Zn^{++} > Ni^{++} > Ca^{++} > Co^{++} > NH_4^{+} > K^{+} > Au^{+++} > Na^{+} > Mg^{++} > Li^{+}$. For the ion-exchange of A zeolites, the decreasing order of affinity is: $Ag^{+} > Cu^{++} > H^{+} > Zn^{++} > Sr^{++} > Ba^{++} > Ca^{++} > Co^{++} > Au^{++} > K^{+} > Na^{+} > Ni^{++} > NH_4^{+} > Cd^{++} > Hg^{++} > Li^{+} > Mg^{++}$ (80).

2.1.2. Catalytic Activity

Zeolites have acquired new prominence and value as a catalyst in petroleum and petrochemical industries during the last decade.

The catalytic activity exists on the exterior surface of the zeolitic crystal, but mostly on the interior surface (98). The external surface area of A and X zeolites is about 1-3 $m^2/gm.$, whereas the internal surface area is about 700 to 800 $m^2/gm.$ (33). Therefore, the reaction on the exterior surface is negligible compared with that on the interior surface if the whole surface fully participates in the reaction.

Molecular sieving action of zeolites affects the reaction. This is so-called molecular-shape-selective

catalysis. Weisz and co-workers (99) first demonstrated it in the dehydration of butyl alcohols on CaX and CaA. The dehydration of n-butyl alcohol occurs on both CaA and CaX, but only CaX can dehydrate sec-butyl alcohol ($<130^{o}C$) and isobutyl alcohol ($<260^{o}C$) since sec-butyl and isobutyl alcohol cannot enter the aperture of CaA. The product distribution of n-hexane cracking is also affected by the pore size of the zeolite catalyst. The ratio of isoparaffin to n-paraffin in the product mixture is very low on CaA compared with CaX and silica-alumina (99). Rálek and Grubner (63) found that the olefin formation from the dehydration of ethyl alcohol on CaA was faster than on CaX whereas the dehydration of diethyl ether on CaX was faster than on CaA. The selectivity of the olefin formation in the dehydration of ethyl alcohol on CaA was higher than that on CaX. Similar results were found by Bryant and Kranich (15). They studied the effect of pore geometry on the reaction rate and the selectivity for the dehydration of ethyl and n-butyl alcohol on various ion-exchanged zeolites including type A, X and mordenite. Olefin formation was more favorable on A zeolites and mordenites than X zeolites. For the dehydration of ethyl alcohol to ether and olefin, the selectivity of the olefin formation on mordenite was often higher than

on A zeolites. It was suggested that the long cylindrical pore structure of mordenite, in contrast to the roughly spherical cages of type A and X, made it difficult for the ether chain to form and move.

The catalytic activity of zeolites for the cracking of hydrocarbons such as n-hexane exceeds greatly that of conventional silica-alumina. Some synthetic zeolites in the hydrogen form are reported to have activities, based on extrapolated rate constants from Arrhenius plots, greater than 10,000 times that of silica-alumina (26, 51, 100). The activities of ion-exchanged X, Y and mordenites for the isomerization of o-xylene have been compared with silica-alumina (38). The most active catalyst is HZ and the activity is about 266 times that of silica-alumina. Many X and Y zeolites are less active than silica-alumina. Those are Mn, Ca, Mg and ZnX and Ca, Sr, and CaY. Therefore, the superactivity of zeolites compared with silica-alumina found for the cracking of n-hexane, is not a universal character of zeolites.

Zeolites are versatile catalysts for many organic reactions (89). Venuto and co-workers have performed a variety of organic reactions using zeolite catalysts: the alkylation of aromatics with olefins, alcohols and alkyl halides and the disproportionation of alkyl benzenes

(86, 87); the condensation of carbonyl compounds with phenol, thiophenol, m-xylene, and the self-condensation of ketones (88); the Beckmann rearrangement of ketoximes to amides (40); the dehydrohalogenation of alkyl halides and the reaction of ethyl alcohol and hydrogen chloride (85). Generally, these reactions are catalyzed by acid catalysts and the reactions are ionic.

Many theories have been proposed regarding the source of catalytic activity of zeolites, including acidic hydroxyl groups (Brönsted acid sites), tricoordinated aluminum atoms (Lewis acid sites), electrostatic fields, and cations.

For NaX and NaY, evacuated at 430° to 500°C, Uytterhoeven and co-workers (84) found the surface hydroxyl groups, which could be exchanged with deuterium, to be $0.29 - 0.68 \times 10^{20}$ OH/gm. The amount of hydrogen is enough to cover the surface with hydroxyl groups. Calcium zeolites have more hydroxyl groups than the corresponding sodium zeolites. The hydrogen content increases as much as 50 times if the zeolites are decationized. New infrared OH-stretching bands appear in a deaminated, 75% decationated zeolite. On adsorbing ammonia, these hydroxyl groups disappear with the increase of the ammonium ion on the surface. This can be visualized as follows.

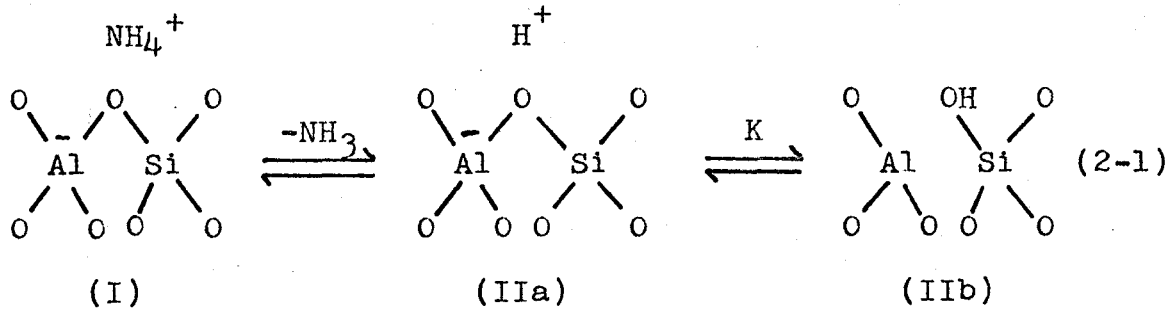

(2-1)

A classical Brönsted form (IIa) is proposed as being in equilibrium with the silanol form (IIb), and proton donation can occur upon the approach of a strong base (NH_3); with weaker bases, the magnitude of the equilibrium constant, K, is critical (84).

The hydroxyl groups can be dehydrated by heating (10, 84, 94) and then a tricoordinated alumina and positively charged tricoordinated silicon ion pair and the negatively charged alumina-oxygen tetrahedra are proposed to form as follows:

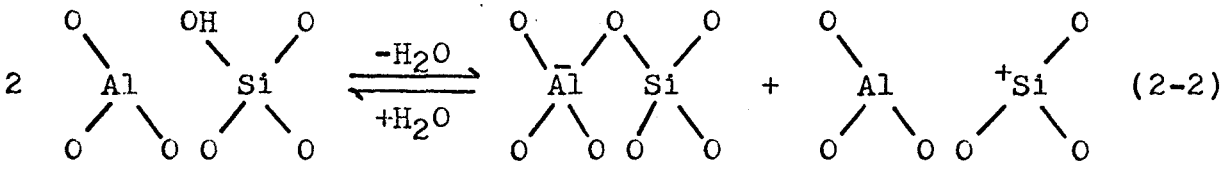

(2-2)

The hydroxyl groups can be reformed by adding water.

The infrared spectra of chemisorbed pyridine are useful for determining Brönsted and Lewis acidities (32, 94, 95). The concentration of the pyridinium ion parallels

that of the acidic hyroxyl group (Brönsted acid site). The concentration of coordinately bound pyridine corresponds to that of the tricoordinated aluminum atom (Lewis acid site). The Brönsted and the Lewis acidities are a function of the calcining temperature and the concentration of the acidic hydroxyl group on HY reaches a maximum at 350°C, remains constant to 550°C, and decreased with increasing temperature. The concentration of the Lewis acid site on HY is low below 475°C, but increases rapidly with increasing calcination temperature (94). Similar results are found for magnesium Y (95). Hattori and Shiba (32) studied infrared OH stretching vibration in connection with the adsorption of water and pyridine over K, NH_4, Mg, Ca, Sr, Zn, La(III), Ce(III), and MnX and found two kinds of Lewis acid. The stronger Lewis acid can easily be converted into Brönsted acid by the addition of water. The weaker Lewis acid cannot be easily converted into Brönsted acid. The catalysts studied can be classified into four groups as follows. In their study, all catalysts except NH_4X were calcined and evacuated at 450°C. NH_4X was evacuated at 270° or 300°C.

First group: NH_4, La and CeX have both Brönsted and strong Lewis acid sites which can be converted into Brönsted acid by the addition of water.

Second group: Almost all of the acid on Ca and SrX is strong Lewis acid which can be converted into Brönsted acid by the addition of water.

Third group: Zn, Mn, and MgX have Lewis acid sites which are too weak to be converted easily into Brönsted acid by the addition of water.

Fourth group: NaX has only weak Lewis acid which cannot be converted into Brönsted acid by water.

The comparison of the catalytic activity for cumene cracking with Brönsted and Lewis acid concentrations shows that the Brönsted acid site has a direct relation with the activity (94, 95). Benesi (10) studied the disproportionation of toluene on HY and HZ and the cracking of n-butane and n-pentane on HZ as a function of calcination temperature. He found a similar change of activity with calcination temperature. Venuto and co-workers (87) studied the alkylation of benzene with ethylene on rare-earth exchanged Y(REY), rare-earth exchanged X(REX) and HY as a function of calcination temperature. The activities reached their maxima at 400° (REX), 250° (REY) and 600° (HY) and decreased with the increase of calcination temperature. Thus, it has been postulated that the acidic hydroxyl group (Brönsted acid) is the active center for these reactions and the carbonium ion which forms by the donation of proton from the surface

is the reaction intermediate.

Turkevich and co-workers (82) studied cumene cracking, ethylene polymerization and butene isomerization on decationated NaY by changing the sodium content. The number of decationated sites was very close to the number of active sites determined by a pulse poisoning technique using gas chromatography. Quinoline was used as the poison. The Lewis acid site (tricoordinated aluminum atom) was found on the decationated NaY using the ESR technique and the intensity of the ESR signal corresponding to the Lewis acid site was proportional to the number of decationated sites.

Silica-alumina whose activity is attributed to Lewis and/or Brönsted acid sites is virtually inactive for the isomerization of n-hexane, whereas bivalent cation Y zeolites are active. The bivalent cation Y zeolites give rise to strong carboniogenic activity, i.e. catalytic activity indicative of the formation of a carbonium ion intermediate, which greatly increased with the decrease in cation radius. Pickert and co-workers first reported that the electrostatic field generated by the cation is responsible for the activity and the cations in low coordination with structural oxygen ions are the catalytically active sites (59).

Tung and McInich (81) studied the cracking and isomerization of n-hexane on NaY zeolite by changing the content of Ca ions. The isomerization activity increases remarkably above the ion-exchange level of 60%. The point where sites I of Y zeolites are fully occupied by calcium ions corresponds to about a 61% level of exchange. The excess calcium ions reside in site II and will set up a surface electrostatic field. This is because a Ca^{++} ion, while replacing two Na^{+} ions, can be physically present only near one site, thus leaving the other site empty. Electrostatically, the filled site will have one net positive charge and the empty site will have one negative charge. The hydrocarbon can be adsorbed on the positive-negative pair charge site and polarized or completely ionized. They proposed that the electrostatic field had a dynamic character which was caused by the surface diffusion of cations and had an important role for the adsorbed species to desorb from the sites.

Butler and co-workers (16) dehydrated n- and sec-propyl alcohol over NaX in a static reactor at 240° and 270°C at alcohol pressure up to 10 torr. They suggested that the potentially active sites on NaX were alkali metal ions at type II and III sites since the Brönsted and Lewis acid sites were negligible on NaX.

2.2. Silica-Alumina

Silica-alumina is a typical solid-acid catalyst that is effective in a variety of hydrocarbon reactions similar to those observed for acidic catalysts such as aluminum chloride, hydrogen fluoride, sulphuric acid, phosphoric acid and boron trifluoride. It has been postulated that the reaction intermediates are carbonium ions. The silica-alumina catalyst is prepared by precipitating sodium silicate with sodium aluminate, adding either sulphuric acid or sodium hydroxide to control the pH. After aging and washing, sodium ions in the hydrogel are exchanged for ammonium ions and the gel is then dried and finally calcined (78). Final catalysts have a very low sodium content. Oblad and co-workers (54) suggest that most silica-alumina catalysts are mixtures of silica and alumina particles with the silicon and aluminum ions sharing oxygen ions at the points of contact.

By adsorption and desorption experiments in a flow system using a nitrogen stream saturated with quinoline, Oblad and co-workers (54) found that a small amount of quinoline was irreversibly chemisorbed on silica-alumina at 300°C whereas silica-gel which was inactive for cracking hydrocarbons could only reversibly adsorb quinoline under the same condition. The amount of

quinoline chemisorbed irreversibly on silica-alumina was independent of the partial pressure. Similar results were obtained using ammonia (77). By the titration of silica-alumina with n-butylamine in a non-aqueous medium such as benzene, it was found that silica-alumina was comparable in acid strength to very strong acids, but that the concentration of acid sites was very small (77). The infrared spectra of chemisorbed pyridine shows that both Lewis and Brönsted acid sites are present on the surface of silica-alumina (9, 57).

A direct relation between the activity of silica-alumina for hydrocarbon cracking and its acidity was found (54, 77). The Brönsted acidity was measured by means of the infrared spectrum of chemisorbed pyridine and a linear relationship was found between Brönsted acidity and the catalytic activity for o-xylene isomerization over silica-alumina containing up to 14% alumina (96). For propylene polymerization and hydrogen transfer between decalin and isobutene, the catalytic activity was correlated better with protonic acid content, which was determined by base exchange with 0.1 N ammonium acetate solution followed by pH measurement, than with total acid determined by butylamine titration for the entire composition range from pure silica

to pure alumina (37). The concentration of protonic acid sites reached a maximum at 82% silica. Shiba and co-workers (71, 75) reported that the activity for the cracking of cumene, the polymerization of propylene and 1-butene, and the double-bond migration of 1-butene were closely correlated with the Brönsted acidity and that the activity for the cracking of isobutane was proportional to Lewis acidity.

2.3. Reactions

2.3.1. Chemical Equilibrium

The free energies of formation of n- and sec-butyl acetate are not known. Rudy and Fugassi (68) calculated the equilibrium constant for the decomposition of tert-butyl acetate to acetic acid and isobutene. The equilibrium constant was about 10^5 at 252°C and therefore the reaction was irreversible. They also calculated the equilibrium constant for the dissociation of the dimer of acetic acid. The constant was about 5×10^4 at 252°C and the amount of the dimer was negligible. Warrick and Fugassi (97) calculated the equilibrium constant for the decomposition of tert-butyl propionate to propionic acid and isobutene. The constant was about

3×10^5 at 240°C and the reaction was irreversible. Sashihara and Syverson (70) estimated the equilibrium constant for the decomposition of n-hexyl acetate at 300°C to be 10^2 to 10^4. The approximated value indicated that the equilibrium conversion of ester was greater than 99%.

The thermodynamic properties of n-butenes are known (73). Experimental studies have been done extensively in the temperature range of 235° to 300°C (11), 200° to 630°C (90), 87° to 332°C (28) and 123° to 451°C (44). The equilibrium concentrations of n-butenes (44) are given in Figure 2-4.

2.3.2. Pyrolysis of n- and sec-Butyl Acetate

If a β-hydrogen is present in the alkyl group of ester, the ester decomposes to carboxyl acid and olefin. The reactivity of ester increases with the increasing number of β-hydrogens (39). The pyrolysis of esters shows a much lower heterolytic character than halides (46). Hurd and Blunck (39) have postulated that a six-membered ring intermediate forms through an intramolecular rearrangement and this mechanism is now generally accepted. For the pyrolysis of n- and sec-butyl acetate, Froemsdorf and co-workers (27) have found that

the selectivity of n-butenes produced is consistent with the cyclic intermediate which can form via random hydrogen bonding between β-hydrogens and carbonyl oxygen (Fig. 2-5).

sec-Butyl acetate decomposes cleanly to acetic acid and 1-, trans-2- and cis-2-butene at 303° to 525°C (23, 27, 30, 72). The ratio of cis- to trans-2-butene is about 0.54 at 450°C compared with an equilibrium ratio of about 0.89 (44) and the ratio of 2-butenes to 1-butene is 0.75 compared with 0.67 calculated on the basis of the number of β-hydrogens available for forming of the cyclic intermediate as shown in Figure 2-5 (27).

n-Butyl acetate decomposes to acetic acid and 1-butene at 489° to 500°C (27, 72). The isomerization of n-butene does not occur during the gas-phase decomposition of n- and sec-butyl acetate (27, 30).

The decomposition of n- and sec-butyl acetate follows first order kinetics (23, 72). The kinetic constants are shown as follows.

	n-Butyl	sec-Butyl	Reference
ε(Kcal/mole)	---	46.60	(23)
log A	---	13.30	(23)
ε(Kcal/mole)	1. 44.5 ± 0.8 2. 47.8 ± 1.2	47.2 ± 1.2	(72)
log B	1. 8.869 2. 7.958	10.880	(72)
log A	1. 11.751 2. 10.840	13.715	(72)

Where, $k = Ae^{-\varepsilon/RT}$ and $k = BTe^{-\varepsilon/RT}$.

2.3.3. Catalytic Decomposition of Esters

Maihle found that thorium oxide is a catalyst for the decomposition of ethyl, propyl and butyl acetates to acetic acid and the corresponding olefins at 310° to 340°C (47). Copper borate (4) at 480° to 620°C and zinc, zinc oxide, lead, lead dioxide and ferric oxide (17) were also catalysts for the reactions. Obolentsev and co-workers (55) studied the decomposition of isoamyl acetate on an aluminosilicate catalyst at 350°C. Sashihara and Syverson (70) studied the decomposition of n-hexyl acetate on activated bauxite and metal oxide-bauxite catalysts at 255° and 305°C in a fixed-bed flow reactor. They found that a boric oxide-bauxite catalyst was superior. During the reaction, the catalysts showed aging. The kinetic study was carried out using the boric oxide-bauxite catalyst at 305°C and 0.98 to 3.98 atm. Semi-empirical rate equations based on the Langmuir-Hinshelwood rate expression correlated the conversion-space time data satisfactorily. The rate expression suggests that the surface reaction on dual-sites is the controlling step. The rate equation and kinetic constants were as follows.

$$r = \frac{kE\left(\frac{\pi_e}{\pi_e - \pi}\right) P_e}{\left(1 + \left(\frac{\pi_e}{\pi_e - \pi}\right)EP_e + HP_h + AP_a\right)^2} \qquad (2\text{-}3)$$

Where π_e = 6.57 atm.

k = 0.0294 gm. mole/ hr. gm. catalyst

E = 0.501 $atm.^{-1}$

H = 0.0521 $atm.^{-1}$

A = 5.01 $atm.^{-1}$

(refer to the table of notations on p. 196)

The retarding effect of acetic acid on the rate was large and of n-hexene small. Macarus and Syverson (43) studied the adsorption of acetic acid, n-hexene and n-hexyl acetate under the reaction condition and confirmed that acetic acid inhibited the reaction rate. They found the adsorption of n-hexene was reversible, but acetic acid was partly irreversibly adsorbed on boric oxide-bauxite catalyst at 305°C.

Pettit and Anderson (58) studied the decomposition of sec-butyl acetate on charcoal at 300° to 400°C and atmospheric pressure. The ester decomposed to acetic acid, 1-, cis-2- and trans-2-butene. Traces of n-butane, methane and carbon dioxide were found. The butene

selectivity was independent of the conversion of ester. The ratio of 1-butene to 2-butenes was close to the ratio for gas-phase decomposition and far removed from the equilibrium butene ratio. The following rate equation was found:

$$r = \frac{kEP_e}{1 + EP_e} \qquad (2\text{-}4)$$

The rate expression corresponds to the first order surface reaction of ester chemisorbed on a single-site or adsorbed physically. The gas chromatographic measurements confirmed that the ester was the principal adsorbate. The activation energy was 32.7 Kcal/mole compared with 46.6 Kcal/mole for the gas-phase decomposition.

Sanyal and Weller (69) studied the decomposition of ethyl acetate on aluminas, silica-aluminas and zeolites. The zeolites were NaY, CaY, HY, SK-500, H- and Na-mordenite. On the Y zeolites, the conversion at comparable times increased in the order of NaY < CaY < HY < SK-500. Except for NaY and CaY, all zeolites showed aging.

2.3.4. Isomerization of Butenes

The isomerization of n-butenes is one of the simplest hydrocarbon reactions in the aliphatic series. The

reaction is catalyzed by a wide range of materials under a variety of conditions. Typical catalysts include liquid (76), gaseous (45) and solid (56) acids; bases (60); transition metal hydrides (18) and coordination complexes (31); salts (52); semiconductor (1) and insulator (24) oxides.

In many cases, the thermodynamically less stable cis-2-butene is kinetically favored in 1-butene isomerization. This process, called stereoselectivity, was first reported by Pines and Haag (60) over sodium dispersed on alumina. They proposed that the double-bond migration occurred through a chain mechanism involving a carbanion attack on an allylic hydrogen as shown in equation (2-5) and the transition state of a cyclic intermediate (IV) was involved. Stereoselectivity was also found in the isomerization of 1-butene on alumina and in the dehydration of n- and sec-butyl alcohol and sec- and tert-pentyl alcohol. Foster and Cvetanović (24) studied the stereoselectivity of n-butene isomerization on a wide range of catalysts. The highest stereoselectivity in the isomerization of 1-butene was found on the basic catalysts and the smallest on some metals such as nickel and silver. They found that the isomerization of 2-butenes proceeded by exclusive double-bond shift on some basic

$$\underset{\text{I}}{CH_2 = CH - CH_2CH_3} \xrightarrow{R^-Na^+} \underset{\text{II}}{(CH_2 = CH - \bar{C}HCH_3)\ Na^+} + RH \qquad (2\text{-}5)$$

$$\underset{\text{II}}{\text{II}} \rightleftharpoons \underset{\text{III}}{(\bar{C}H_2 - CH = CH - CH_3)\ Na^+} \qquad (2\text{-}6)$$

$$\underset{\text{III}}{\text{III}} \rightleftharpoons \underset{\text{IV}}{H_2\bar{C}\overset{CH = CH}{\underset{Na^+---H}{\diagdown\ \diagup}}CH_2} \qquad (2\text{-}7)$$

catalysts such as KOH or by exclusive cis-trans conversion on some acidic catalysts such as H_2SO_4 or by combination of the two processes. For the isomerization of 1-butene the reaction on acid catalysts proceeded through the carbonium ion mechanism and the carbanion mechanism was associated with base-catalyzed reactions. Hightower and Hall (36) investigated the mechanism of n-butene isomerization on silica-alumina and alumina with carbon-14 and deuterium tracers. They suggested that the 2-butyl-carbonium ion was the common reaction intermediate over silica-alumina. Over alumina, no single mechanism could be formulated to explain the results. A large primary kinetic isotope effect ($k_H/k_D = 4$) was found on alumina suggesting that the carbon-hydrogen bond cleavage was involved in the

rate determining step for all reactions over alumina.

Dimitrov and Leach (19) studied the isomerization of n-butenes on NaX and a series of copper X which was prepared by partial exchange of the sodium ion. All catalysts were active for cis-trans isomerization and double-bond shift. The reaction was reversible first order according to a triangular reaction scheme in which all possible reaction paths between the three component mixture of isomers were involved. The isomerization on NaX occurred over a temperature range 200° to 300°C and was in marked contrast to that reported for amorphous silica-alumina; in particular NaX exhibited a marked preference for double-bond shift rather than cis-trans isomerization. The ion-exchange by cupric ion had a profound effect on the reaction rate, activation energy, and stereoselectivity, but the effect was not linear with exchange. When the extent of exchange was below about 30%, CuX showed a very strong preference for the formation of trans-2-butene from 1-butene. The initial rate of isomerization was low and the rate was accelerated with time. They suggested that cupric ion in S_I sites reduced to cuprous which were capable of forming unstable complexes with olefins and that the reduction process was responsible for the induction period. When the extent of exchange was

higher, stereoselectivity appeared and the reaction was similar to the isomerization on acid catalysts which occurred through the carbonium ion mechanism.

Chapter 3

EXPERIMENTAL METHODS

3.1. Apparatus

3.1.1. Reaction System

A schematic diagram of the continuous flow reaction system is shown in Figure 3-1. The fixed-bed reactor consisted of 5/8 inch 316 stainless steel tubing 13.5 inches long and 1/2 inch 316 stainless steel tubing 10.0 inches long with a 200-mesh stainless steel screen at the end. The 1/2 inch tubing was silver-soldered to a Swagelok union tee. This tube was inserted into the 5/8 inch tubing and connected by a Swagelok nut. A Teflon front ferrule and stainless steel back ferrule were used so that the reactor could be detached from the furnace. A 1/16 inch outside diameter stainless steel-sheathed thermocouple was attached to the Swagelok union tee by silver-soldering. The catalyst bed temperature was measured at 0.2 inch above the 200-mesh screen since the temperature difference along the axis of the catalyst bed was small. Under the steady reaction condition used in this study, the axial temperature differences within 1.5°C were measured in

a preliminary experimental run. The catalyst was loaded in the 1/2 inch tube. The inlet part of the tube (8.5 to 9.5 inches long) was packed with 3mm. diameter Pyrex glass beads and used as preheater to heat the reactant to reaction temperature. The top part of the reactor which was outside the furnace was heated by electric heating tape at about 150°C to prevent the condensation of reactant inside the reactor and to vaporize the reactant inside fine inlet tubing. The reactor was heated by a metal block furnace which was fabricated from 3 inches OD and 3/4 inch ID stainless steel cylinder wound doubly with nichrome wire.

The electrical power was maintained constant using an A/C voltage stabilizer. The furnace was heated about 5°C below the setting temperature using the outside heating wire. The voltage of the outside heating wire was kept constant. The temperature was controlled by the inside heating wire using a voltage regulator and 2 ohm variable resistance. The temperature in the catalyst bed was kept within $\pm 1^{\circ}C$ by controlling the voltage manually.

Liquid reactant was fed by a Harvard Infusion/ Withdrawal Pump, model 940, using 20 and 50 milliliter syringes. The pump was installed for the outlet to be

upward so that air did not remain inside the infusing syringe. The reliability of liquid feed was excellent (APPENDIX 1). The fluctuation was within 1.2% of the setting feed rate. The reactant was stored in a glass reservoir sealed with calcium chloride tubing. The liquid line was 1/8 inch 316 stainless steel tubing. The line was connected to 1/16 inch stainless steel tubing which was silver-soldered to the Swagelok union tee of the reactor and extended to the preheating part of the reactor. The outlet line from the reactor was 1/8 inch 316 stainless steel tubing. An Aerograph six-way gas sampling valve was attached to the outlet tubing, and the tubing and the valve were heated to 150°C to prevent condensation. Teflon seals were used for the gas sampling valve. The sampling valve was connected to a Beckman 2A gas chromatograph.

3.1.2. BET Apparatus

Nitrogen adsorption isotherms on catalysts were measured by a conventional glass volumetric adsorption apparatus. The burettes were maintained at 30°C by circulating water from a thermostat. A glass U tube with a 4-way capillary stopcock was used as the adsorption vessel (2). The vessel was small and light

enough to be weighed in an analytical balance to determine the weight loss upon burning the catalyst. The bores of the stopcock plug were arranged so that both were open or only one was open. The U tube had a catalyst chamber which was made just large enough to accommodate the sample required, less than 1 cc. The tubes leading to the stopcock contained loosely packed wads of glass wool to prevent the catalyst from blowing out of the chamber. The adsorption vessel was connected to the adsorption or burning systems by a 10/30 capillary ground-glass joint. With the 4-way stopcock the sample could be connected to the system for adsorption or evacuation with one bore open, and with both bores open a stream of oxygen could be passed over the catalyst.

3.2. Materials

3.2.1. Organic Compounds

Organic compounds used in this study were n- and sec-butyl acetates, acetic acid, and 1- and cis-2-butenes. Reagent grade n- and sec-butyl acetate were purchased from British Drug House and Eastman Organic Chemicals. Reagent grade acetic acid was obtained from Canadian Industry. 1-Butene was Matheson technical grade and

cis-2-butene was Matheson C.P. grade. No impurity was found in sec-butyl acetate and cis-2-butene by gas-liquid chromatography. The purity of 1-butene was higher than 99.9% by gas-liquid chromatography. Traces of trans- and cis-2-butene were found. n-Butyl acetate contained n-butyl alcohol, which was partly removed by storage over CaA zeolite. The purity of n-butyl acetate used was higher than 99%. Acetic acid contained water and unknown impurities. Water was removed by phosphorus pentoxide and distilled. The purity of acetic acid used was higher than 99% by gas chromatography.

3.2.2. Catalysts

Powders of Linde 3A(KA) Lot No. 340224, 4A(NaA) Lot No. 450339, 5A(CaA) Lot No. 550043, 10X(CaX) Lot No. 1080001, 13X(NaX) Lot No. 1350001, and SK-40(NaY) Lot No. 3606-224, and of Norton sodium mordenite (NaZ) Lot No. BG-11, and hydrogen mordenite (HZ) Lot No. BG-10 were used. The ammonium Y(NH_4Y), hydrogen Y(HY), silver Y(AgY) and nickel Y(NiY and NiHY) were prepared by ion-exchanging NaY powder (APPENDIX 2). Table 3-1 shows the level of ion-exchange and the Si/Al ratio.

The powdered zeolites in the hydrated form were

compressed to large pellets at about 200°C and 10,000 p.s.i. using a Buehler 20-1301 AB Simplimet Press. The large pellets were crushed and sieved to 30 to 35, 70 to 80 and 30 to 80 mesh. None of the zeolites used in this work contained binders.

The silica-alumina was 3/16 inch pellets of Davison 87% silica-13% alumina. 3/16 x 3/16 inch pellets of Girdler T-708 (α-alumina) and Girdler T-126 (γ-alumina) were used. Silica-gel was Davison medium pore volume beads. The particle size of silica-alumina, α- and γ-alumina, and silica-gel used for reactions was 30 to 80 mesh. The preparation of the coconut shell charcoal was described previously (58). All catalysts except charcoal were dried in air at 270°C for more than 3 days before use. The charcoal was calcined in flowing nitrogen at 900°C for 5 minutes.

3.3. Analyses

Reaction mixtures were analyzed by gas-liquid chromatography. The gas chromatograph was a Beckman Model GC 2A, which uses a thermal conductivity cell as the detector. For the decomposition of esters, the two chromatographic columns were used in series as shown in Figure 3-1. The first column was 3 feet of 1/4 inch copper tubing packed

with Porapak P which was operated at 190°C to separate butenes, acetic acid, and butyl acetates. The second, 50 feet of 1/4 inch copper tubing packed with 18 wt. % propylene carbonate on Chromosorb P, was operated at room temperature to separate 1-butene, trans- and cis-2-butene. Helium was used as a carrier gas at 120 cc. (S.T.P.)/min. For the isomerization of 1-butene, 20 feet of 1/4 inch copper tubing packed with 10 wt. % bis (2-(2-methoxy-ethoxy)ethyl) ether on Chromosorb P was used at room temperature to separate 1-, trans-2- and cis-2-butene. The carrier gas was helium at 110 cc. (S.T.P.)/min. The typical analyses by gas-liquid chromatography are given in APPENDIX 4.

The relative thermal response factors of n- and sec-butyl acetate to total butenes were 0.574 and 0.646, respectively. The relative thermal response factor between n-butene isomers was taken as 1.0. The detector current used in this study was 200mA. The output signal from the detector was recorded and integrated by a Disc Chart Integrator, model 231.

3.4. Experimental Procedures

3.4.1. Decomposition of n- and sec-Butyl Acetates

A dried catalyst was weighed and charged into the

reactor for each experiment, and purged with helium at about 20 cc./min. for 1 1/2 hours at the reaction temperature before introducing the ester. To shorten initial unsteady behavior, the ester was fed at a high rate, so that the amount of the reaction was negligible, for 10 to 20 seconds. Then, the feed was set at a desired rate. Simultaneously, process time was started to be recorded with a stop watch. The gas chromatographic analysis was usually done once every 15 to 20 minutes. After the reaction, helium was passed over the catalyst overnight at about 10 cc./min. and reaction temperature to purge the product mixture. The used catalyst was kept in a stoppered bottle for further examination.

3.4.2. Isomerization of 1- and cis-2-Butenes

The liquid inlet was sealed and 1-butene was fed from 1-butene cylinder. A pressure regulator and a fine metering valve were used to control the feed rate. The feed rate was measured by a soap film meter connected to the outlet of the reactor.

Pulses of acetic acid were injected by a 10 microliter syringe into a 1/4 inch stainless steel union tee with a silicon rubber septum at one end which was installed on

the gas inlet line and heated by electric heating tape.

Other procedures were the same as in the previous section.

3.4.3. Adsorption Isotherms

The empty sample vessel was weighed and about 0.2 gm. of sample was loaded. The sample was evacuated at 200° to 250°C overnight. Then, the stopcock of the sample vessel was closed and the sample tube was detached from the vacuum system. Grease used on the glass joint was cleaned using n-hexane. The sample and the vessel were weighed to obtain the weight of the sample after evacuation. The sample vessel was attached to the adsorption apparatus and the dead space was measured by helium. After the nitrogen adsorption measurement, organic compounds deposited on the catalyst were burned in the sample vessel by passing oxygen at 480° to 500°C and about 5 cc./min. overnight. Then the sample was evacuated for 3 to 5 hours at this temperature. The sample was weighed and the weight of the deposit and the catalyst was calculated before starting the adsorption measurement.

3.5. Definition of Terms

3.5.1. Conversion

Conversion is the percentage of ester consumed as calculated by equation (3-1).

$$X = \frac{S_b}{S_b + S_e \cdot R_e} \times 100 \qquad (3\text{-}1)$$

Where S_b and S_e are peak areas in arbitrary units for total butenes and ester, respectively, obtained by gas-liquid chromatography. R_e is a relative thermal response factor of ester to 1-butene (APPENDIX 4).

3.5.2. Process Time

Process time is the actual time on stream after the reaction was started, expressed in minutes.

3.5.3. Reaction Rate

Reaction rate is the instantaneous differential rate of conversion of ester expressed in gm. mole ester/hr./ gm. catalyst.

3.5.4. Selectivity of Butenes

Selectivity of butenes is the percentage of a particular isomer in the total butenes.

3.5.5. Space Time

Space time is the reciprocal molar feed rate of ester per unit weight of catalyst expressed in gm. catalyst/gm. mole ester feed/hr.

Chapter 4

DECOMPOSITION OF sec-BUTYL ACETATE

4.1 Experimental Results

Under the reaction conditions of the present study, no decomposition was observed using the reactor packed with glass beads. sec-Butyl acetate decomposed cleanly to acetic acid and n-butenes on silica-alumina and synthetic zeolites. Material balance of moles of n-butenes and unconverted ester to the ester fed was higher than 99%. Traces of methane and carbon dioxide were found, and the mole ratio of methane to carbon dioxide was always less than one. In gas chromatographic analysis, at least four components appeared after the n-butenes (APPENDIX 4). Two of them were identified as trans- and cis-2-pentene by their retention times. Possibly peak X1 corresponded to 1-pentene and peak X2 to a branched pentene or n-hexane. A greater amount of by-products was found on the hydrogen zeolites, CaX and silica-alumina than on the sodium zeolites. The amount increased at higher temperature. Isobutene was not observed. The distributions of components in product mixtures on some catalysts are shown in Table 4-1.

1-Butene and cis-2-butene isomerized on CaX at 290°C and a feed rate of 1.11 (gm. mole butene feed/hr./gm. catalyst) and several by-products were found. The product distributions

at process time 4 minutes are shown in Table 4-2. The mole percents of trans-2-pentene and X2 were calculated using the relative thermal response factor of pentane in the reference (67).

Figure 4-1 shows typical aging patterns for the catalysts. All of these tests were made with one gram of catalyst at a feed rate of 3.38×10^{-2} gm. moles of ester per hour. The catalytic activity of NaY did not change with process time up to 210°C (APPENDIX 3). The catalytic activity of AgY increased slowly with process time at 140° and 170°C (Fig. 6-9 and 6-10). Other zeolites and silica-alumina showed aging as exemplified by curves shown for HY, HZ, NaX, NaA and silica-alumina. Conversions as a function of process time for silica-alumina, NaY, HY, HZ, NaZ, NaX, CaX, CaA, NaA and KA are given in Table 4-3. The distributions of n-butenes could be correlated with conversion of ester, apparently independent of aging. For instance, aging and selectivity plots are given in Figures 4-2 and 4-3 for NiHY at 170°C and feed rates of 0.273, 0.0931, 0.0545 and 0.0454 (gm. mole ester feed/hr./gm. catalyst). The study of the selectivity of n-butenes was carried out on silica-alumina, NaY, HY, NiY, NiHY, AgY, CaX, NaX, HZ, NaZ, CaA, NaA and KA over the temperature range of 140° to 290°C. The results are given in Table 4-4. The initial distributions of n-butenes obtained by extrapolating to zero conversion and equilibrium

compositions of n-butenes (44) are also given in Table 4-4. The change of n-butene distribution with process time on HY at 290°C is shown in Figure 4-4. The conversion of ester was always 100%.

4.2 Discussion

For the decomposition of sec-butyl acetate on synthetic zeolites and silica-alumina, some of the products observed in the reaction of butenes were not found; these were propylene, propane, n-butane and isobutene. Traces of methane, carbon dioxide, X1, X2, trans- and cis-2-pentene were found. Methane and carbon dioxide were probably produced by the decomposition of acetic acid. The reactivity of cis-2-butene for the skeletal isomerization was lower than 1-butene as seen in the product distributions for the isomerization of 1- and cis-2-butene .
Traces of isobutene were observed from the decomposition of n-butyl acetate on HY, CaX, and silica-alumina at 290°C. For this ester, 1-butene was the principal primary product. However, for sec-butyl acetate, the quantity of 1-butene produced was smaller than 2-butenes which were less reactive for the skeletal isomerization. A similar observation has been reported regarding the reactivities of 1-butene and 2-butenes for the skeletal change (3).

Table 4-3 shows that the conversion decreases in the

order: HY > silica-alumina > HZ > NaY > CaX > NaZ > NaX > CaA > NaA > KA. For the same type zeolite, the hydrogen and calcium forms had higher activity than the sodium form. A similar effect of the cations on catalytic activity has been observed in many organic reactions on zeolite catalysts (89). The hydrogen and calcium zeolites have strong Brönsted and/or Lewis acid sites, whereas NaY and NaX have no strong acid sites (32, 48, 92, 93). The higher activity of the hydrogen and calcium zeolites may be due to the strong Brönsted acid sites. However, it is noteworthy that the conversion on NaY was higher than on CaX (Table 1), since, for the cracking of cumene, NaY was inactive up to 500°C (29, 65), while CaX was active at 470°C (26, 29). NaX was also inactive at 483°C (29) for the cracking of cumene, but was active for the decomposition of sec-butyl acetate.

Furthermore, sec-butyl acetate decomposes at a moderate rate, greatly exceeding the gas-phase reaction rate, on charcoal at 303° to 375°C, and the carbon surface is neither ionic nor acidic (58). Butler and co-workers have reported that the dehydration of n- and sec-propanol occurs on NaX (16). They suggested that the potentially active sites were the alkali cations at S_{II} and S_{III} positions. These results suggest that decomposition proceeds on nonacidic and weakly acidic surfaces, but the rate is greater on strongly acidic surfaces; however, the rate must also depend on other factors than acidity.

The effective pore diameters of KA, NaA and CaA are about 3Å, 4Å and 5Å (12) respectively. The minimum molecular size of sec-butyl acetate calculated from the Fisher-Hirschfelder-Taylor model is about 5.5Å. Therefore, sec-butyl acetate is too large to enter into the internal cavities of the A zeolites. The external surface of A zeolites is about 1 to 3 m^2/g compared with an internal surface area of 700 to 800 m^2/g (33). Weisz and co-workers (99), in their study of molecular-shape-selective reactions, have observed that CaA does not dehydrate sec-butyl alcohol, which is about the same size as sec-butyl acetate, up to 130°C, whereas appreciable conversion was achieved on CaX. At temperatures higher than 190°C, dehydration occurred on CaA, probably on the external surface. The ratio of rate constants of CaX to CaA based on first-order kinetics was approximately equal to the ratio of the total surface area of CaX to the external surface area of CaA. The conversions of sec-butyl acetate at 290°C, extrapolated to zero process time, were about 70, 19, 95, and 48% on NaX, NaA, CaX and CaA respectively. The ratio of first-order rate constants for NaX to NaA and CaX to CaA were approximately 4.6 and 3.5 respectively, whereas the ratio of the total surface of NaX and CaX to the external surface of NaA and CaA were 250-800. Thus the simple relationship found by Weisz does not hold for ester decomposition. Possibly the total area does not participate in the ester decomposition, even on NaX and CaX which have larger apertures than A zeolites.

The conversion on HZ is lower than on HY as shown in Table 4-3; however, it has been reported that HZ has higher activity than HY for the cracking of n-hexane (51), n-butane and n-pentane (10) and the disproportionation of toluene (10). For the decomposition of ethyl acetate, Sanyal and Weller (69) have also observed the lower catalytic activity of HZ than HY. The diffusional limitation in the pores of HZ might be considerably larger because of its one dimensional tubular structure of small diameter, 6.6Å (12). Eberly (21) has observed that the diffusional resistance for the gases, Ar, Kr, and SF_6, which can easily enter the pores, decreases in the order of NaZ > HZ > CaA > Na faujasite > silica-alumina.

The thermodynamic stability of n-butenes increases in the order, 1-butene, cis-2-butene and trans-2-butene (44). For the gas-phase pyrolysis of sec-butyl acetate, the distribution of n-butenes does not follow this order and the ratio of 2-butenes to 1-butene is 0.75 (27). For the decomposition on charcoal n-butenes of similar composition were found (58). On the zeolites and silica-alumina the fraction of 1-butene in total n-butenes was near the amount corresponding to equilibrium for the three isomers, and the fraction of 1-butene did not change very much with increasing conversion of ester as shown in Table 4-4. On NaY, 1-butene was unchanged with temperature, but as the reaction temperature increased, the equilibrium value approached the percentage of 1-butene (Table 4-4).

Trans- and cis-2-butenes deviated from the chemical equilibrium and the compositions were dependent on the catalyst and the temperature. The interpretation of n-butene isomers is complicated because n-butenes are produced at different positions along catalyst bed and the n-butenes may subsequently isomerize. It was notable that, with increasing conversion of ester, the fractions of cis- and trans-2-butene changed whereas 1-butene stayed constant on silica-alumina (170°, 190°C), NaZ, HZ, NaX, CaX, NaY (170°, 190°, 210°C), HY, NiY (170°C), and AgY (140°C) and that the changes of the distribution of n-butenes were often away from the equilibrium composition. Apparently, these eccentric changes should not occur for the isomerization of n-butenes in absence of ester and acetic acid. One interpretation is that the butenes produced changes along catalyst bed, and isomerization of butenes does not occur to a significant extent. Yashima and co-workers have reported the alkylation of toluene with methanol to o-, m- and p-xylene on Y zeolites (102). The distribution of xylene isomers on HY at 225°C changes first toward and then away from the equilibrium composition with increasing contact time.

The present results suggest that subsequent isomerization of olefins does not occur to an appreciable extent, except under very severe conditions when the ester is decomposed completely (Fig. 4-4). The change of n-butene distribution on HZ at 290°C might occur because of the catalyst aging with

the activity for the isomerization decreasing faster than for the decomposition of sec-butyl acetate. By the addition of a small quantity of alkali to alumina, the isomerization capacity was greatly reduced, while the dehydration of n-butyl alcohol was not greatly decreased (62). Changes of butene composition with conversion of ester may result from modification of the surface by acetic acid. During the isomerization of 1-butene on NaX in a continuous flow fixed-bed reactor, a small amount of acetic acid, injected as a pulse by a syringe, increased isomerization. Injection of a larger pulse of acetic acid decreased isomerization.

For the gas-phase pyrolysis of sec-butyl acetate, cis-elimination through a six-center ring intermediate has been proposed (27). The important support for this reaction mechanism is that the ratio of 2-butenes to 1-butene is 0.75, which is close to the ratio, 0.67, predicted based on the β-hydrogens available to form the intermediate. Similar ratios were observed for the decomposition on charcoal (58). On synthetic zeolites and silica-alumina, the ratio of 2-butenes to 1-butene was substantially larger, varying from 3.35 to 21.2. Therefore, the mechanism of decomposition on the synthetic zeolites and silica-alumina seems to be different from the homogeneous reaction and that on charcoal.

The cyclic intermediate may not be necessary for the decomposition of esters on aluminosilicates. The carboxyl oxygen of sec-butyl acetate could remove a hydrogen from a

surface hydroxyl group and the butyl group donate a hydrogen to a surface oxide. The elimination of a β-hydrogen is the easiest route to the olefins; however, the present data are of no diagnostic value in deciding whether β-hydrogens in the methyl or methylene groups or other hydrogens are removed. The reaction favors the production of cis- rather than trans-2-butenes, and the trans- isomer is certainly not the exclusive product of the primary reaction. If the butyl species produced is strongly chemisorbed, it might rearrange on the catalyst surface before desorbing. Thus, the composition of the butenes produced may not have relevance to the mechanism of the primary reaction.

Chapter 5

DECOMPOSITION OF n-BUTYL ACETATE

5.1 Experimental Results

n-Butyl acetate decomposed cleanly to acetic acid and n-butenes on synthetic zeolites, silica-alumina and γ-alumina. The material balances of moles of n-butenes and unconverted n-butyl acetate to n-butyl acetate fed were higher than 99 percent. Traces of methane, carbon dioxide, propylene, n-butane, trans-2-pentene, cis-2-pentene, X1 and X2 were found on some catalysts (Table 5-1). On CaX, HY and silica-alumina, a trace of isobutene was found (Table 5-1). α-Alumina, silica-gel, active charcoal and KA were virtually inactive at 290°C. Except for these inactive catalysts, the activity always decreased with time as shown in Figure 5-1. All of the tests were made at 290°C with one gram of catalyst at a feed rate of 0.0341 gm. mole of ester per hour. Conversions as a function of process time for all catalysts are given in Table 5-2.

The distribution of n-butenes could be correlated with conversion of ester and was independent of aging. Aging patterns of CaX at 290°, 270° and 245°C and of NaX at 290° and 270°C are shown in Figures 7-1 to 7-5, respectively. The selectivities of butenes on CaX and NaX are shown in Figures 5-2 to 5-6. The selectivities on NaA, CaA and silica-alumina

(Fig. 5-7); NaZ and NaY (Fig. 5-8); and HZ and HY (Fig. 5-9) at 290°C are shown as a function of conversion. In Figure 5-10, the selectivity of 1-butene on NaA, CaA, NaZ, HZ, NaY, HY, silica-alumina and γ-alumina are given. The ratios of cis-2-butene to trans-2-butene on these catalysts are shown in Figure 5-11.

A study of isomerization of 1-butene on NaA, CaA, NaX and CaX was performed at 290°C. The conversion of 1-butene and the ratio of cis-2-butene to trans-2-butene in the product on NaX and NaA are shown in Figure 5-12. 1-Butene was fed over 0.5383 gm. of NaX and 0.7813 gm. of NaA at a feed rate of 0.622 gm. mole per hour. The effect of pulse injection of acetic acid on the isomerization activity of NaX and NaA was studied (Fig. 5-12). In the figure, the injections are indicated by the arrows and the amounts of acetic acid injected are given. The conversion of 1-butene and the ratio of cis-2-butene to trans-2-butene on CaX and CaA are shown in Figure 5-13. 1-Butene was fed over 0.0655 gm. CaX and over 0.2512 gm. CaA at a feed rate of 0.736 and 0.622 gm. mole per hour, respectively.

5.2 Discussion

The same by-products, methane, carbon dioxide, X1, X2, trans- and cis-2-pentene, were found for the decomposition of sec-butyl acetate on synthetic zeolites and silica-alumina

(Chapter 4). The carbon dioxide and methane might be produced from the decomposition of acetic acid. Other by-products including methane could form from butenes as indicated in the previous chapter. Skeletal isomerization of n-butenes might occur on strong acid sites of HY, CaX and silica-alumina but not on sodium zeolites which do not have strong acid sites. The small size tubular pores of HZ might be unfavorable for the formation of isobutene and/or the isobutene could produce a polymeric compound inside the pores because of its slow mobility and longer contact time. Thus no isobutene might be found on HZ.

Table 5-2 shows that the conversion at a process time of 15 minutes decreases in the order: silica-alumina > HY > NaY > CaX > HZ > CaA > NaX > NaA > NaZ > γ-alumina. The hydrogen and the calcium zeolites had higher activities than the corresponding sodium form. The same effect of cations was found for the decomposition of sec-butyl acetate. For the decomposition of n- and sec-butyl acetate, the order of activity; HY > NaY > CaX > NaX > NaA, was the same. CaA was more active for n-butyl acetate than for sec-butyl acetate. The minimum diameter of n-butyl acetate is about the same as n-paraffins which can enter the pores of CaA. Therefore, n-butyl acetate might enter the pores of CaA whereas sec-butyl acetate could not. Thus the higher relative activity for the decomposition of n-butyl

acetate than sec-butyl acetate might result. Weisz and co-workers (99) found a similar molecular sieving effect of CaA on the dehydration of n- and sec-butyl alcohol.

The extrapolated conversions of ester on NaX and NaA at zero process time are about 30 and 20% at 290°C, respectively (Fig. 5-1). The ratio of first-order rate constant of the ester decomposition on NaX to NaA is about 1.7. n-Butyl acetate cannot enter the aperture of NaA but it can enter that of NaX. If the ester decomposed on the whole surface area of NaX and on the exterior surface area of NaA crystals, the ratio of rate constant would be similar to the ratio of the total surface area of NaX to the exterior surface area of NaA which is about 250 to 800 (33). However, the present result shows that the molecular-shape-selective reaction does not occur clearly in the decomposition of n-butyl acetate and also in the decomposition of sec-butyl acetate (Chapter 4). Possibly, the total surface area of NaX might not participate in the reaction.

For the isomerization of 1-butene whose critical diameter was about 5.1Å, NaX had appropriate activity, but NaA had very low activity as shown in Figure 5-12. The ratio of first-order rate constants, neglecting reverse reactions, of NaX to NaA was approximately 37. The ratio was smaller than the ratio of interior to exterior surface area of the zeolites which is 250

to 800. One interpretation may be that, at 290°C, n-butenes could enter the pores of NaA to some degree. Breck found that propylene with a diameter of about 5Å could diffuse into NaA at 25°C (12). Another explanation may be that there was diffusional limitation on NaX and the total surface area did not participate in the reaction. Both phenomena might occur at the same time. For the isomerization of 1-butene on CaA and CaX, the ratio of first-order rate coefficient of CaX to CaA was about 7.9. The effective pore size of CaA is about 5Å whereas that of NaA is about 4Å (91). The larger aperture size of CaA may be responsible for the lower ratio of rate constants for the calcium zeolites; 7.9, compared with the sodium zeolites; 37.

The reactivity of n-butyl acetate was lower than sec-butyl acetate. The temperature difference for similar conversion on silica-alumina and HY was about 100°C. For the gas-phase pyrolysis, the reactivity of butyl acetates increases with the increasing number of β-hydrogen: tert-butyl acetate > sec-butyl acetate > n-butyl acetate > isobutyl acetate (72).

Figure 7-1 shows that aging occurred rapidly on CaX at 290°C. The aging was a function of process time and space time. However, the composition of butene isomers falls on a single curve when plotted against conversion of n-butyl acetate and there was apparently no significant effect of aging (Fig. 5-2). The same type of correlation was found on

other catalysts. The isomerization of n-butenes and the decomposition of n-butyl acetate might occur on the same active sites. Dzis'ko and co-workers (20) have reported that the degree of isomerization of 1-butene from dehydration of n-butyl alcohol on aluminas increases with the conversion of alcohol. The composition of butene isomers could be correlated with the conversion of n-butyl alcohol. This correlation was independent of catalytic poisoning by NaOH; apparently the same centers were active in both dehydration of alcohol and isomerization of 1-butene.

There was no large effect of temperature on the distribution of n-butenes up to about 30% conversion of n-butyl acetate. This was found on CaX from 245° to 290°C (Fig. 5-2 to Fig. 5-4) and on NaX from 270° to 290°C (Fig. 5-5 and 5-6). At conversion higher than 30% the isomers approached equilibrium composition. For the decomposition of sec-butyl acetate on aluminosilicates, the composition of butenes produced in the primary decomposition changed with temperature, but the subsequent isomerization did not occur to a significant extent.

Figure 5-10 shows a fraction of 1-butene in the butenes as a function of conversion of n-butyl acetate

on all active catalysts. The relative rate of the consecutive isomerization to the decomposition of n-butyl acetate on γ-alumina and NaX was slower than on CaX, HY, NaY and silica-alumina. The decomposition activity of γ-alumina and NaX was also lower. The relative rates of isomerization on HZ, NaZ, CaA and NaA were faster than on CaX, HY, NaY and silica-alumina, whereas the latter were more active catalysts for the decomposition. The pore size of HZ, NaZ, CaA and NaA might play an important role for the fast relative rates of isomerization. The difference of pore diffusion between n-butenes and n-butyl acetate would be greater on zeolites with smaller pore diameter. Larger molecular size and weight and higher polarity might reduce the diffusivity of n-butyl acetate significantly. Consequently, a larger portion of surface area could participate in the isomerization than in the decomposition of n-butyl acetate and the high relative rate of isomerization might result. For CaX, HY, NaY and silica-alumina, the difference of diffusion between n-butenes and n-butyl acetate should not be as large as for HZ, NaZ, CaA and NaA because of their larger pore diameter.

The ratio of cis- to trans-2-butene decreased very rapidly on NaA, CaA and NaZ (Fig. 5-11). These catalysts have smaller aperture diameters than the others. Sodium ions located on the

wall of a tubular pore of NaZ might reduce the effective pore diameter. Eberly found that diffusional resistance of NaZ was greater than HZ (21). From a Fisher-Hirschfelder-Taylor atom model, the critical diameter of cis-2-butene is about 5.4Å while 1- and trans-2-butene are about 5.1Å. The diffusion of cis-2-butene inside the pore of these zeolites might be slower than 1-butene and trans-2-butene because of its larger critical diameter. The concentration of cis-2-butene in the pore might become high, since cis-2-butene could be produced from 1- and trans-2-butene and diffuse slowly from the pore to gas-phase whereas 1- and trans-2-butene could diffuse faster from the pores. Thus, the low ratio of cis- to trans-2-butene might result. However, on the catalysts with large pores, the difference of diffusion between cis-2-butene and 1- and trans-2-butene should not be large because there was enough aperture space for all n-butenes to diffuse in and out. For the isomerization of 1-butene as shown in Figure 5-12 and 5-13, the ratios of cis-2-butene to trans-2-butene on NaA and CaA are 0.57 and 0.16 compared with about 1.20 and 1.45 on NaX and CaX, respectively.

As seen in Figure 5-2, 2-butenes were found even at very low conversion of n-butyl acetate. If the initial product was 1-butene at primary decomposition, 1-butene would have isomerized very rapidly at low conversion. Suppose n-butyl

acetate decomposed to acetic acid and 1-butene and then 1-butene isomerized to 2-butenes, the reaction scheme will be written as follows.

n-Butyl Acetate $\longrightarrow$ Acetic Acid

$$+ \text{ 1-Butene} \begin{cases} \xrightarrow{k_t,\ r_t} \text{trans-2-Butene} \\ \xrightarrow{k_c,\ r_c} \text{cis-2-Butene} \end{cases}$$

The reverse reactions are neglected for the low concentration of 2-butenes. k, k_t and k_c are reaction rate constants for the steps. r, r_t and r_c are reaction rates for the steps. Assuming the first-order rate expression, the reaction rates of decomposition and isomerization at low conversion may be:

$$r = kP_e \fallingdotseq k \tag{5-1}$$

$$r_t = k_t P_b \fallingdotseq k_t ZX \tag{5-2}$$

$$r_c = k_c P_b \fallingdotseq k_c ZX \tag{5-3}$$

P_e and P_b are partial pressures of ester and 1-butene. X is a conversion of n-butyl acetate

and Z is a fraction of 1-butene in total butenes. The differential rates for the decomposition and the isomerization of 1-butene are:

$$\frac{dX}{d\ W/F} = r \qquad (5\text{-}4)$$

$$\frac{dXZ}{d\ W/F} = r - r_t - r_c \qquad (5\text{-}5)$$

From equations (5-1) to (5-5), one can obtain

$$\frac{dZ}{dX} = \frac{1 - Z}{X} - \alpha Z \qquad (5\text{-}6)$$

Where α is the ratio of rate constants for isomerization to decomposition, $\frac{k_t + k_c}{k}$. Integrating equation (5-6), the fraction of 1-butene is

$$Z = \frac{1 - e^{-\alpha X}}{\alpha X} \qquad (5\text{-}7)$$

The ratios, α, on CaX and NaX at 290°C were calculated from equation (5-7) using data shown in Figures 5-2 and 5-5.

Catalyst	X	Z	α
NaX	1.0%	0.860	31
CaX	0.5	0.657	182

The conversions of n-butyl acetate at process time zero on CaX and NaX were obtained from Figures 7-1 and 7-4. Applying first-order kinetics, the rate coefficients on NaX and CaX at 290°C were 8.48×10^{-3} and 3.95×10^{-2} (gm. mole ester decomposed/hr. gm. catalyst/atm.). For the isomerization of 1-butene on NaX and CaX at 290°C, the conversions at process time zero were about 12 and 45% (Fig. 5-12 and 5-13). The first order rate coefficients were 0.191 and 6.70 (gm. mole butene converted/hr. gm. catalyst/atm.) on NaX and CaX respectively. Therefore, the ratios, α , are about 23 on NaX and 170 on CaX at 290°C. These are close to the values calculated from equation (5-7). This result supports the postulate that the consecutive isomerization of 1-butene occurs very rapidly at low conversion as shown in Figures 5-2 and 5-5 and that 1-butene was the principal product at primary decomposition. For dehydration of n-butyl alcohol, the initial product was 1-butene (20, 62). As considered in the previous chapter, if carboxyl oxygen accepts a hydrogen from the surface of a catalyst and the butyl group donates a β -hydrogen to the surface, the easiest olefin to form from n-butyl acetate will be 1-butene. However, other mechanisms are possible. Pine and Manassen (61) suggested that γ -hydrogen might be eliminated from n-butanol producing 2-butenes. On the strong acid sites, the butyl species produced in the primary decomposition

of n-butyl acetate might rearrange before desorption.

On NaX, acetic acid might react with sodium cations located in the supercage forming sodium acetate and generating acid hydrogen on the surface. This may explain the increased catalytic activity for the isomerization of 1-butene by pulse injection of acetic acid as shown in Figure 5-12. The catalytic activity of NaA was also increased slightly by acetic acid (Fig. 5-12). By injecting acetic acid the ratio of cis-2-butene to trans-2-butene on NaX did not change significantly, whereas the ratio decreased on NaA. Acetic acid might react with sodium cation near the aperture of NaA generating acid hydrogen and enlarging the aperture diameter. Then, a larger portion of interior surface could participate in the reaction, resulting in the lower ratio of cis-2-butene to trans-2-butene as described above.

Chapter 6

KINETICS

6.1. Experimental Results

No significant aging of NaY was found during the decomposition of sec-butyl acetate up to 210°C. A kinetic study was carried out using three feed compositions at atmospheric pressure and temperatures from 170° to 210°C. The feed compositions were pure, 81.87 mole % and 17.50 mole % ester diluted with acetic acid. The results are given in APPENDIX 3. The conversions of ester at 210°C obtained for 17.50 mole % ester feed are plotted versus space time in Figure 6-1. Figure 6-2 shows the conversions of ester at 170°, 190° and 210°C obtained for the pure and 81.87 mole % ester feed.

The decomposition of sec-butyl acetate over HY, NiY, AgY and silica-alumina was studied using pure ester feed at 140° and 170°C and at atmospheric pressure. Moderate aging of HY, NiY and silica-alumina occurred (Fig. 6-3 to 6-8). The conversions of ester on these catalysts were extrapolated to zero process time. The extrapolated conversions are plotted as a function of space time in Figures 6-11 (140°C) and 6-12 (170°C). The activity of AgY increased or remained constant with

process time (Fig. 6-9 and 6-10). The conversions at process time 200 minutes are plotted in Figures 6-11 and 6-12.

The curves in Figures 6-2, 6-11 and 6-12 were obtained by integrating the rate equation (d) in Table 6-1 using the kinetic constants given in Table 6-2. The integration was performed by a fourth order Runge-Kutta method.

6.2. Analysis of Data

The various Langmuir-Hinshelwood rate equations were converted into linear forms. For instance, if irreversible surface reaction controls the rate and an adsorbed ester reacts with an adjacent vacant site, the rate expression (79) is given by equation (6-1). Where k is the surface

$$r = \frac{kEP_e}{(1 + EP_e + BP_b + AP_a)^2} \qquad (6\text{-}1)$$

reaction constant and E, B and A are the adsorption constants of ester, butenes and acetic acid, respectively. P_e, P_b and P_a are the partial pressures of ester, butenes and acetic acid, respectively. If the concentration of empty sites and butenes adsorbed on the sites are very small, the equation can be approximated by equation (6-2).

$$r = \frac{k/E\ P_e}{(P_e + (A/E)P_a)^2} \qquad (6\text{-}2)$$

In equation (6-2), the constant, k/E, is equal to the initial rate for pure ester feed. Thus, the linear form of equation (6-2) is expressed by equation (6-3).

$$\sqrt{\frac{r_o P_e}{r}} = P_e + (A/E)P_a \qquad (6\text{-}3)$$

The decomposition of ester is stoichiometric and the partial pressures of ester and acetic acid are calculated from conversion, total pressure ($\fallingdotseq$ 1 atm.) and the concentration of ester in feed as follows:

$$P_e = \frac{y\,(1 - X)}{1 + yX} \qquad (6\text{-}4)$$

$$P_a = \frac{1 - y + yX}{1 + yX} \qquad (6\text{-}5)$$

(y: mole fraction of ester in feed.)

The smoothed curves for conversion as a function of space time were drawn and the rates were calculated by numerical differentiation (35). The rates were smoothed and then integrated to obtain new conversions by Simpson's rule. The new conversions were compared to the initial conversion curves and this procedure was repeated until the standard deviation of the initial conversions from the new conversions calculated by

Simpson's rule became less than 0.5%. Three or four trials were required to obtain the adequate curves of rates and conversions. The rates obtained at the first trial are shown in Figures 6-13 to 6-15.

The final conversions and rates corresponding to the equally spaced space time were used for the linear regression of equation (6-3). The increment of space time was 5 gm. catalyst/gm. mole ester feed/hr.

Various rate equations were examined for the experimental results shown in Figure 6-2. For example, equation (6-6) is obtained from equation (6-1) if the concentration of butenes adsorbed on active sites is negligible. The linear-form of equation (6-6) is given by equation (6-7).

$$r = \frac{kFP_e}{(1 + FP_e + AP_a)^2} \qquad (6\text{-}6)$$

$$\sqrt{\frac{P_e}{r}} = \frac{1}{\sqrt{kF}} + \frac{\sqrt{F}}{\sqrt{k}}P_e + \frac{A}{\sqrt{kF}}P_a \qquad (6\text{-}7)$$

All kinetic constants, k, F, A, can be evaluated separately if two different compositions of ester, prepared by being diluted with acetic acid, are used. However, in equation (6-7), if the first term on the right hand

side is very small compared with the other two terms (the concentration of empty sites is very small) and the error on the left hand side is not very small compared with the first term on the right hand side, the evaluation of kinetic constants is seldom successful even if the mechanism is correct. In this study, negative kinetic constants were obtained when equation (6-7) was examined.

Four rate equations shown in Table 6-1 remained after eliminating inadequate rates which gave negative constants or large standard deviations. The standard deviation was calculated based on experimental conversions by equation (6-8).

$$s = \sqrt{\sum_{i=1}^{N} \left\{ X_i - \int_0^{(W/F)_i} r \, d(W/F) \right\}^2 / N} \qquad (6\text{-}8)$$

The kinetic constants and the standard deviations for the four equations are given in Table 6-1. As seen in Table 6-1, the differences of standard deviations are too small to discriminate between the rate equations. Apparently, the reaction conditions were not diagnostic. However, the difference of these rates is increased if the ester is diluted by acetic acid to a large extent.

The curves 1, 2, 3 and 4 shown in Figure 6-1 were the predicted conversion curves for 17.50 mole % ester feed corresponding to the rate equations (a), (b), (c) and (d) in Table 6-1, respectively. The curves were obtained by integrating the rates using kinetic constants given in Table 6-1. The integration was performed by a fourth order Runge-Kutta method.

Figure 6-1 shows that the best expression is rate equation (d).

Assuming the Arrhenius relation for the rate constants, apparent activation energy of ester decomposition and the difference of heat of adsorption between acetic acid and ester are calculated according to equation (6-9) and (6-10).

$$\ln k/E = C + \frac{-(\mathcal{E} + Q_e)}{RT} \qquad (6\text{-}9)$$

$$\ln A/E = C' + \frac{Q_a - Q_e}{RT} \qquad (6\text{-}10)$$

Where C and C' are constants, $\mathcal{E}$ is the activation energy, and Q_e and Q_a are the heats of adsorption of ester and acetic acid, respectively. Figure 6-16 shows Arrhenius plots of rate constants for the decomposition of ester on NaY. The apparent activation energy, $\mathcal{E} + Q_e$, was 28.0 $\pm$ 4.13 Kcal/mole and the difference of the heats of adsorption of acetic acid and ester was 5.4 $\pm$ 2.07 Kcal/mole at the confidence limit of 95%.

For the reactions on HY, NiY, AgY and silica-alumina, the rate equation (d) was applied to the conversion-space time data shown in Figures 6-11 and 6-12. The initial rates were obtained from the conversion-space time curves. The ratios of adsorption constant, A/E, were obtained by a nonlinear regression method. Equation (6-8) was used as an object function for the regression and the value of A/E which minimized the standard deviation was obtained. The kinetic constants, standard deviations, apparent activation energies and the differences of heat of adsorption are listed in Table 6-2.

The computations in this chapter were made by a CDC 6400 computer.

6.3. Discussion

If the reaction rate is limited by mass transport process between catalyst particles, the reaction rate increases with increasing linear velocity of feed. The effect of pore diffusion on the reaction rate is a function of the particle size of the catalyst and decreases with the decrease of particle size (41). For the decomposition of sec-butyl acetate on NaY of two different particle sizes, 30 to 35, and 70 to 80 mesh, showed no significant difference (APPENDIX 3). The feed rates of

reactant were changed 10 times and there was no significant influence on the reaction rates (APPENDIX 3). Therefore, it is considered that the effects of mass transport process between particles and in macro-pores of catalysts on the reaction rate are not important. However, the effect of intracrystalline pore diffusion on the reaction rate is not known.

The best rate equation found for the reaction on NaY suggests that the decomposition of ester occurs on dual-sites, the retarding effect of acetic acid and ester is large and the concentration of empty sites and the coverage of sites by butenes are negligible. Sashihara and Syverson (70), in their study of the decomposition of n-hexyl acetate on a boric oxide-bauxite catalyst at 305°C, found that the inhibiting effect of acetic acid was great and of n-hexene small. The adsorption equilibrium constants of acetic acid, n-hexyl acetate and n-hexene in their semi-empirical rate equation based on dual-site surface reaction were 5.01, 0.501 and 0.0521 $atm.^{-1}$, respectively. For the decomposition of ester on zeolites, the strong inhibition of acetic acid and ester might be expected since the affinities between zeolite surface and polar compounds such as acetic acid and ester are very high (89) and the active sites are covered almost completely with these two

compounds. Dimitrov and Leach (36) found that the isomerization of n-butenes on NaX and CuX at 305° and 105°C followed first-order kinetics, and apparently, no retarding effect of n-butenes occurred. Their results may confirm that the coverage of butenes is negligible on the zeolites. For the decomposition of sec-butyl acetate on charcoal, Pettit and Anderson (58) found that ester was the principal adsorbate and the retarding effects of acetic acid and butenes were negligible. The surface of charcoal is greatly different from that of aluminosilicates; it has neither ionic nor polar character. Therefore, the surface may not have high affinities for functional groups such as carbonyl and hydroxyl groups as the zeolite surface has.

Figures 6-9 and 6-10 show that activity of AgY increases at higher space time suggesting that some product effects the process of activation. The pulse injection of acetic acid and water during the reaction did not influence the activity. Possibly, traces of hydrogen which may be produced in dehydrogenation or cracking of hydrocarbon reduce silver ions with the formation of Brönsted acid sites.

Kinetic constants are greatly dependent on catalysts (Table 6-2). The increasing order of k/F is NaY < silica-

alumina < AgY < HY < NiY. The metallic ion on the surface may participate in the adsorption of acetic acid and ester. An electrostatic (ionic) interaction between cation and acetyl group of acetic acid and ester can be expected. However, the acetyl group of acetic acid may have much stronger interaction than that of ester because of its stronger ionic property. The electrostatic force increases with the charge density of cations. The ionic radii of Ag^{+}, Na^{+} and Ni^{++} are 1.25, 0.95 and 0.75 Å, respectively. Therefore, the increasing order of the charge density of cations is $Ag^{+} < Na^{+} < Ni^{++}$. This order corresponds to the increasing order of A/E as shown in Table 3. The low value of A/E on silica-alumina compared with zeolites may be due to the absence of cations on the surface. Except for NaY, k/E increases with the increase of A/E (Fig. 6-17). Possibly, the catalyst on which the stronger adsorption of acetic acid occurs is more active for the decomposition of ester and the cation can act as active site or has direct relation with active site. The apparent activation energies vary from 10.3 to 28.0 Kcal/ mole (Table 6-2). Active sites of different nature may be involved. One of the possible direct relations between the cation and the active site may be that a cation reacts with acetic acid and the

protonic acid site is produced. This process may be enhanced if the charge density of cation is high and if the cation is in low coordination with structural oxygen ion. The reaction of acetic acid and nickel ion may be visualized as follows.

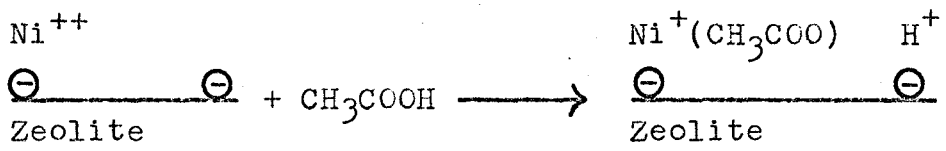

A similar reaction may occur on NaY and results in the increase of activity as seen in Figure 5-15. However, sodium ion is highly coordinated with structural oxygen ion and the dissociation of acidic hydrogen from the acetyl group may not occur as easily as on NiY.

The activation energy cannot be separated from the heat of adsorption and the apparent activation energies in Table 6-2 are larger than the actual activation energies by the heat of adsorption of ester as shown by equation (6-9). However, these values are still smaller than 47.2 Kcal/mole for the gas-phase reaction (72) and 32.7 Kcal/mole on charcoal (58).

In the previous chapters, it was suggested that the carboxyl group of the ester could accept a hydrogen from the surface hydroxyl group and that the butyl group could

donate a hydrogen to the surface oxide. The present kinetic model does not contradict this mechanism. Possibly, the ester may adsorb on a protonic acid site through a hydrogen bond with a carbonyl oxygen. The ester may also adsorb on some cation. The acidic hydrogen of the adjacent vacant site may be accepted by another carboxyl oxygen, the butyl group of ester may donate a hydrogen to the same site and the ester decomposes to acetic acid and butene as visualized below.

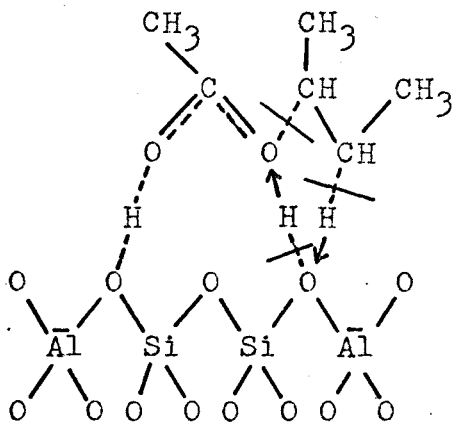

Chapter 7

AGING OF CATALYSTS

7.1. Treatment of Data

For the correlation of conversions of n-butyl acetate on NaX and CaX with process time, an empirical aging equation (7-1) was converted into a linear-form given by equation (7-2) and then the constants were calculated by linear regression for the assumed value of C_2. From the plot of standard deviation as a function of C_2, the optimum constants which made the standard deviation of experimental from calculated conversions minimum were determined.

$$X = C_1 e^{-pt} + C_2 \qquad (7\text{-}1)$$

$$\ln(X - C_2) = \ln C_1 - pt \qquad (7\text{-}2)$$

Where p is the first-order aging rate constant, t is the process time, and C_1 and C_2 are constants.

For the decomposition of n-butyl acetate on NaX and CaX, the first-order rate equation, $r = kP_e = k\,\frac{1 - X}{1 + X}$, was applied to the conversions of ester extrapolated to zero process time. The first-order rate constant, k,

was obtained by nonlinear regression. The object function for the regression was defined by equation (7-3) and (7-4).

$$s = \sqrt{\sum_{i=1}^{N} \{X_i - Y_i\}^2 / N} \qquad (7\text{-}3)$$

$$Y_i = k \int_{o}^{(W/F)_i} \frac{1 - Y}{1 + Y} \, d\,(W/F) \qquad (7\text{-}4)$$

Where X_i is an experimental conversion, Y_i is the calculated conversion and $(W/F)_i$ is the space time. The conversions are expressed in mole fractions. The integration of equation (7-4) was performed using a fourth order Runge-Kutta method and the best value of rate constant k that made the object function minimum was determined.

Generally, the differential reaction rate is a function of process time and space time and is expressed by $r((W/F)_i, t_j)$. If the concentration term is separable, the rate can be expressed by equation (7-5),

$$r((W/F)_i, t_j) = f((W/F)_i, t_j) \cdot g(X_{ij}), \qquad (7\text{-}5)$$

where, $f((W/F)_i, t_j)$ is a local relative activity at $(W/F)_i$ and t_j and is 1.0 at zero process time. Therefore, the rate at zero process time is given by equation (7-6).

$$r((W/F)_k, 0) = g(X_{kl}) \qquad (7\text{-}6)$$

From equations (7-5) and (7-6), if X_{ij} is equal to X_{kl}, the local relative activity at $(W/F)_i$ and t_j is given by equation (7-7).

$$f((W/F)_i, t_j) = r((W/F)_i, t_j) / r((W/F)_k, 0) \qquad (7\text{-}7)$$

The rate at $(W/F)_i$ and at t_j can be obtained from the conversion-space time curve as shown in Figures 7-7 and 7-8 by numerical differentiation (35).

7.2. Experimental Results

The decomposition of n-butyl acetate was carried out on CaX at 290°, 270° and 245°C and on NaX at 290° and 270°C. The reaction was performed at atmospheric pressure using pure ester feed. The conversions of ester first decreased rapidly, then became constant with increasing process time. Aging was also a function of space time and was faster at higher space time. The aging patterns are shown in Figures 7-1 to 7-5. The conversions were correlated satisfactorily with aging equation (7-1). The optimum constants and the standard deviations of

experimental from calculated conversions are given in Table 7-1. The curves in Figures 7-1 to 7-5 were calculated by equation (7-1) using the optimum constants. The first-order rate equation for ester decomposition was applied to the conversions at zero process time which were calculated by equation (7-1). Table 7-2 shows the rate constants and the standard deviations obtained by equations (7-3) and (7-4). The Arrhenius plots of rate constants are shown in Figure 7-6. The apparent activation energies were about 30 Kcal/mole for the ester decomposition on both CaX and NaX. For the decomposition of n-butyl acetate on CaX and NaX at 290°C, the conversions calculated by aging equation (7-1) are shown as a function of space time in Figures 7-7 and 7-8. The local relative activities were calculated based on the conversion curves shown in Figures 7-7 and 7-8. The local relative activities are shown as a function of space time in Figures 7-9 and 7-10.

The decomposition of n-butyl acetate was conducted on acetic acid-treated NaX, Ac-NaX. The catalytic activity was compared with that of fresh NaX. Figure 7-11 shows that the conversions obtained over 3.4944 gm. Ac-NaX at a feed rate of 3.41×10^{-2} gm. mole ester feed/hr. are almost the same as on 1.4126 gm. of fresh NaX at the same feed rate.

Table 7-3 shows the X-ray diffraction analysis of used catalysts.

The activities of fresh and regenerated catalysts dried at 270°C in air were compared for the decomposition of n-butyl acetate at 290°C (Fig. 7-12). The catalysts were silica-alumina, HY, CaX and NaA. Silica-alumina and HY could be regenerated by burning the deposit with air, but CaX was only partly regenerated. The activity of NaA was partly recovered by purging with helium. The purge with helium did not effect the activity of silica-alumina and NiHY used for the decomposition of sec-butyl acetate (Fig. 7-13), but the activity could be regenerated by burning the deposit with air.

The activity change of NaX was compared with that of NaY for the decomposition of sec-butyl acetate at 210°C (Fig. 7-13). The activity of NaX decreased with process time, but NaY did not.

The color of HZ, HY and silica-alumina was black after being used for the decomposition of n-butyl acetate at 290°C, whereas the color of NaZ, NaY, NaX, CaX, NaA and CaA was light brown.

The nitrogen adsorption isotherms at -195°C for the catalysts used in the reaction are shown in Figures 7-14 and 7-15. The catalysts were NaY, HY, NaX, CaA, HZ-1,

HZ-2, NaZ and silica-alumina. The isotherms were measured before and after burning the deposit. HZ-1 was used for the decomposition of sec-butyl acetate at 290°C on one gram catalyst at feed rate 0.0338 gm. mole/hr. All other catalysts were used for the decomposition of n-butyl acetate at 290°C on one gram catalyst at feed rate 0.0341 gm. mole/hr. The reaction periods for the catalysts are given in the last column of Table 7-4. The volume of pores smaller than 100 Å was estimated from the adsorption isotherms by assuming that the adsorbate has the density of normal liquid nitrogen, 0.8081 gm./cc. For zeolites with isotherms that flatten at low relative pressures, the pore volumes were estimated from amount adsorbed at a relative pressure of 0.2 except for NaZ where 0.086 was used. For silica-alumina, pore volume was estimated at a relative pressure of 1.0. The amount of nitrogen adsorbed on the used catalysts and on the regenerated catalysts, expressed in cc. (S.T.P.) per one gram of regenerated catalyst (after burning the deposit), are given in the second and third column of Table 7-4, respectively. The difference of pore volumes between the used and the regenerated catalysts, V_1, which was calculated using a liquid nitrogen density of 0.8081, is given in the fourth column of Table 7-4. In the

fifth column, the percentages of the blocked pore volume to the pore volume of regenerated catalyst are given. The weights of deposit on one gram of regenerated catalyst are given in the sixth column. The volume of the deposit, V_c, was calculated assuming that the deposit was carbon having the density of 1.8.

7.3. Discussion

If aging of the catalyst occurs rapidly, it is extremely difficult to obtain accurate conversions extrapolated to zero process time. Therefore, the application of a complicated rate equation to these extrapolated conversions is not so significant. In this study, the simple first-order rate equation, which was the best among half-, first- and second-order rate equations, was applied to the conversions of n-butyl acetate on NaX and CaX at zero process time which were calculated by aging equation (7-1).

In equation (7-1), p is a first-order aging rate constant. The values of p in Table 7-1 show that the aging rate of NaX is faster than that of CaX and that the aging rate increased with increase of temperature. The reaction rate of ester decomposition on CaX is faster than on NaX and the activity of CaX at 290°C in terms

of the first-order rate constant is about 4.7 times that of NaX (Table 7-2). Therefore, the aging rate does not parallel the catalytic activity for ester decomposition. The effect of temperature on the aging rate was not as large as on the rate of ester decomposition. On CaX, the aging rate at 290°C is about 1.7-fold greater than at 245°C, whereas the reaction rate is about 9.6-fold greater. On NaX, the aging rate at 290°C is about 1.3-fold greater than at 270°C, whereas the reaction is about 2.9-fold greater.

Assuming the Arrhenius relation for the aging rate constants, the apparent activation energy is about 8 Kcal/mole for CaX and about 15 Kcal/mole for NaX. These activation energies are smaller than those for the decomposition of ester. The apparent activation energy for the decomposition of n-butyl acetate is about 30 Kcal/mole on both NaX and CaX (Fig. 7-6). This may suggest that NaX and CaX have the same active site. The acidic hydrogens may form on NaX and CaX as discussed in Chapter 6. Another possibility is that NaX contains traces of calcium cation as an impurity and the same active site as CaX may be produced on NaX. These calcium ions normally found in the commercial Linde Na zeolites markedly increases the catalytic activity of NaY (42).

The plots of conversion of n-butyl acetate as a function of space time show that the rates at small values of W/F are not effected much by the aging. But, at high W/F, the effect of aging is large and the conversion curves become horizontal lines as the aging proceeds (Fig. 7-7 and 7-8). In the present study, the space time is proportional to the bed length of the catalyst since the ester feed rate was constant. Therefore, these data indicate that the exit end of the catalyst bed ages more extensively. The plots of the local relative activity demonstrates this more clearly (Fig. 7-12 and 7-13). Probably, reaction products cause the aging of X zeolites, since, if the reactant or an impurity in the feed causes the aging, the deactivation of catalysts should occur most extensively at the inlet of catalyst bed. The moderate aging of NaX occurred during the isomerization of 1-butene at 290°C as seen in Figure 5-12. However, the aging was apparently different from the rapid aging which occurred during the decomposition of esters. In the isomerization of 1-butene, for a large pulse injection of acetic acid the activity of NaX decreased and then recovered slowly. The aging of CaX and NaX is probably caused by acetic acid. The aging of X zeolites may be caused partly by

the collapse of the crystal structure. The acetic acid-treated NaX, Ac-NaX, had an activity of about 1/4 of that of the fresh catalyst (Fig. 7-11). The X-ray analysis of Ac-NaX after being used for reaction shows that crystallinity is lost to a great extent (Table 7-3). However, the initial rapid aging of X zeolites as shown in Figures 7-1 to 7-5 is not due to the crystal collapse since the rapid aging occurs even after acid treatment, as demonstrated by the reaction on Ac-NaX (Fig. 7-11). Furthermore, the catalytic activity of regenerated CaX was not much lower than that of fresh CaX (Fig. 7-12). This suggests that the aging caused by crystal collapse is not large compared with the aging caused by other factors. The information described above suggests that the rapid aging of X zeolites is caused by strong adsorption of acetic acid. On the surface of NaX, for example, a sodium ion may attract an acetyl group through an ionic interaction, and the acidic hydrogen of acetic acid may form a hydrogen bond with an oxygen ion of negatively charged aluminum-oxygen tetrahedra as visualized below. The distance between lattice oxygen ions of X zeolites is about 2.7 Å (14), and between oxygens of the acetyl group is also about 2.7 Å. Therefore, the adsorption on dual sites can occur without constraint. However, the average distance

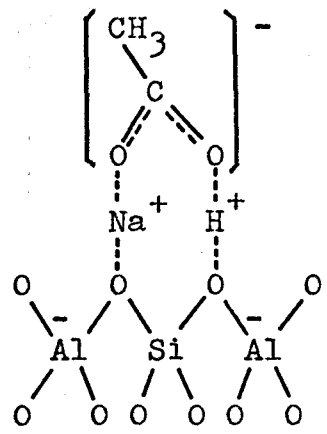

between neighboring aluminum-oxygen tetrahedra of Y zeolites is twice as long as that of X zeolites since the Si/Al ratio is about 1.2 for X zeolites (12) and about 2.5 for Y zeolites (Table 3-1). This may inhibit the strong adsorption of acetic acid on the dual sites of Y zeolites. Consequently, the aging of NaY does not occur (Fig. 7-13). The strong adsorption of acetic acid may also occur on A zeolites since the Si/Al ratio is about 1.0 (12), but not on mordenites of which Si/Al ratio is about 5.8 (Table 3-1).

The acid resistance of zeolites increases with the increase of Si/Al ratio (53). In this study, the degree of crystal collapse decreased in the order: type X> type Y> type Z (Table 7-3), corresponding to the increasing order of Si/Al ratio.

As shown in Figure 7-12, the catalytic activity of

CaX could be partly regenerated by burning the deposit, whereas the catalytic activity of silica-alumina and HY was regenerated completely. NaA could be regenerated partly by passing helium at 290°C overnight (Fig. 7-12). Loss of crystallinity may have prevented complete regeneration of X and A zeolites. The present results suggest that the substance causing the aging of silica-alumina and NiHY is nonvolatile while the substance (probably acetic acid) causing the aging of A and X was, to a certain degree, volatile enough to be removed by purging with helium.

The decrease of pore volumes of catalysts by deposit may be an important factor in interpreting the aging of some catalysts. The process of blocking of pores may be dependent on catalysts. If blocking of pores is caused by the deposit at pore mouths and empty space remains inside the pores, the ratio of volume of carbonaceous deposit, V_c, to the increase in pore volume, V_l, becomes small. The ratio increases and approaches unity as the deposit increases inside the pore. The ratio also increases if the deposition proceeds on the exterior surface of the catalyst. On CaA, NaZ and HZ-2, the ratios of V_c to V_l are low (Table 7-4) and the pores are blocked almost completely (Fig. 7-14 and 7-15)

indicating that on these catalysts the deposition occurs at pore mouths leaving an empty space inside the pores. The ratio of V_c to V_l are higher and closer to unity on NaY and silica-alumina (Table 7-4). The pore volume blocked is smaller compared with other catalysts (Table 7-4, Fig. 7-14 and 7-15), indicating that the deposition proceeded inside the pore without leaving much empty space blocked inside the pores. The behavior of HY and NaX is between the above two groups. During the reaction on HZ-1, the conversion of sec-butyl acetate was 100%. This severe reaction condition possibly caused more deposition on the exterior surface and might result in higher ratio of V_c to V_l on HZ-1 compared with on HZ-2.

The present results show that the blocking of pores easily occurs on zeolites with small apertures. The narrow tubular pore structure of mordenites possibly enhances the rapid blocking. The fast aging of NaZ and HZ during the decomposition of n- and sec-butyl acetate may be due to the blocking of pores. The moderate aging of NaY and silica-alumina during the decomposition of n-butyl acetate at 290 ^{o}C may be the reflection of moderate blocking of their pores.

In contrast to the stable activity of NaY, other Y

zeolites (HY, NiHY and NiY), HZ and silica-alumina showed aging during the decomposition of sec-butyl acetate at 140° to 190°C (Fig. 4-1 and Fig. 6-3 to 6-10). Shephard and co-workers (74) found that propylene polymerized on silica-alumina at 58° to 200°C and the catalyst was poisoned by sodium ions. They proposed that the polymerization occurred on the Brönsted acid sites, but not on the Lewis acid sites. Possibly, on silica-alumina, HY, NiHY, NiY and HZ, polymeric organic material forms from butenes and extensive carbonization of the polymeric material occurs at high temperature.

During the isomerization of 1-butene at 290°C, rapid aging of CaX and moderate aging of CaA were found (Fig. 5-13). The color of CaX turned to black whereas CaA became a yellowish brown. One interpretation of this difference between CaX and CaA may be that polymeric materials do not form extensively in a narrow pore system of CaA.

Chapter 8

CONCLUSIONS

8.1. Reactions

n-Butyl acetate and sec-butyl acetate decompose cleanly to acetic acid and n-butenes on synthetic zeolites and silica-alumina. The principal product from n-butyl acetate is 1-butene and consecutive isomerization of butenes occurs with stereoselective formation of cis-2-butene. 1-Butene, trans-2-butene and cis-2-butene are produced in the primary decomposition of sec-butyl acetate. The 1-butene produced is close to the amount for equilibrium between n-butenes, but trans- and cis-2-butene are not. The thermodynamically less stable cis-2-butene is kinetically favored. The composition of n-butenes produced from sec-butyl acetate is dependent on catalyst and temperature and consecutive isomerization of n-butenes does not occur appreciably except under a very severe condition. sec-Butyl acetate is more reactive than n-butyl acetate for the catalytic decomposition.

8.2. Catalytic Activity

Aluminosilicates with strongly acidic surfaces have higher catalytic activity. Zeolites containing bivalent cations have stronger active sites than those with univalent cations. Acetic

acid modifies the surface of some zeolites and the catalytic activity changes. The catalytic activities of synthetic zeolites for the ester decomposition are affected by aperture size, but the effects are much less than those in the molecular-shape-selective reactions reported by Weisz and co-workers (99). The selectivity for butenes is affected by aperture size of zeolite catalysts and the diffusional consideration gives satisfactory interpretation. The super activity of zeolites compared with silica-alumina, which was found by Weisz and co-workers (100), does not appear for the decomposition of n- and sec-butyl acetate.

8.3. Reaction Kinetics

The decomposition rates of n- and sec-butyl acetates on synthetic zeolites and silica-alumina exceed greatly those in the gas-phase decomposition. For the decomposition of sec-butyl acetate on silica-alumina and Y zeolites, the Langmuir-Hinshelwood rate equation, $r = \frac{k/E\ P_e}{(P_e + (A/E)P_a)^2}$, correlates experimental data satisfactorily. The equation corresponds to the rate controlled by the surface reaction on a dual-site. The affinity of acetic acid and ester for the surface of aluminosilicates is large and active sites are covered almost completely by these two components. The concentration of butenes adsorbed on active sites is negligible. The effect of

cations on the kinetic constants, k/E and A/E, is large. The activation energy is lower than that for pyrolysis.

8.4. Reaction Mechanism

The decomposition of n- and sec-butyl acetate on synthetic zeolites and silica-alumina is different from pyrolysis, and the cyclic intermediate may not be necessary for the catalytic decomposition.

8.5. Aging of Catalysts

The aging of zeolite catalysts is caused by strong adsorption of acetic acid on the surface, collapse of crystal structure and the blocking of pores by deposition of solid organic material. The Si/Al ratio effects the strong adsorption of acetic acid on the zeolite surface. The loss of crystallinity is caused by acetic acid and occurs more easily if the Si/Al ratio is low. The blocking of pores takes place more easily on catalysts with small pore size. The aging by the deposit of polymeric material does not occur in zeolites with sodium and silver cations.

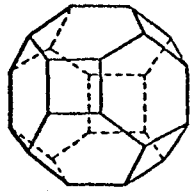

(a)

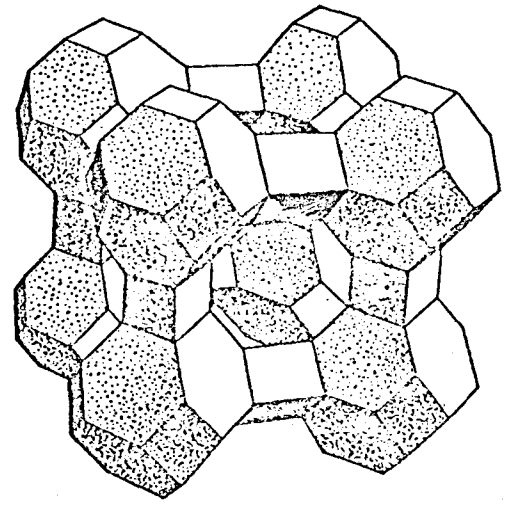

(b)

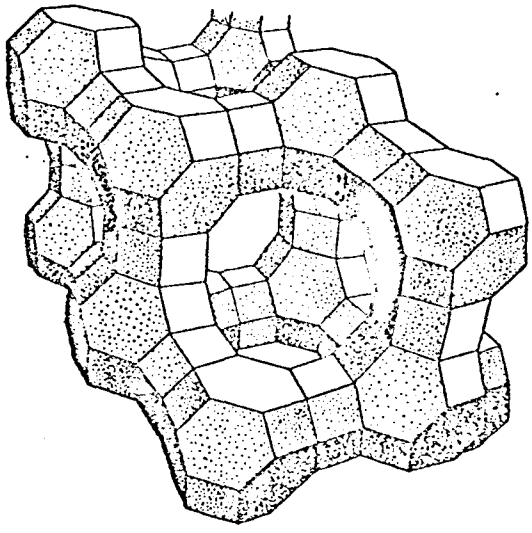

(c)

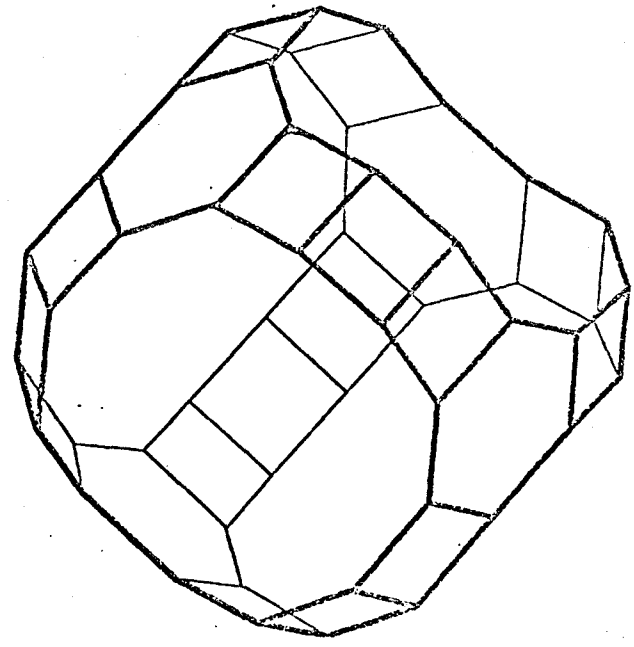

(d)

Fig. 2-1 Crystal structures of A and X zeolites. (a) Truncated octahedron (sodalite unit); vertices represent Si or Al atoms. (b) Line drawing of A zeolite structure. (c) Line drawing of X zeolite structure. (d) Line drawing of supercage of X zeolite. (83, 89)

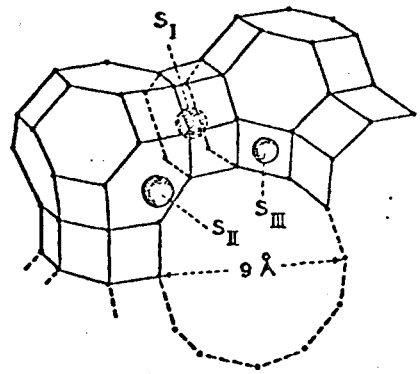

Fig. 2-2 Positions of cations in X and Y zeolites (89).

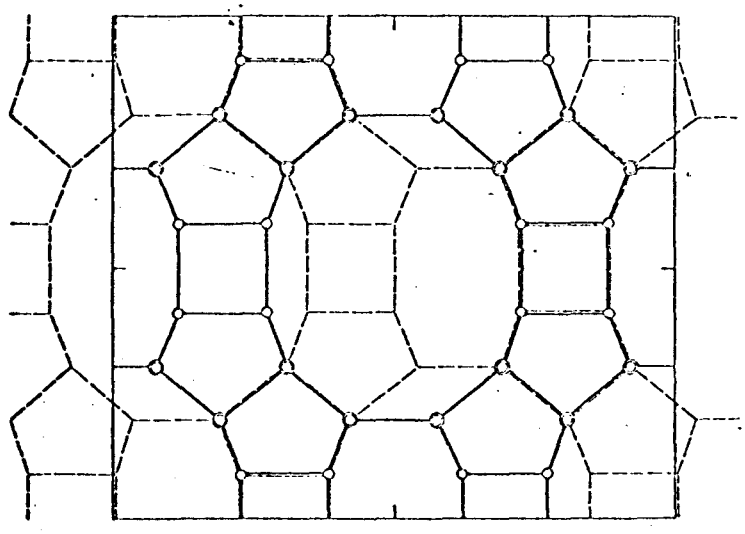

Fig. 2-3 Line drawing of mordenite structure. The displaced region of the structure (stacking fault) is outlined by broken lines (49).

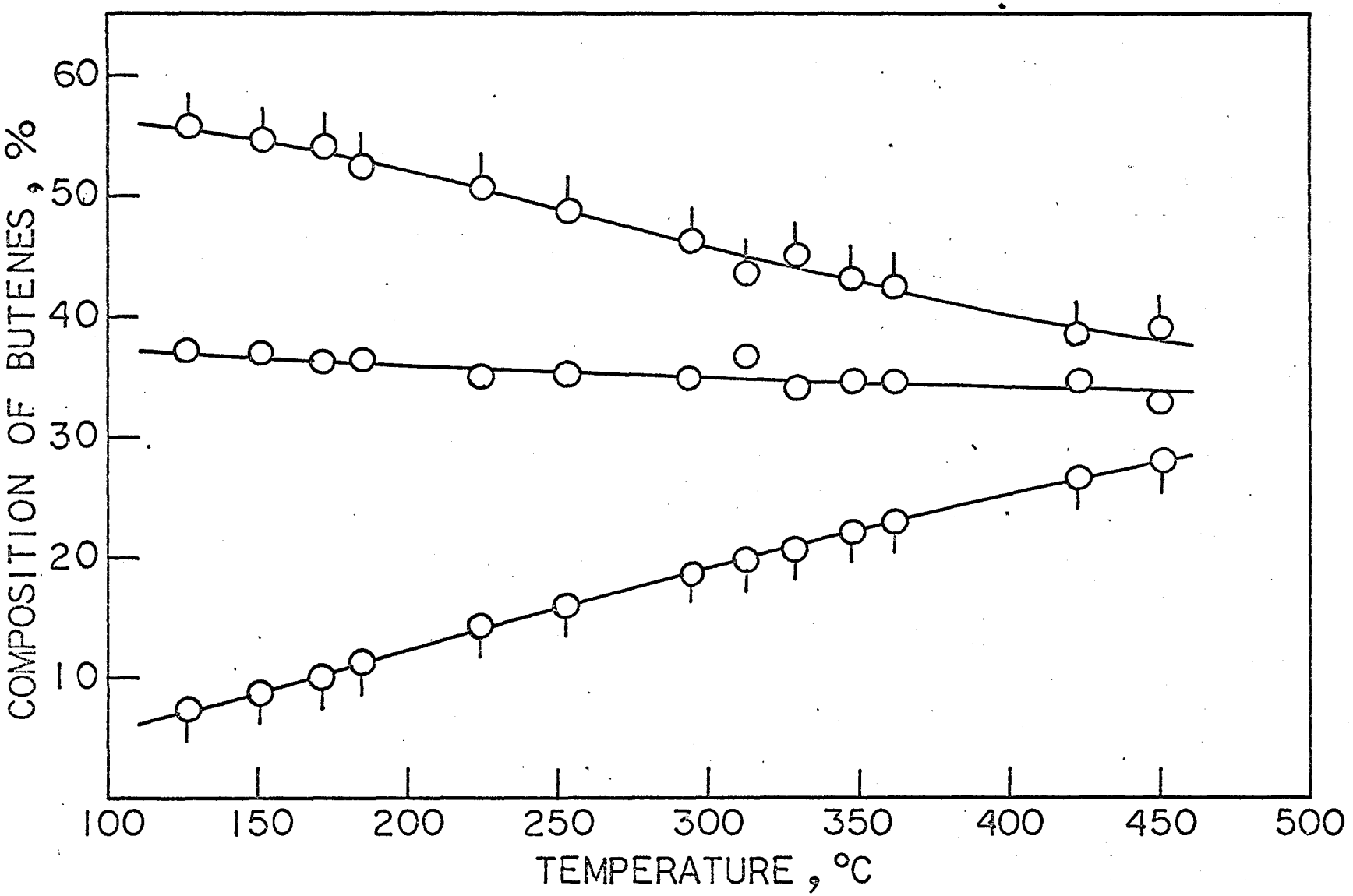

Fig. 2-4 Equilibrium composition of n-butenes: trans-2-( ), cis-2-( ) and 1-butene ( ).

Fig. 2-5 Six-membered ring intermediates for the pyrolysis of n- and sec-butyl acetate.

n-butyl acetate

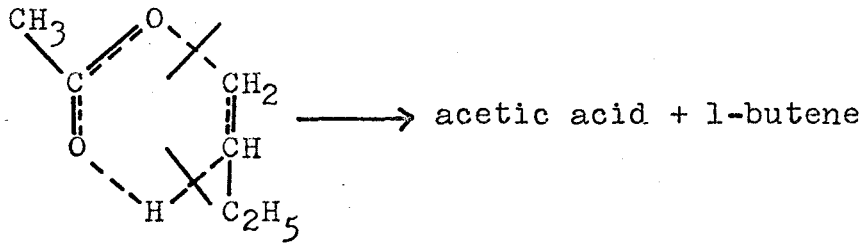

(a) Two β -hydrogens are involved.

sec-butyl acetate

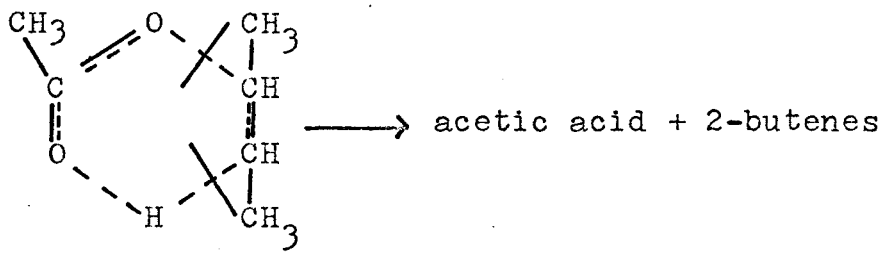

(b) Two β -hydrogens are involved.

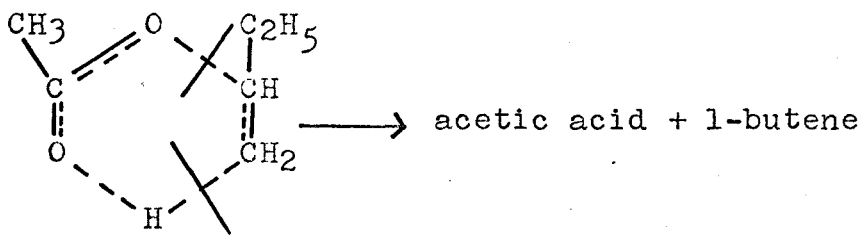

(c) Three β -hydrogens are involved.

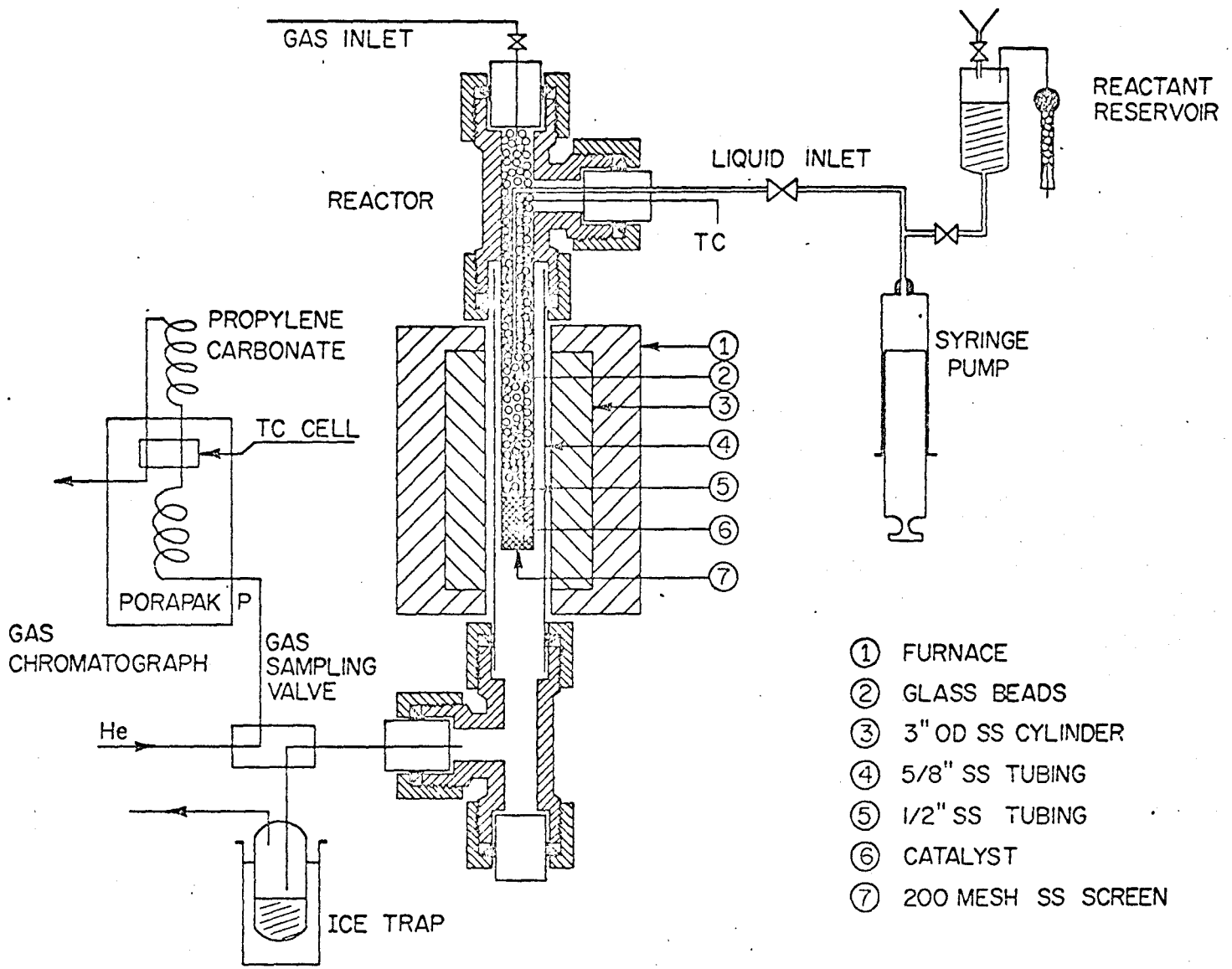

Fig. 3-1 Schematic diagram of reaction system.

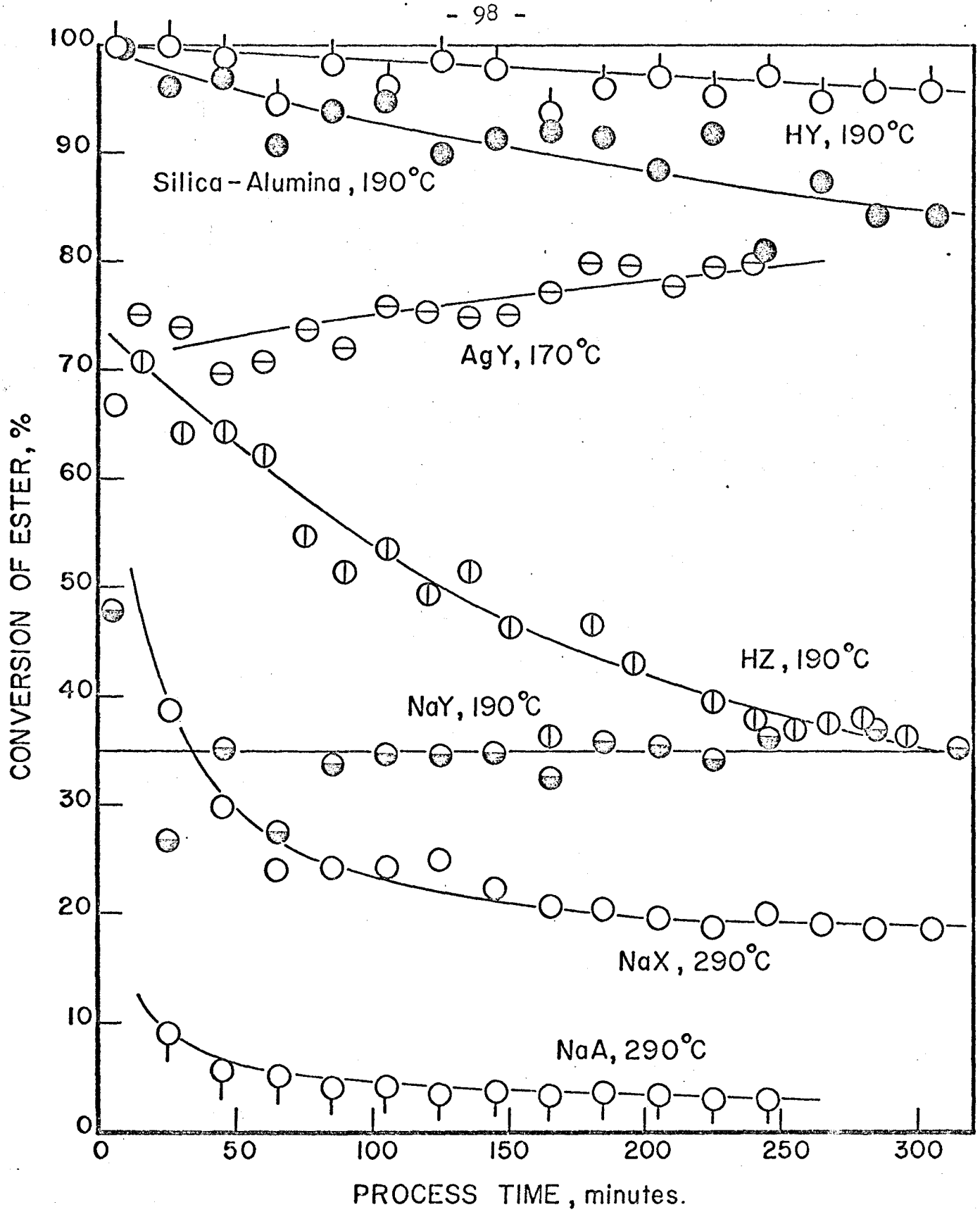

Fig. 4-1 Aging patterns of HY, silica-alumina, AgY, HZ, NaY, NaX and NaA for the decomposition of sec-butyl acetate.

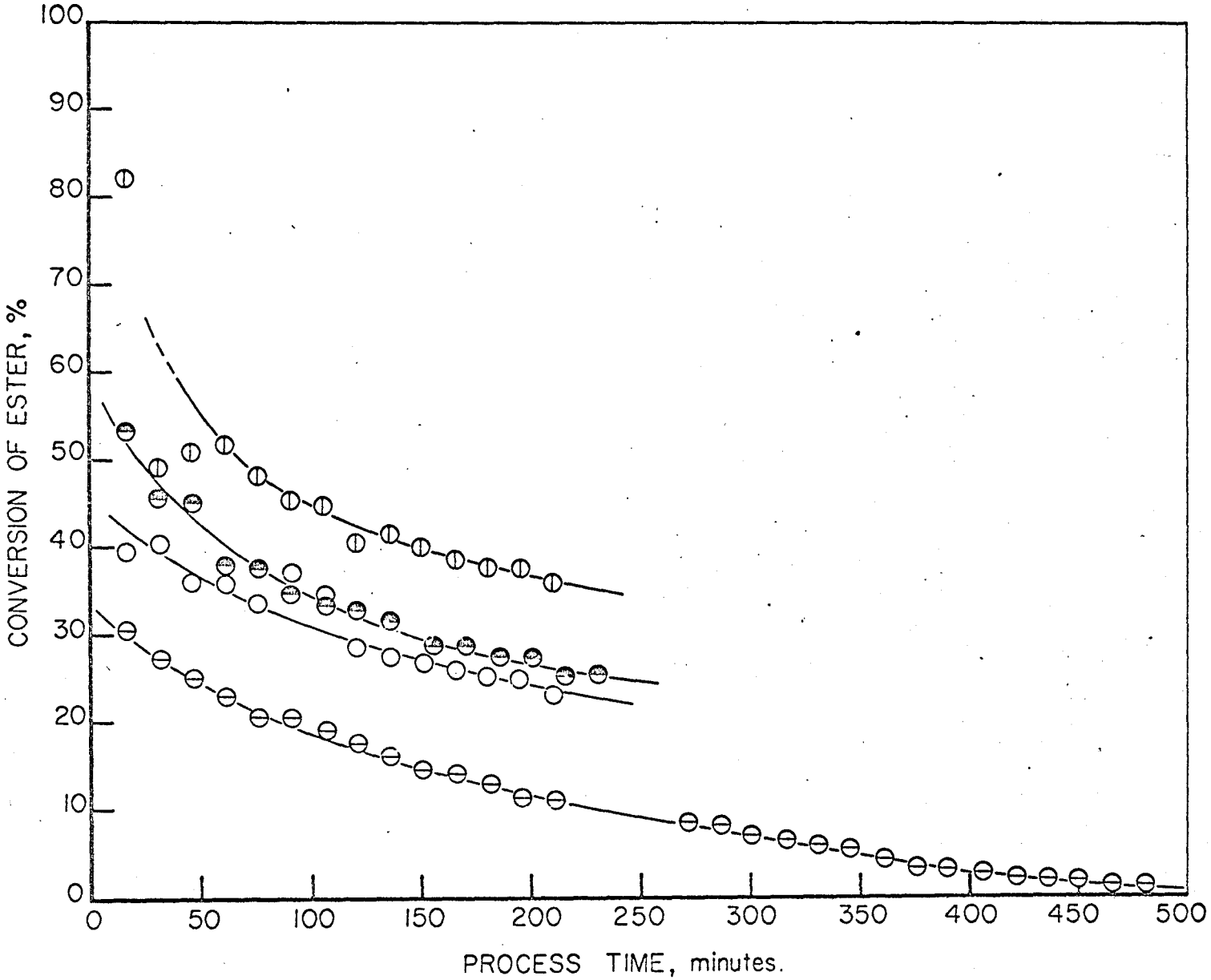

Fig. 4-2 Aging of NiHY during the decomposition of sec-butyl acetate at 170°C; feed rates are 0.273 (⊖), 0.0931 (O), 0.0543 (⊜), and 0.0454 (⊕) gm. mole ester feed/hr./gm. catalyst.

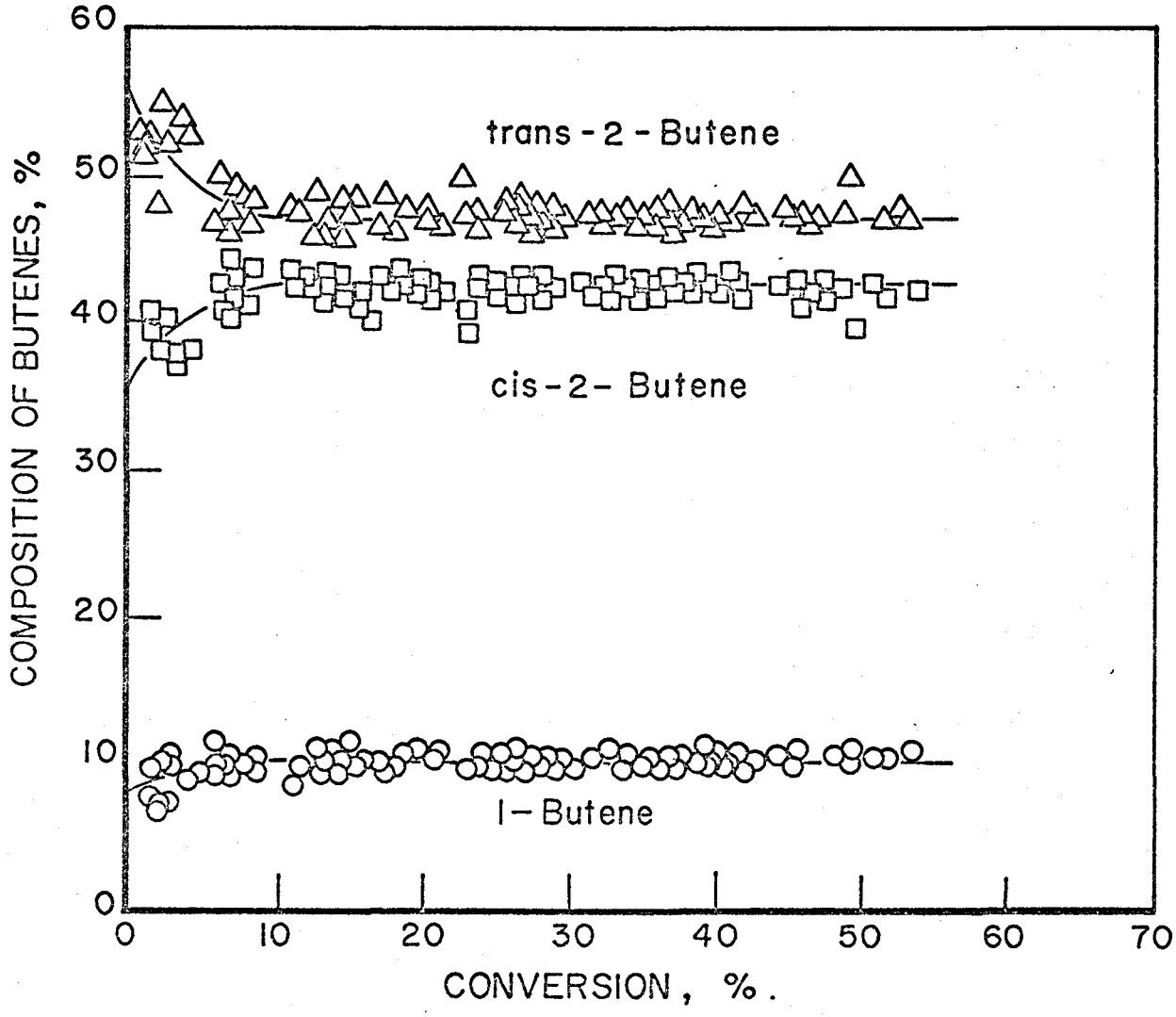

Fig. 4-3 Selectivity of n-butenes for the decomposition of sec-butyl acetate on NiHY at 170°C.

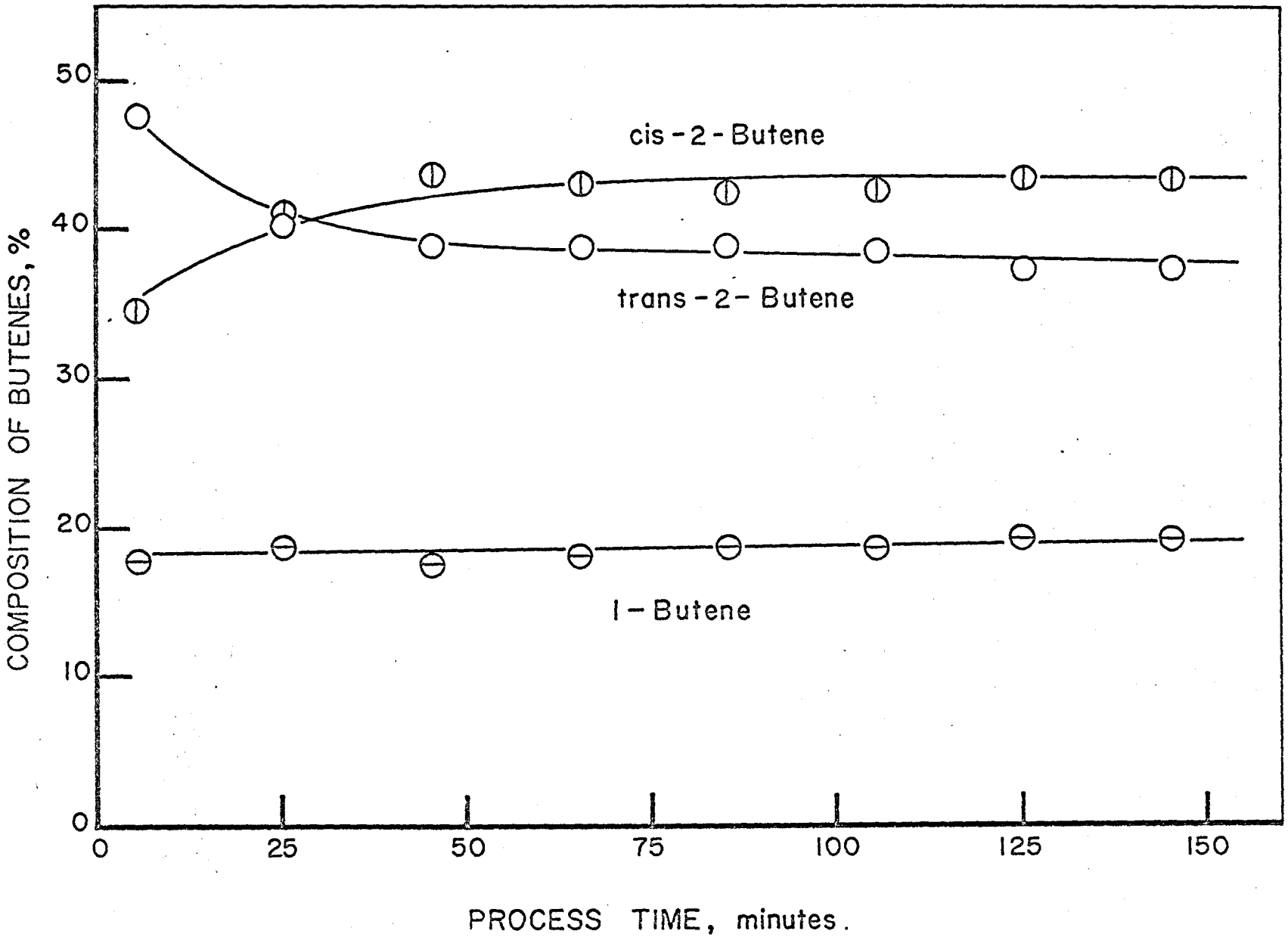

Fig. 4-4 Selectivity of n-butenes for the decomposition of sec-butyl acetate on HZ at 290°C.

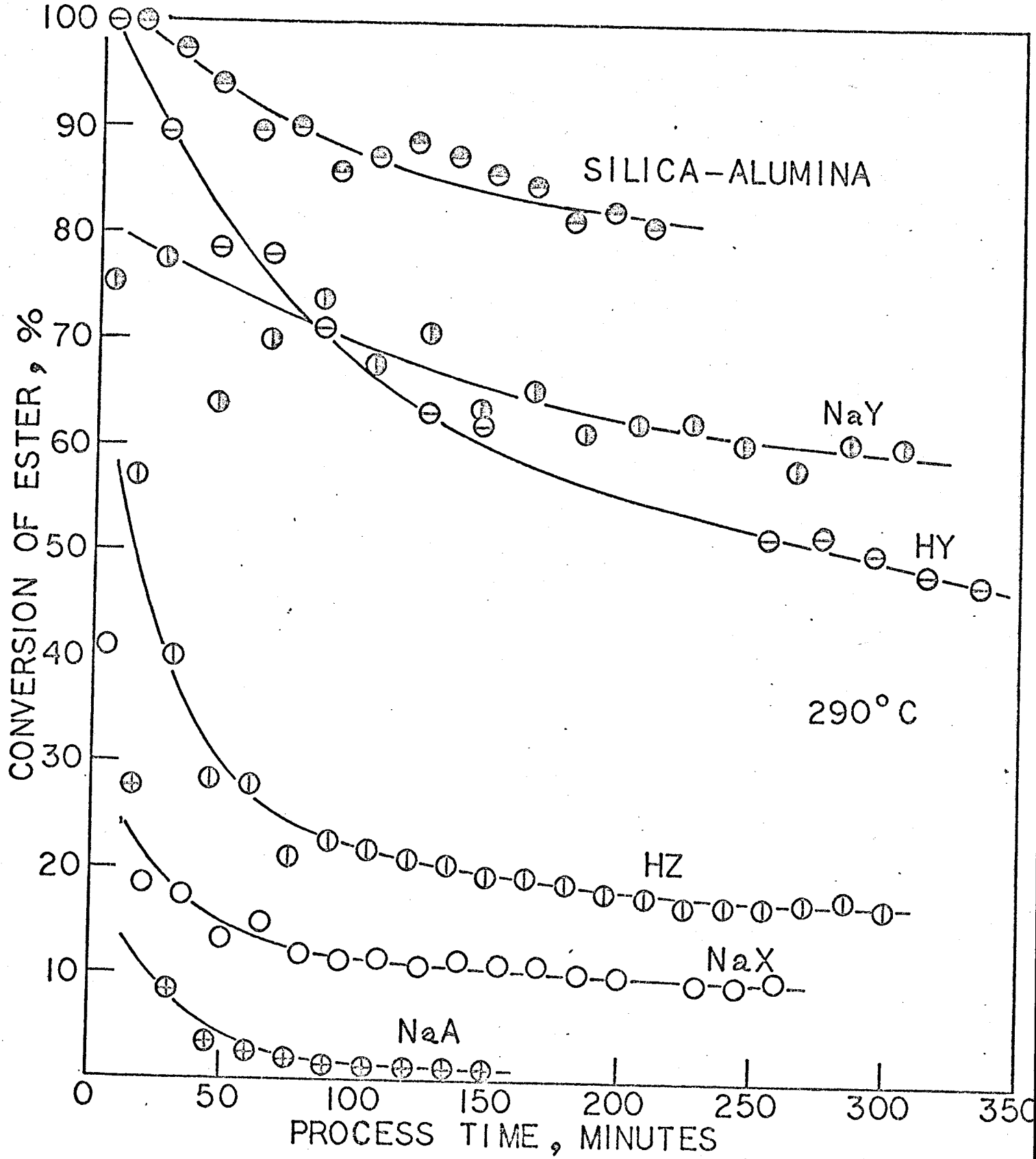

Fig. 5-1 Aging patterns of silica-alumina, NaY, HY, HZ, NaX and NaA for the decomposition of n-butyl acetate.

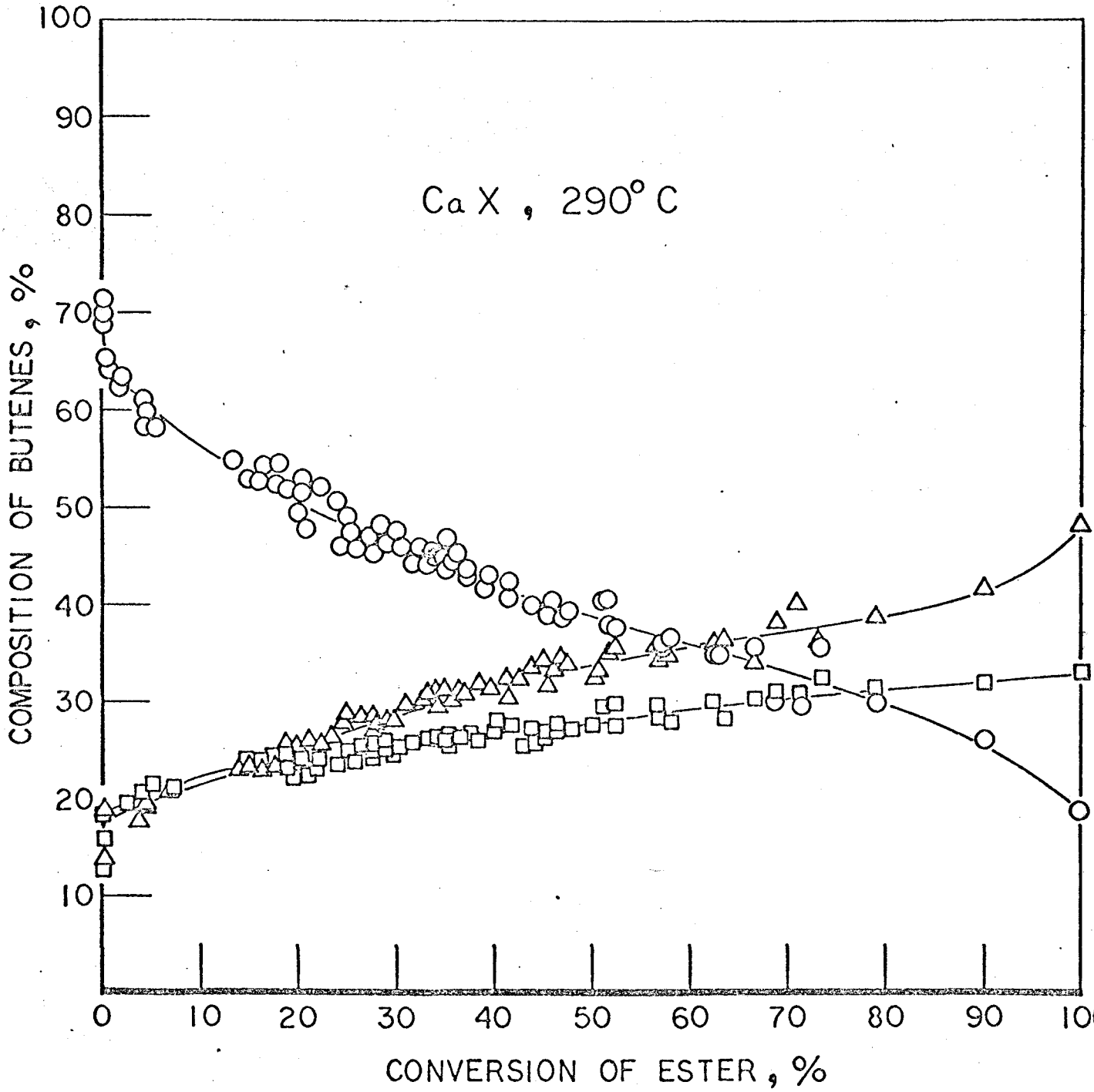

Fig. 5-2 Selectivity of n-butenes for the decomposition of n-butyl acetate on CaX at 290°C; 1-butene (O), trans-2-butene (△) and cis-2-butene (□).

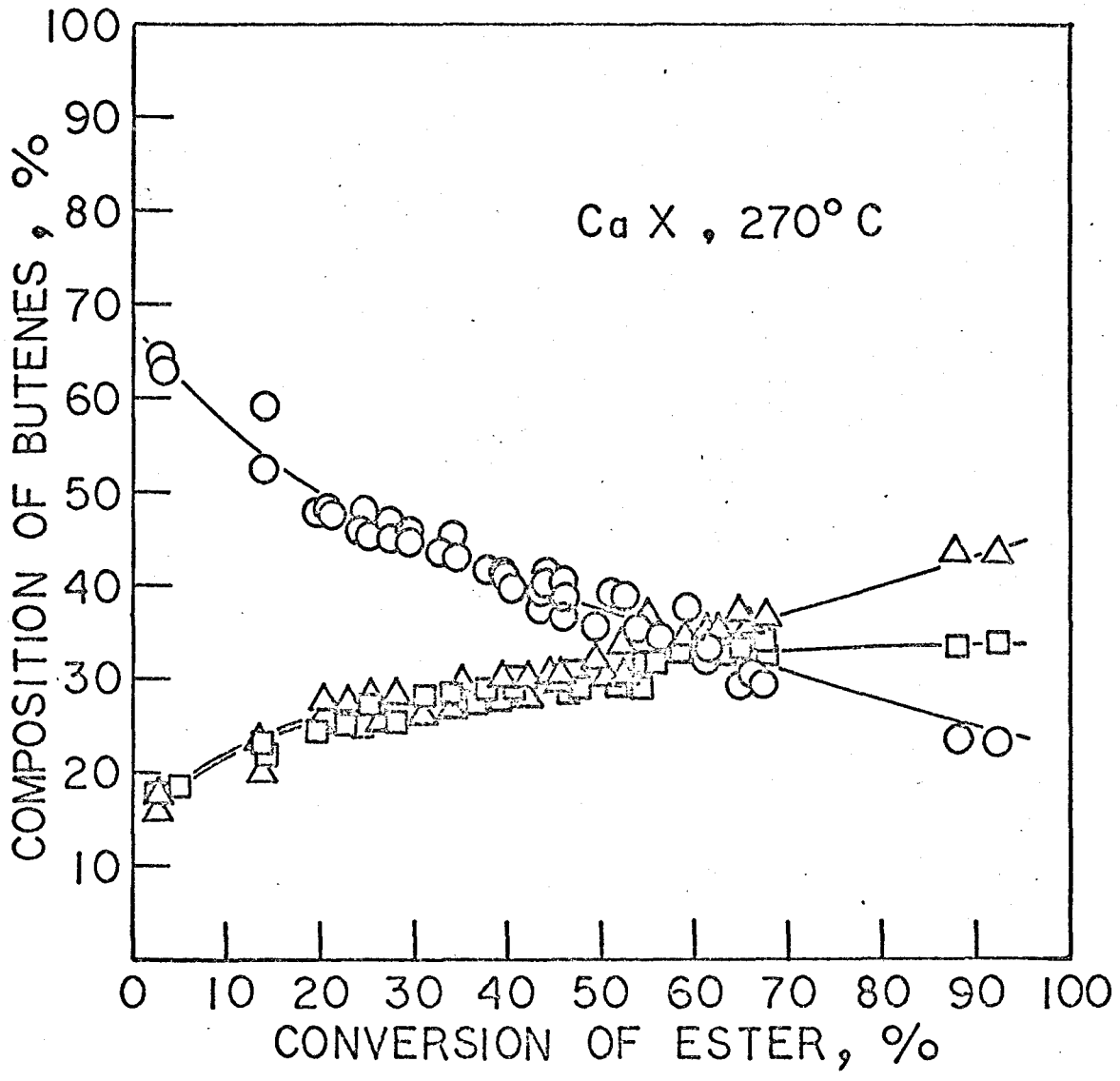

Fig. 5-3 Selectivity of n-butenes for the decomposition of n-butyl acetate on CaX at 270°C; 1-butene (○), trans-2-butene (△) and cis-2-butene (□).

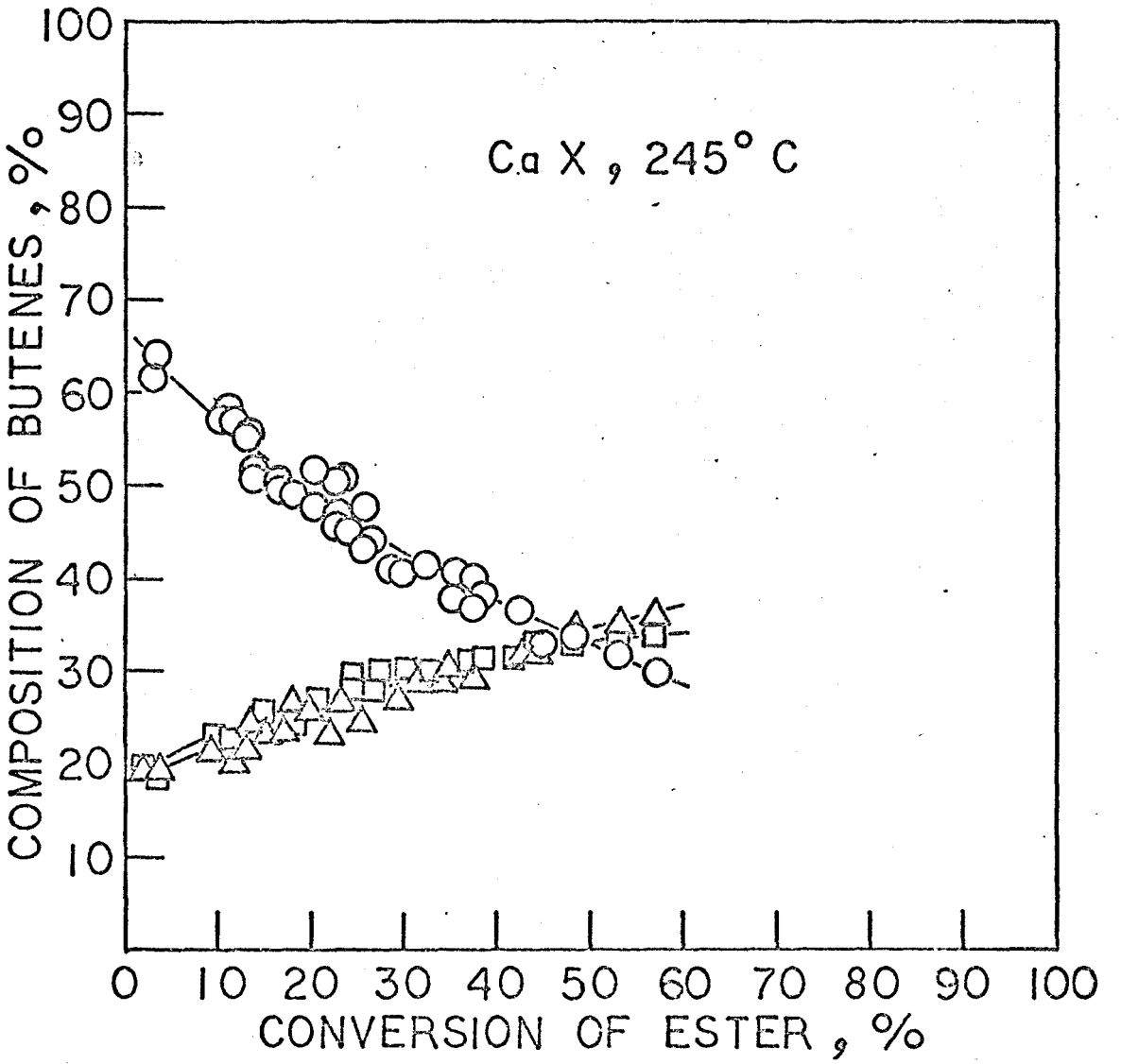

Fig. 5-4 Selectivity of n-butenes for the decomposition of n-butyl acetate on CaX at 245°C; 1-butene (○), trans-2-butene (△) and cis-2-butene (□).

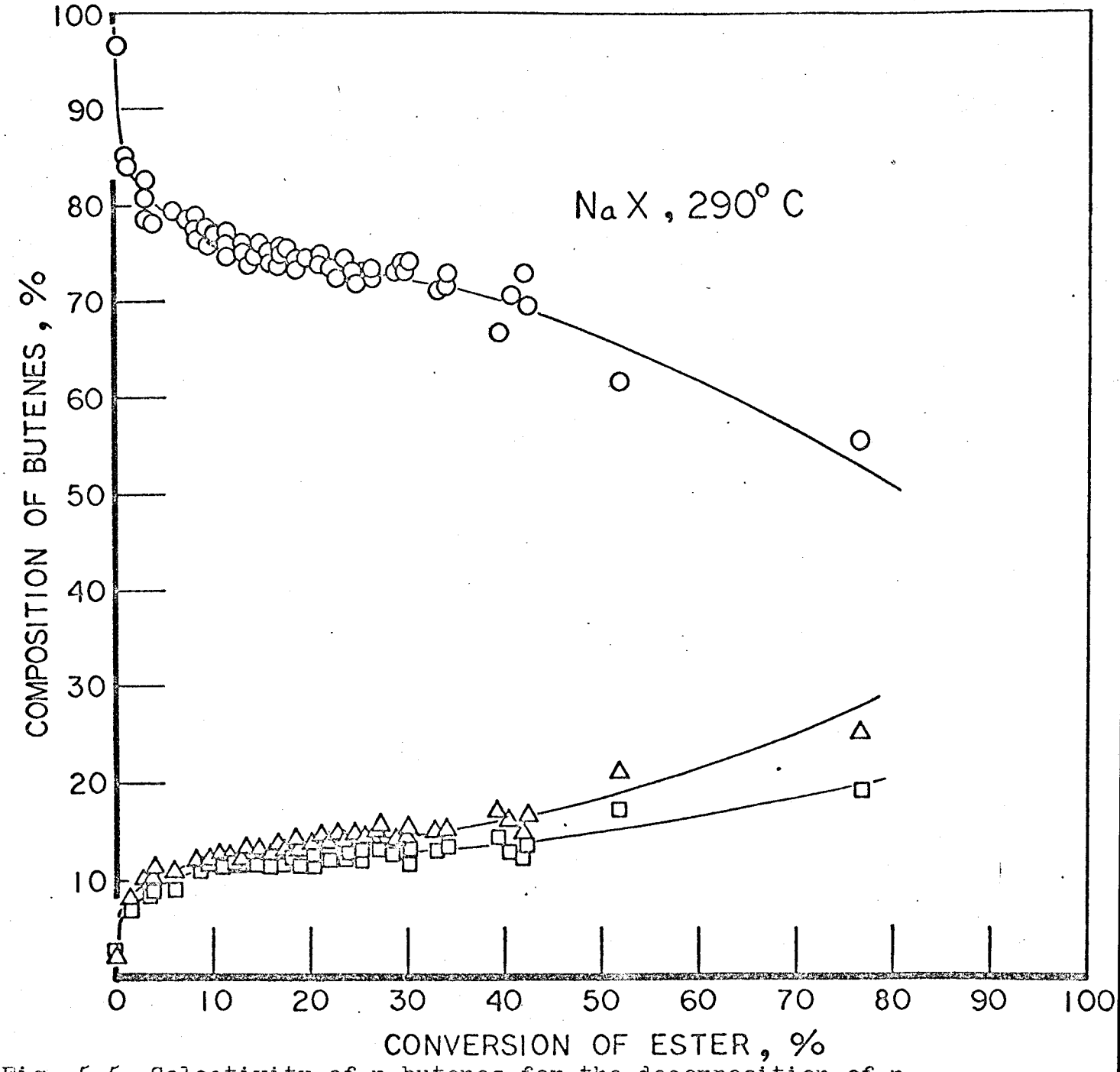

Fig. 5-5 Selectivity of n-butenes for the decomposition of n-butyl acetate on NaX at 290°C; 1-butene (O), trans-2-butene (Δ) and cis-2-butene (□).

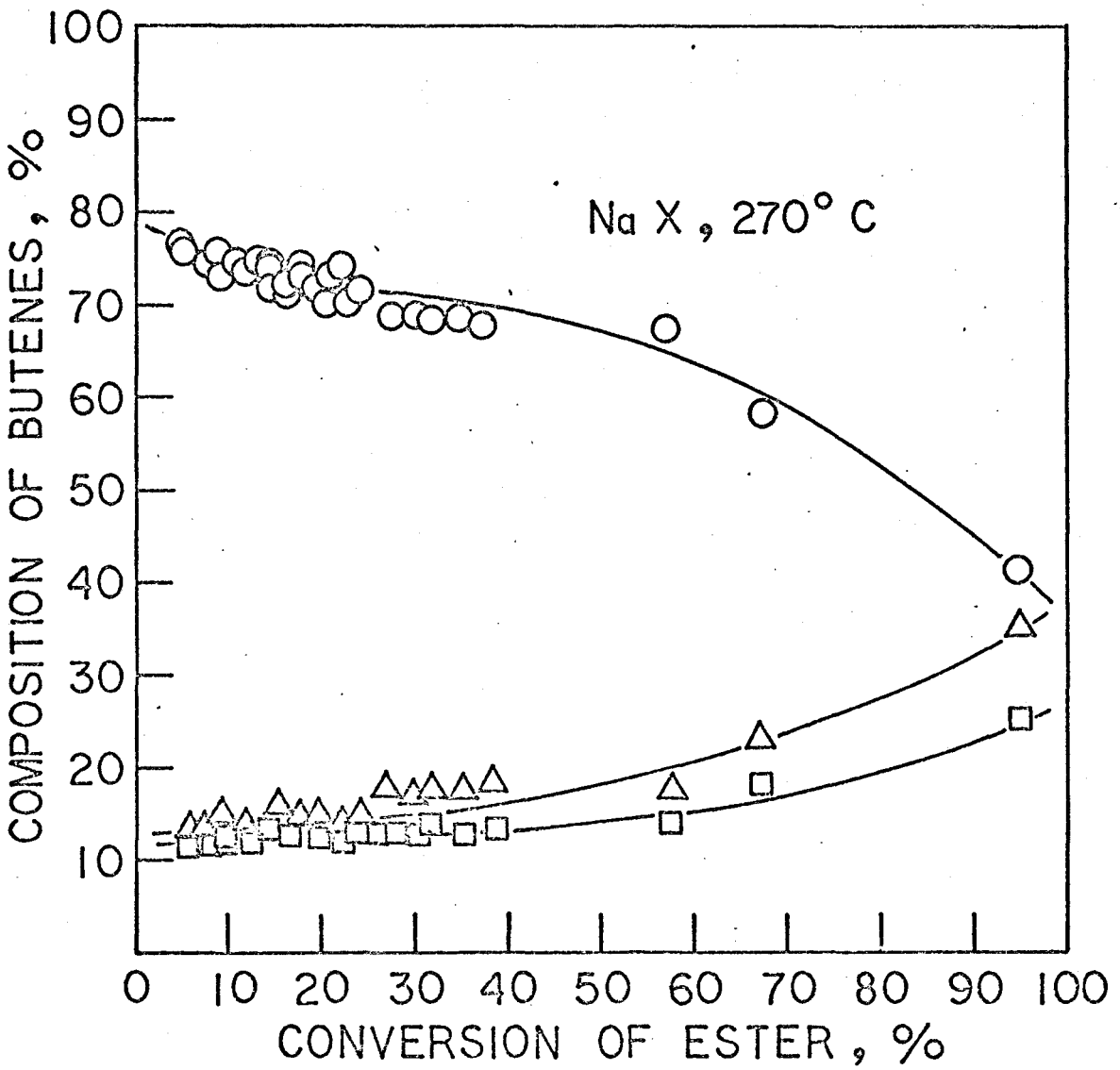

Fig. 5-6 Selectivity of n-butenes for the decomposition of n-butyl acetate on NaX at 270°C; 1-butene (○), trans-2-butene (△) and cis-2-butene (□).

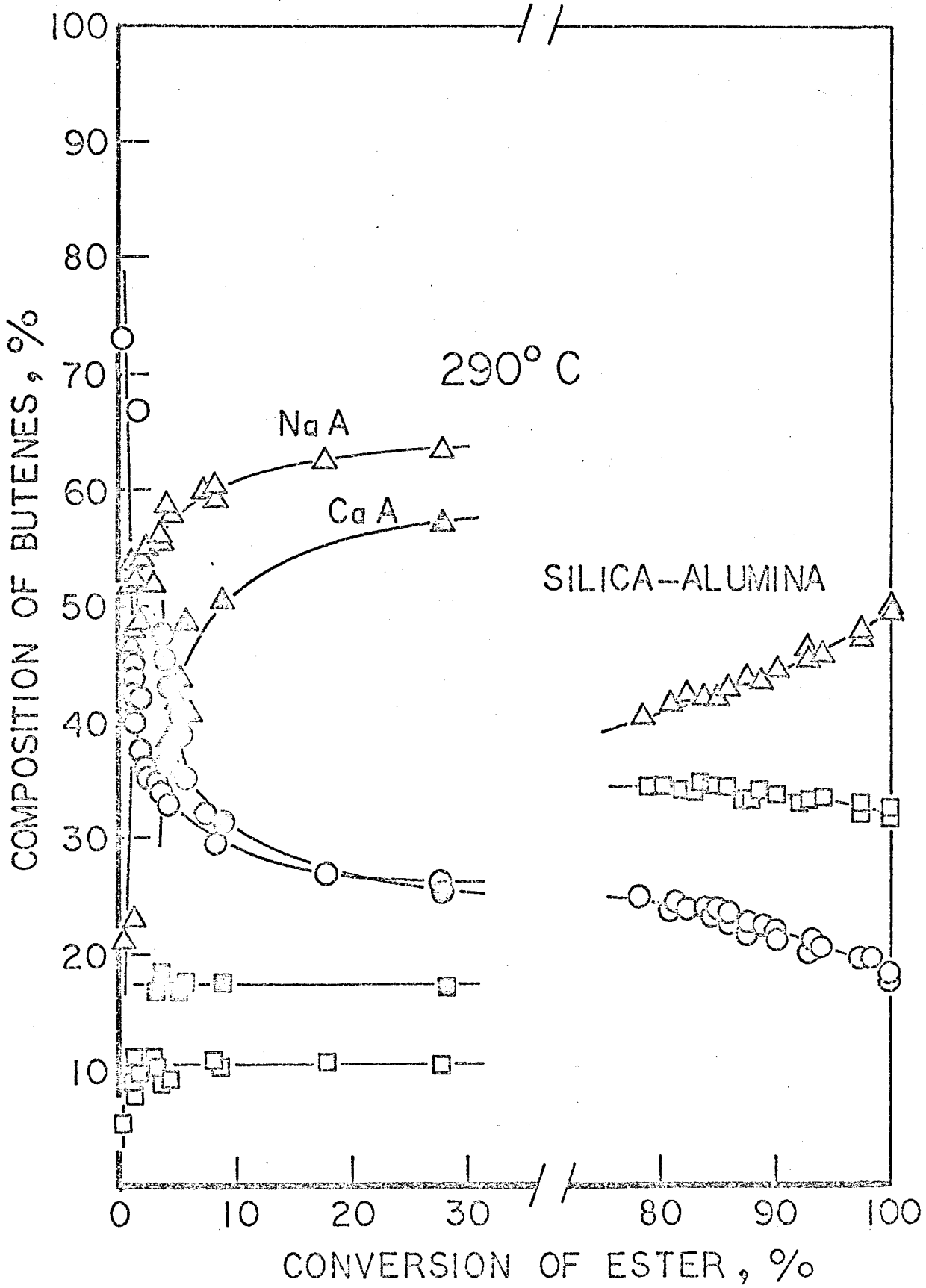

Fig. 5-7 Selectivity of n-butenes for the decomposition of n-butyl acetate on NaA (○ , △ , □), CaA (○ , △ , □) and silica-alumina (○ , △ , □). Symbols in brackets correspond to 1-butene, trans-2-butene and cis-2-butene in the order presented.

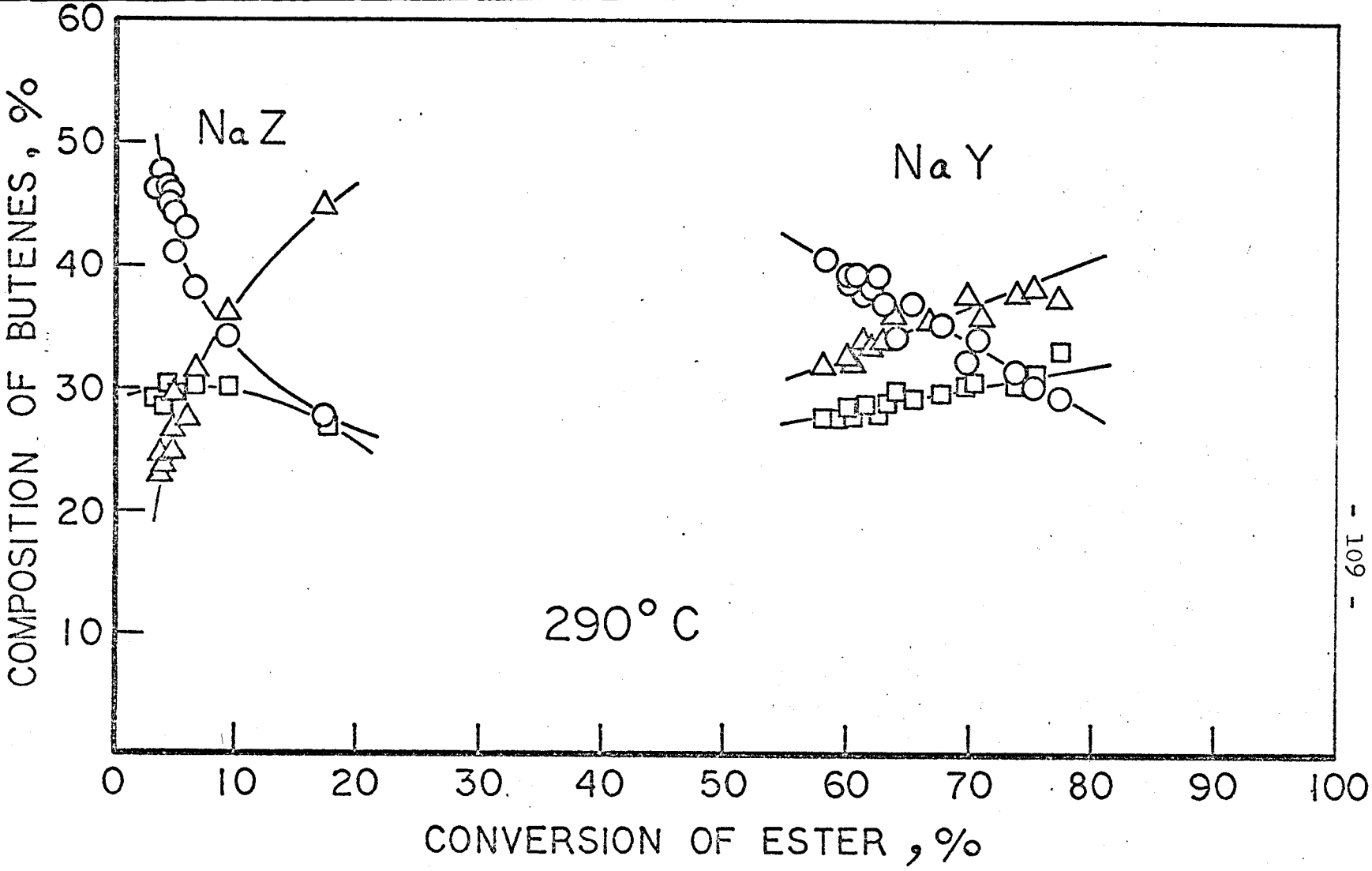

Fig. 5-8 Selectivity of n-butenes for the decomposition of n-butyl acetate on NaZ and NaY at 290°C; 1-butene (○), trans-2-butene (△), cis-2-butene (□).

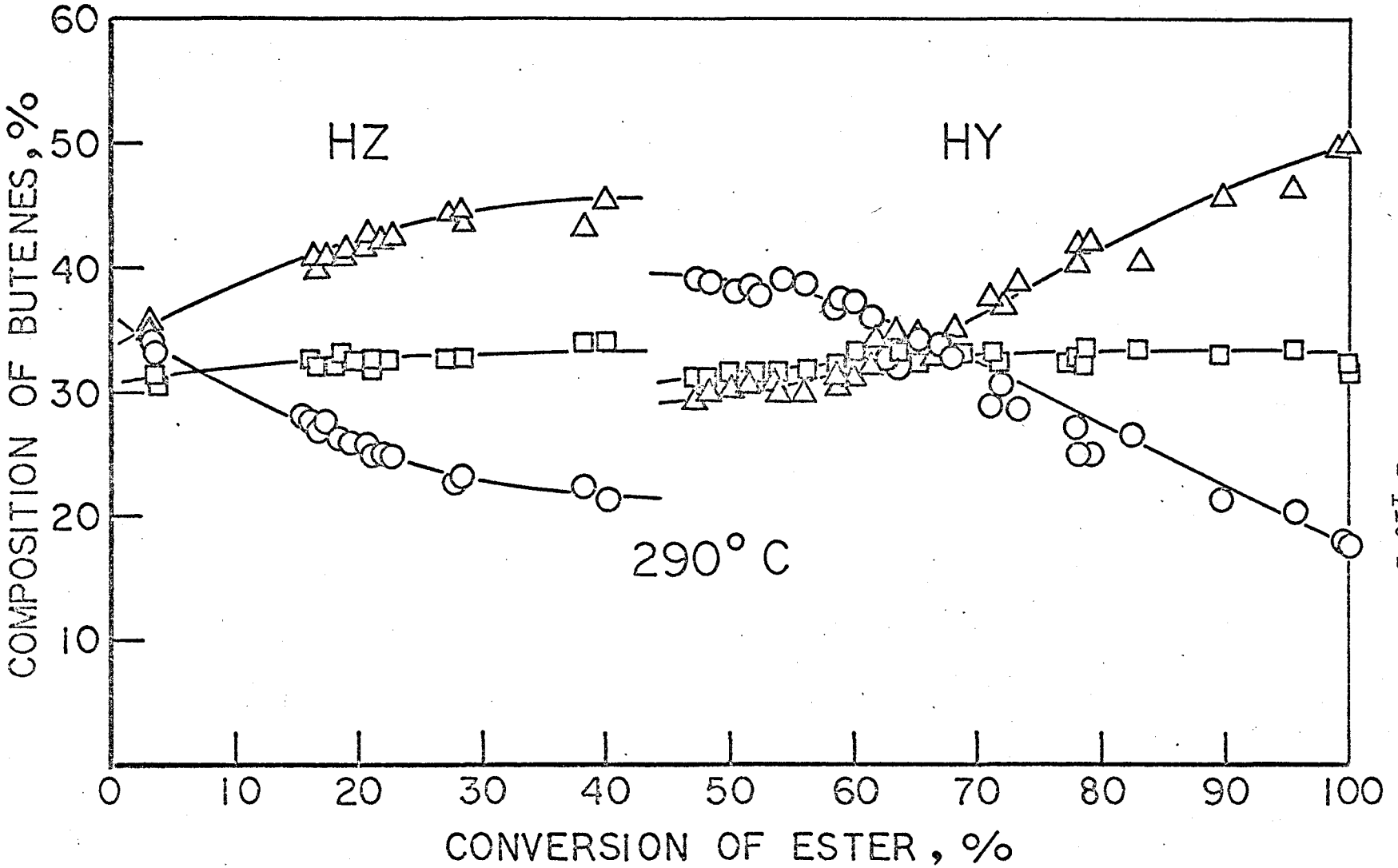

Fig. 5-9 Selectivity of n-butenes for the decomposition of n-butyl acetate on HZ and HY at 290°C; 1-butene (○), trans-2-butene (△), cis-2-butene (□).

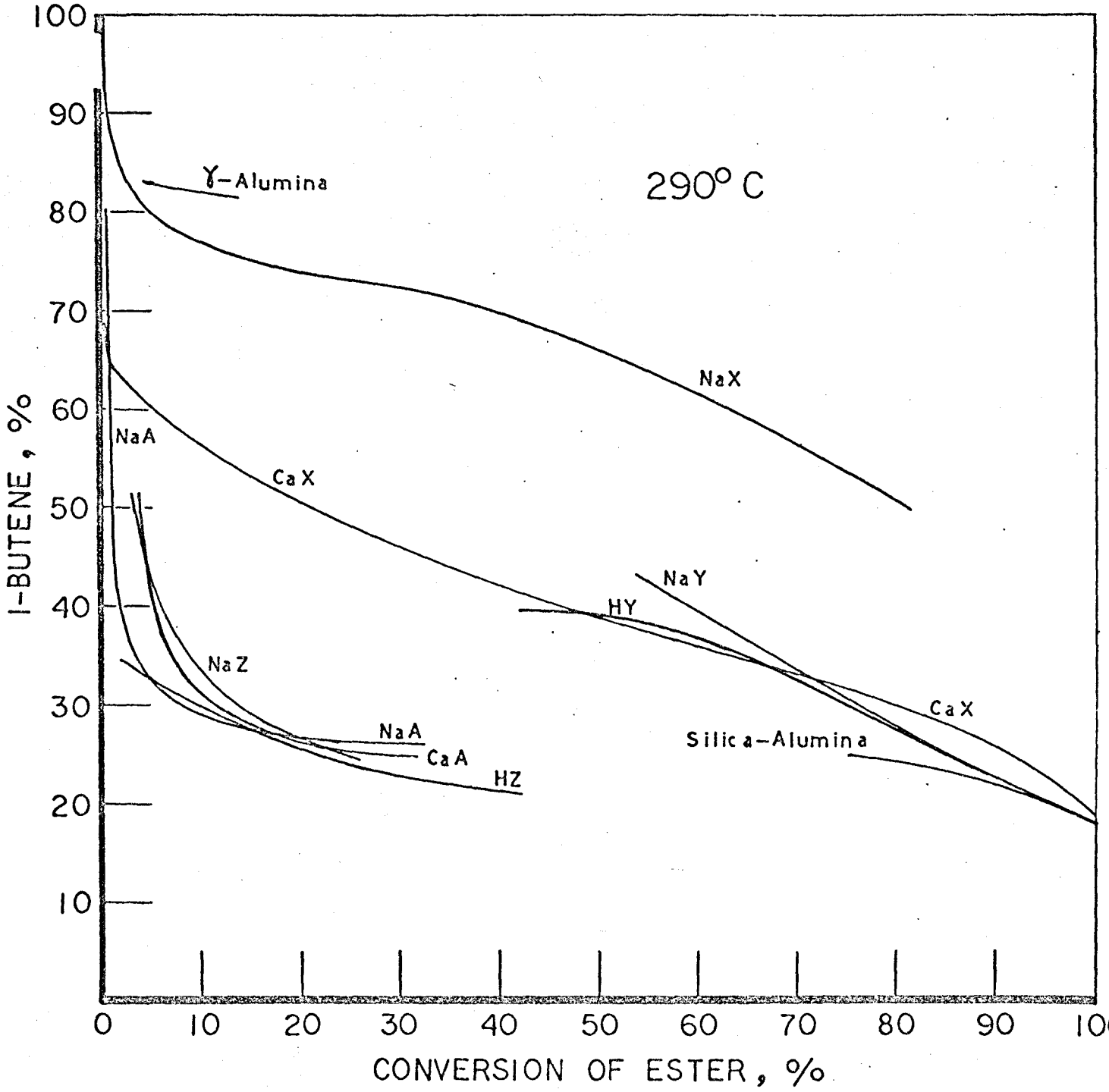

Fig. 5-10 Selectivity of 1-butene for the decomposition of n-butyl acetate on NaA, CaA, NaZ, HZ, NaX, CaX, NaY, HY, silica-alumina and γ-alumina.

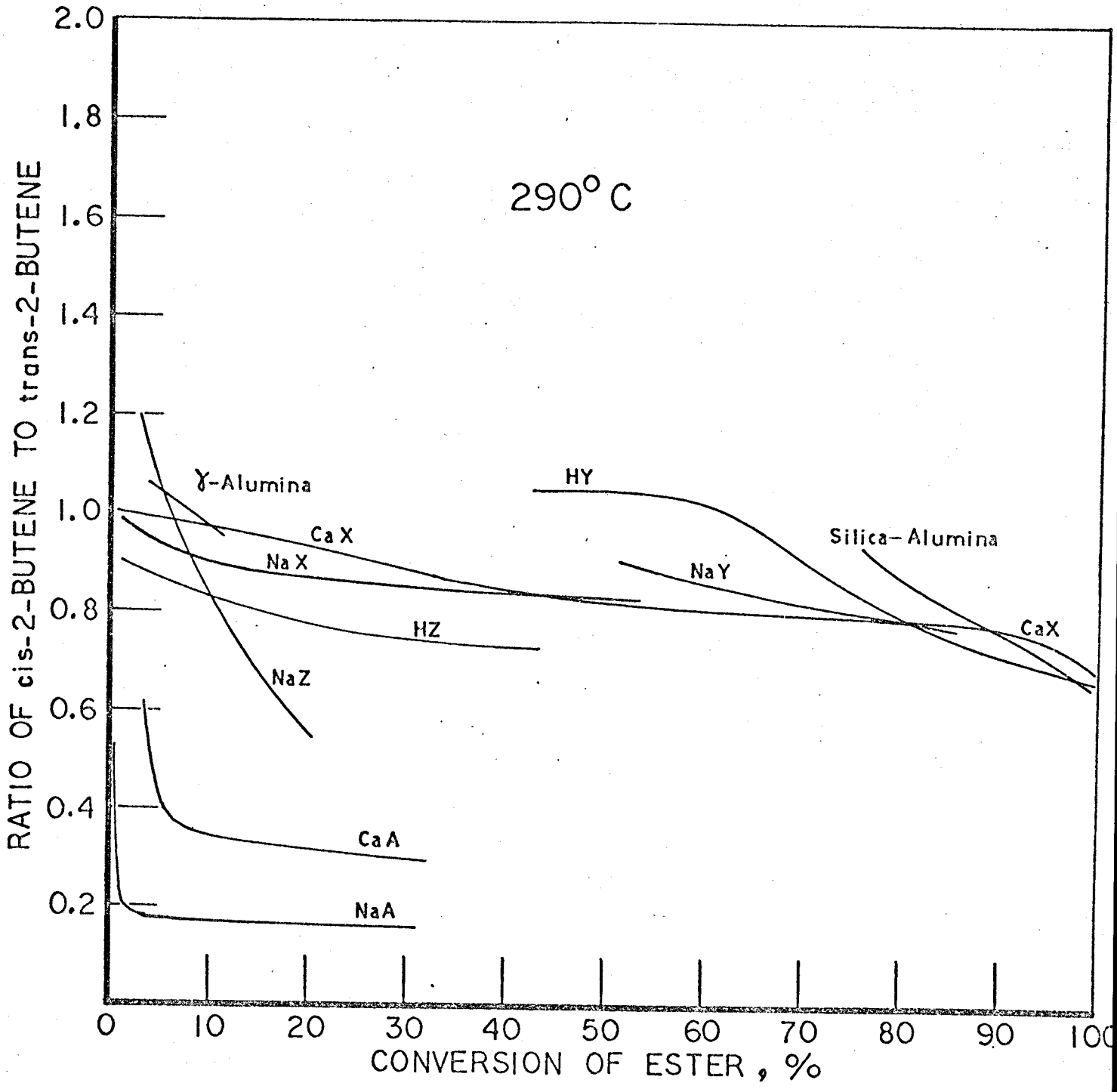

Fig. 5-11 Ratio of cis-2-butene to trans-2-butene for the decomposition of n-butyl acetate on NaA, CaA, NaZ, HZ, NaX, CaX, NaY, HY, silica-alumina and γ-alumina.

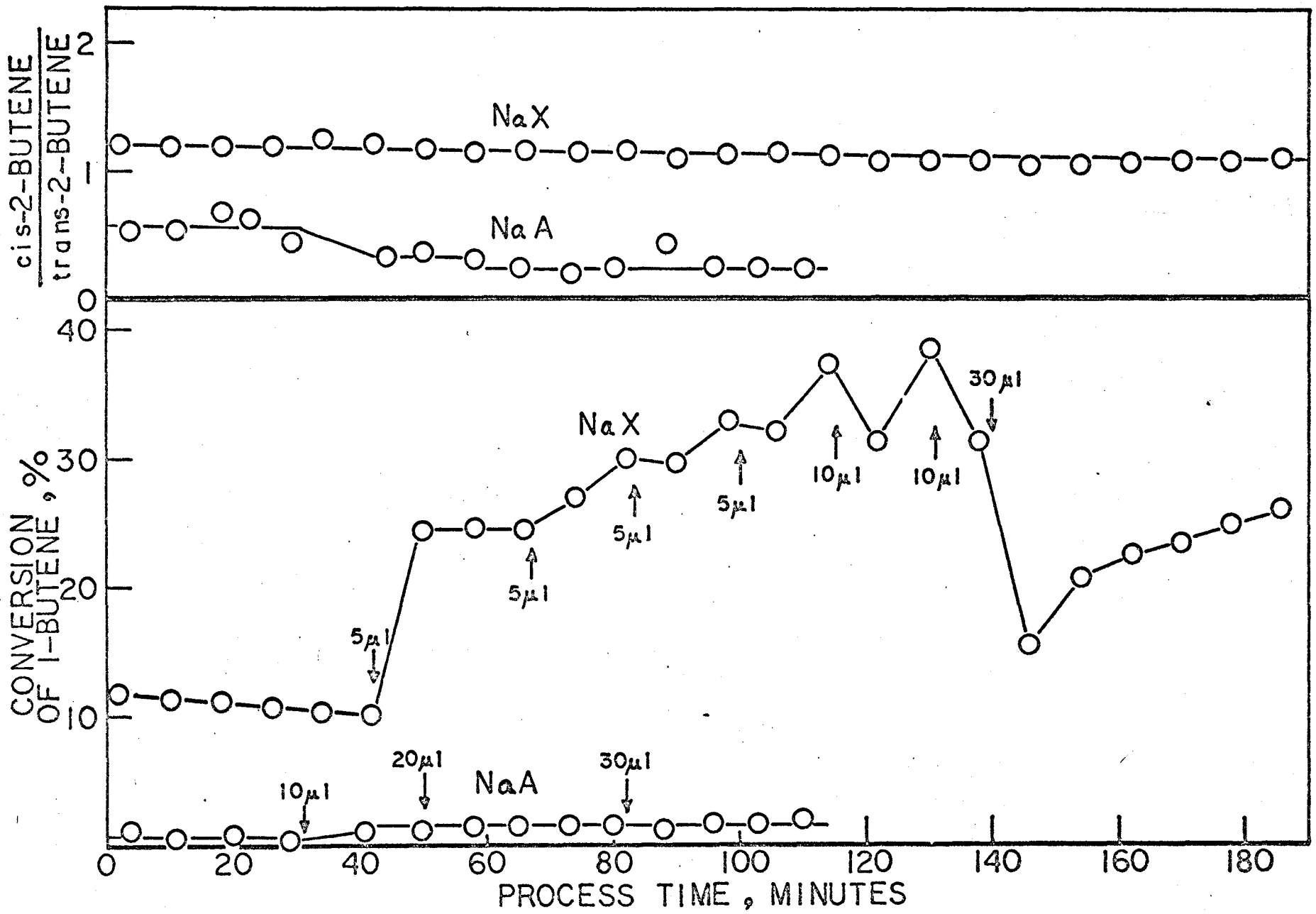

Fig. 5-12 Isomerization of 1-butene on NaA and NaX at 290°C. Pulse injections of acetic acid are indicated by the arrow and the amount injected are given in microliter.

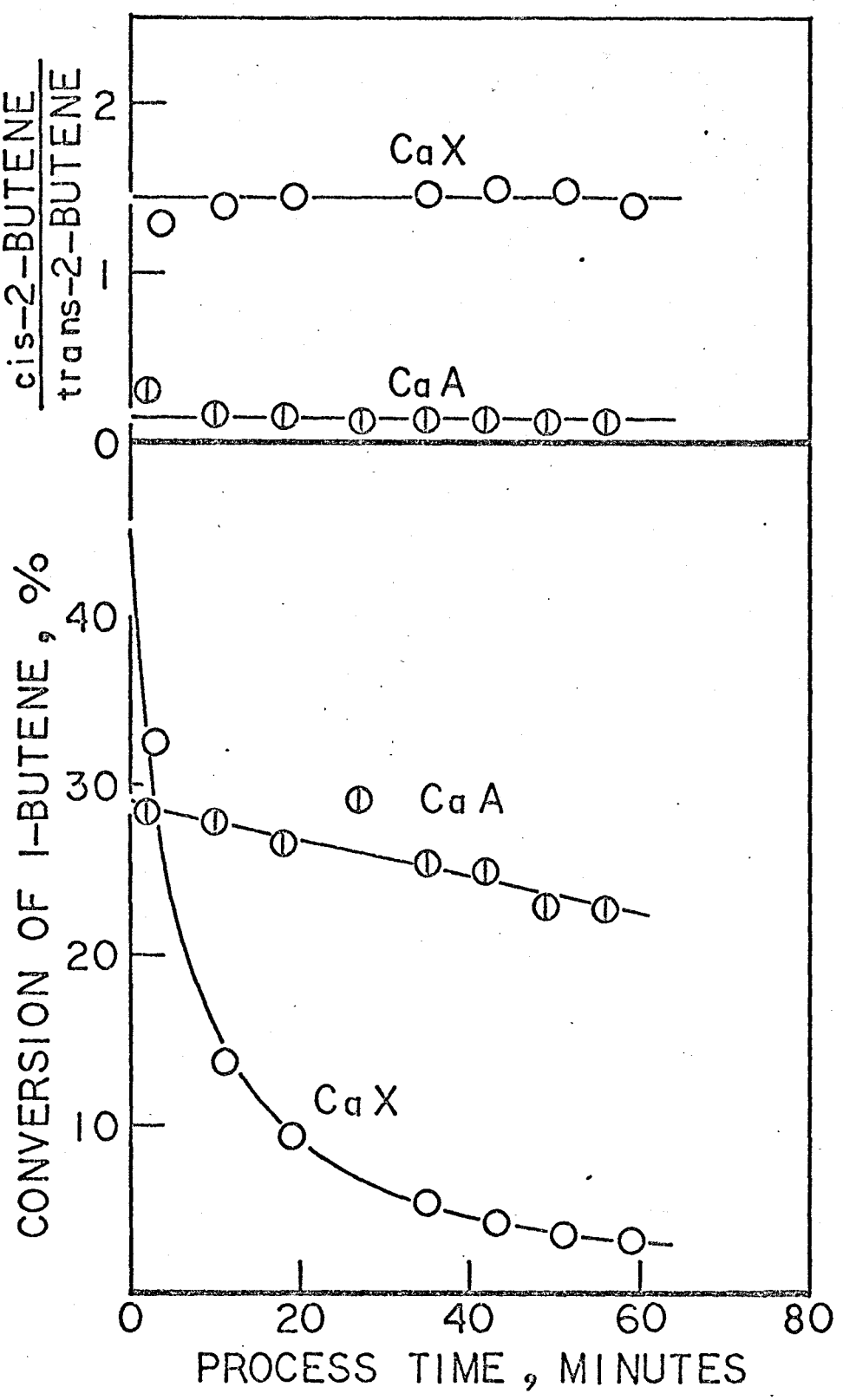

Fig. 5-13 Isomerization of 1-butene on CaX and CaA at 290°C.

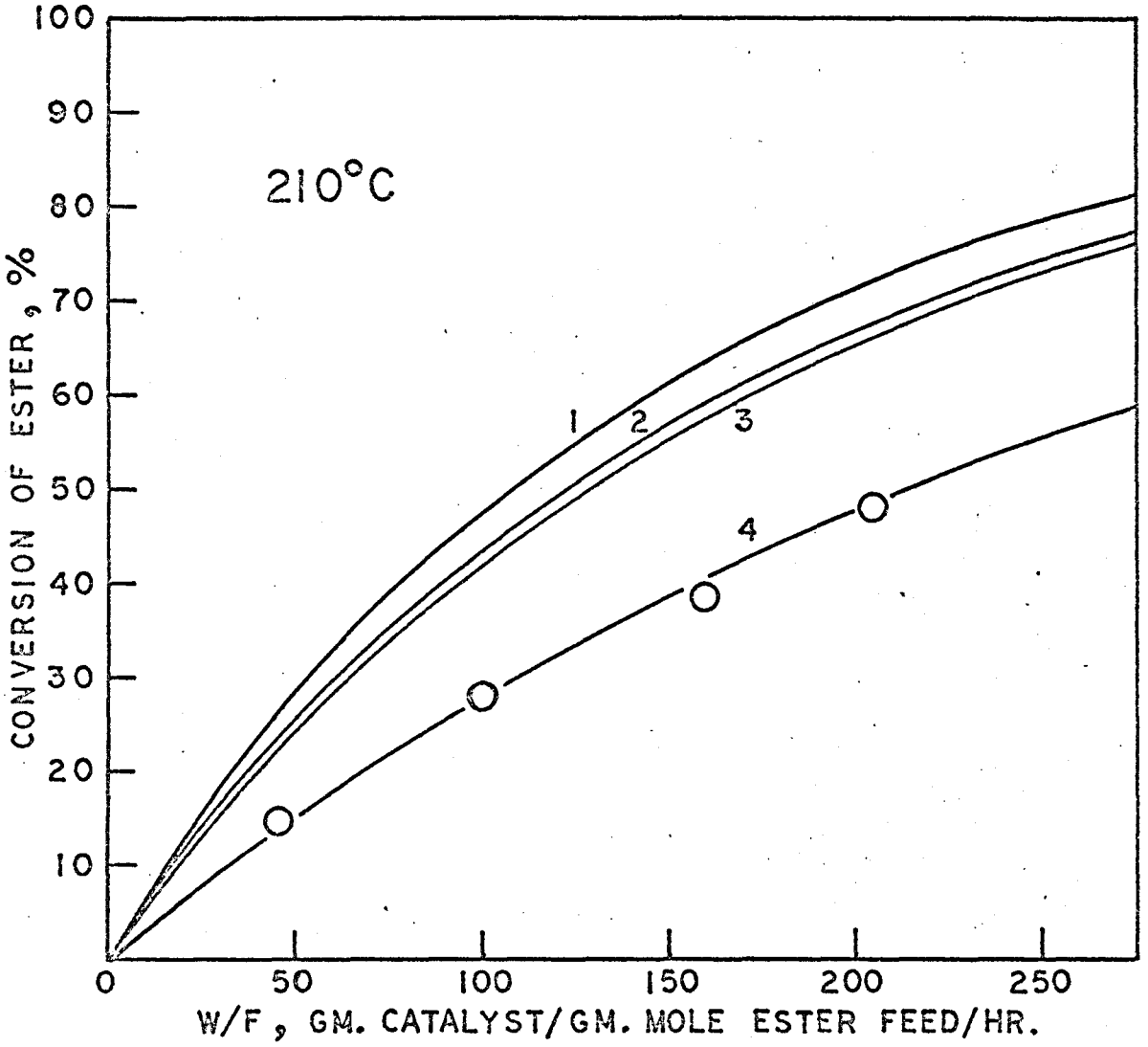

Fig. 6-1 Decomposition of sec-butyl acetate on NaY. The feed was 17.5 mole % ester diluted by acetic acid. The curves were predicted by;

1: $r = \frac{kEP_e}{1 + A\,P_a}$, 2: $r = \frac{kEP_e}{(1 + A\,P_a)^2}$, 3: $r = \frac{k\,P_e}{P_e + (A/E)P_a}$, 4: $r = \frac{k/E\,P_e}{(P_e + (A/E)P_a)^2}$

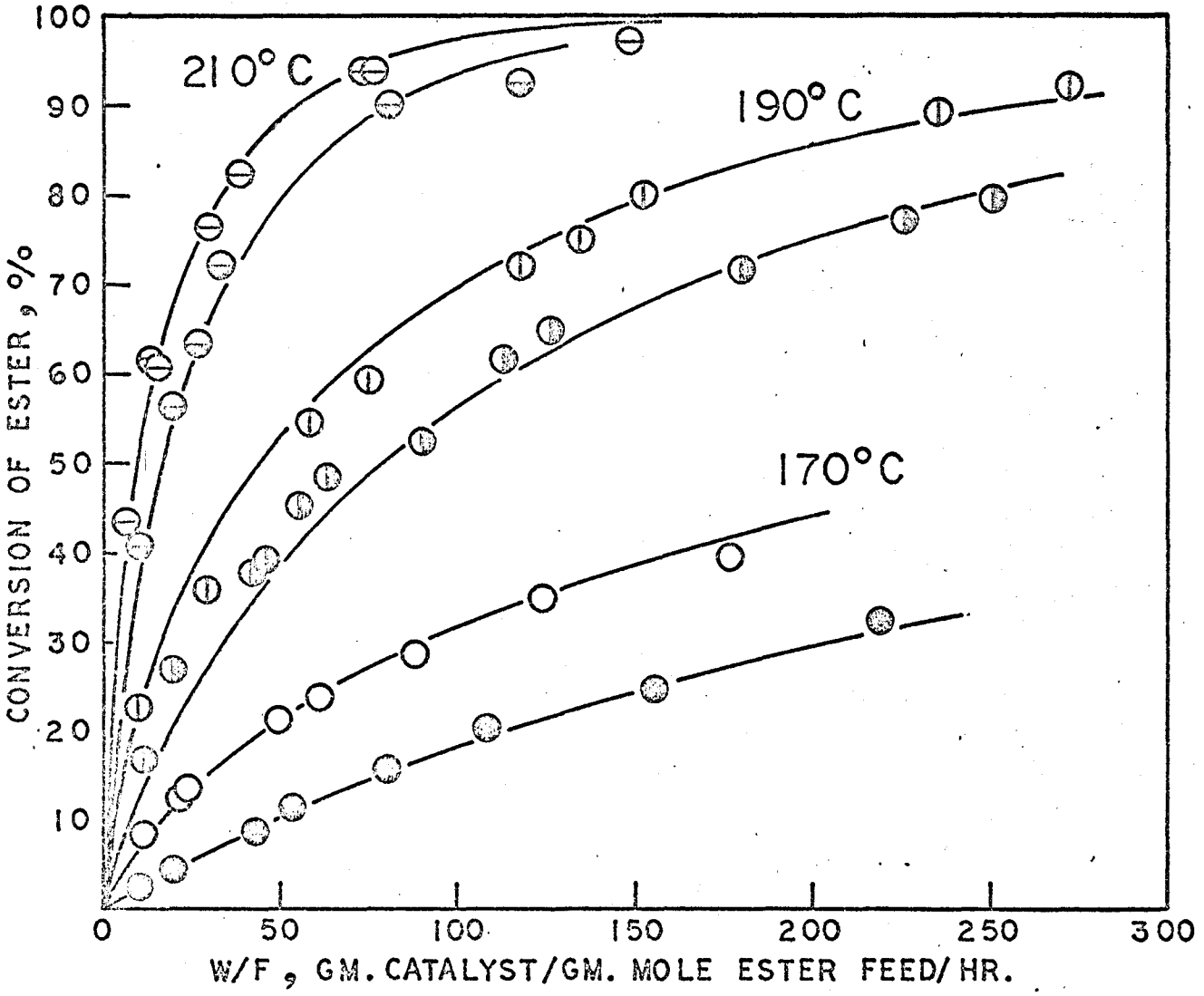

Fig. 6-2 Decomposition of sec-butyl acetate on NaY. ⊖, ◐ and ○ are for pure ester feed. ⊖, ◐ and ◎ are for 81.87 mole % ester feed diluted by acetic acid. The curves were obtained integrating the rate equation,

$$r = \frac{k/E\ P_e}{(P_e + (A/E)P_a)^2}.$$

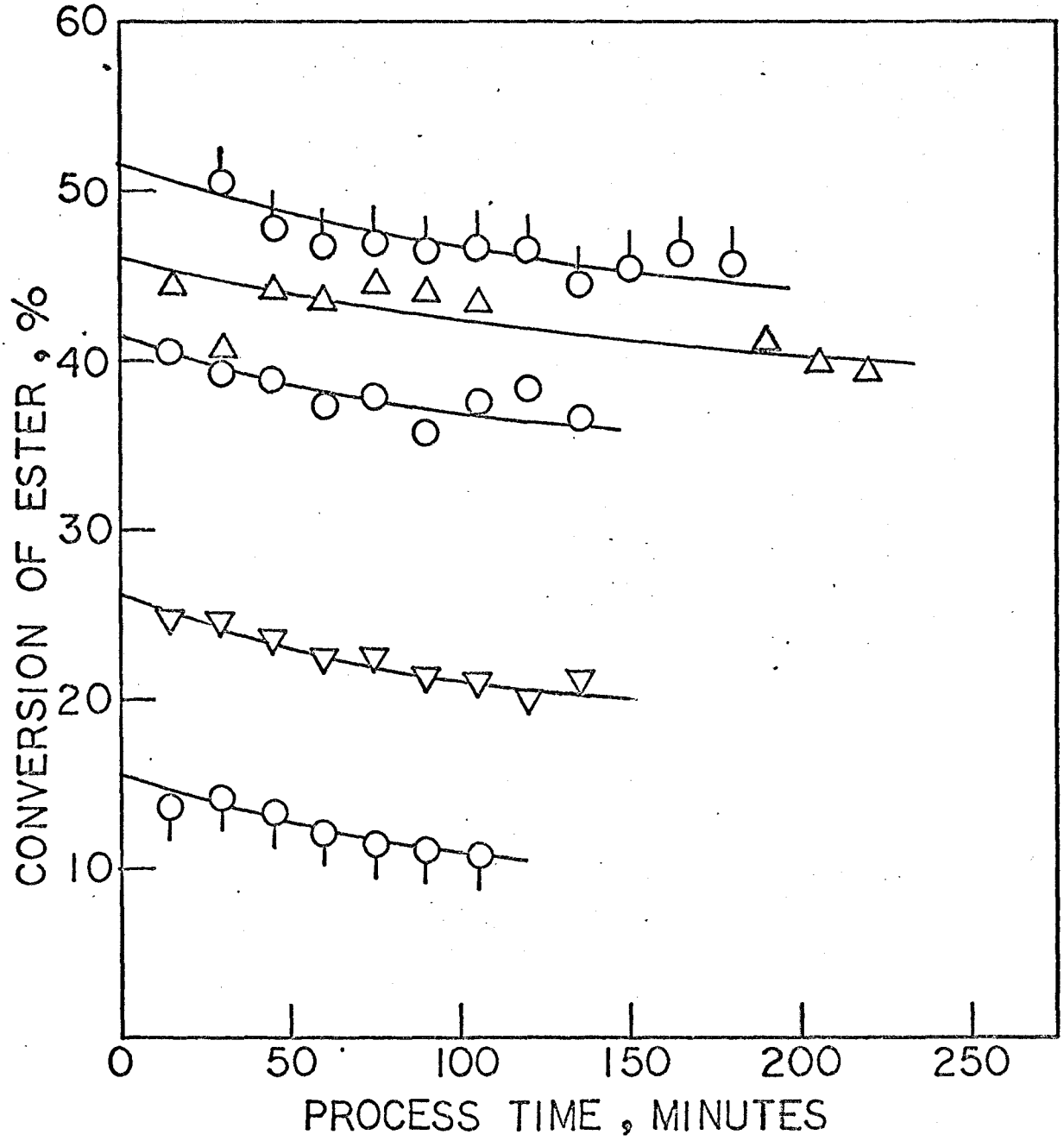

Fig. 6-3 Change of conversions with process time for the decomposition of sec-butyl acetate on HY at 140°C; feed rates are 0.0138 (○), 0.0186 (△), 0.0248 (○), 0.0709 (▽) and 0.192 (○) gm. mole ester feed/hr./gm. catalyst.

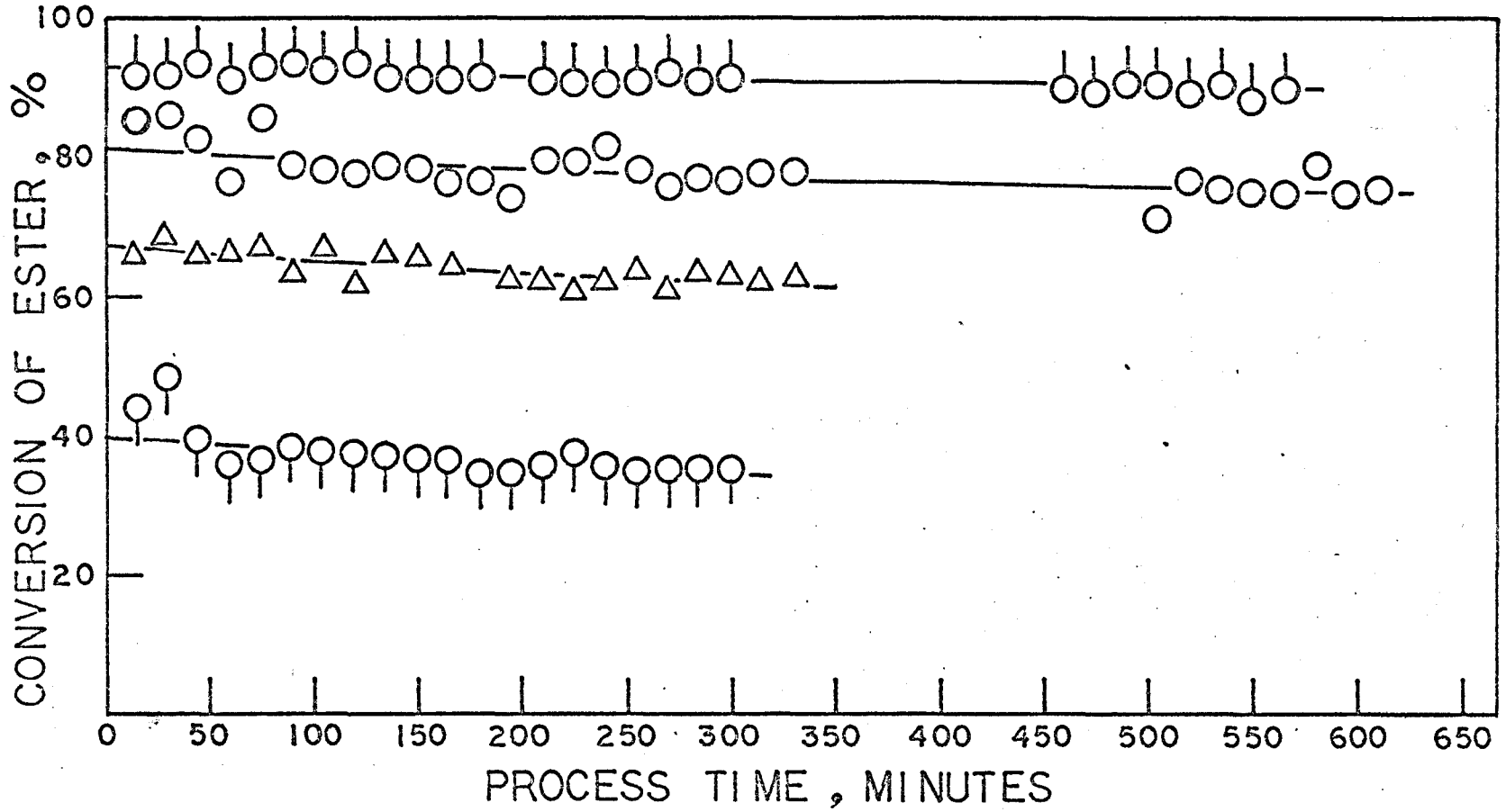

Fig. 6-4 Change of conversions with process time for the decomposition of sec-butyl acetate on HY at 170°C; feed rates are 0.0126 (○), 0.0308 (○), 0.0613 (△) and 0.225 (○) gm. mole ester feed/ hr./gm. catalyst.

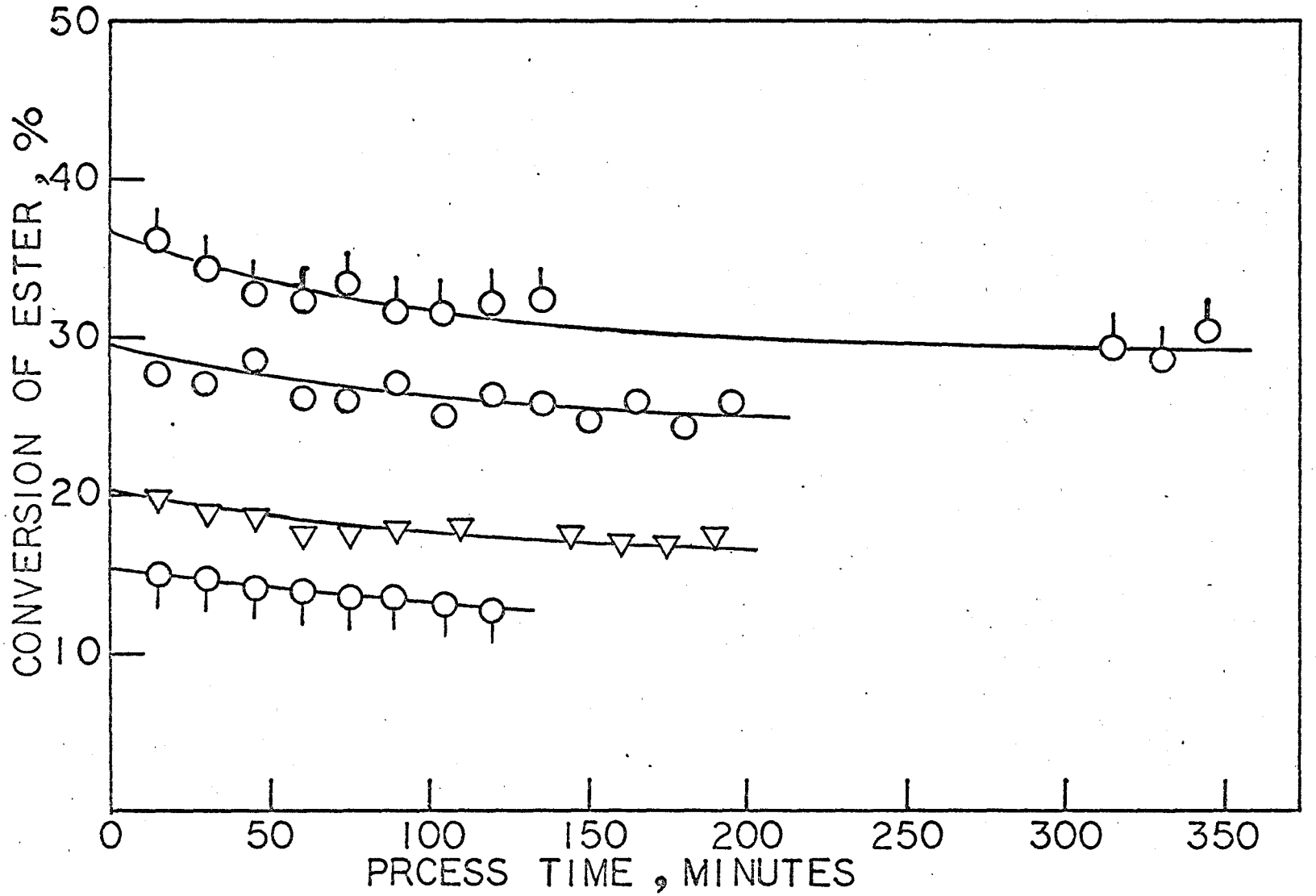

Fig. 6-5 Change of conversions with process time for the decomposition of sec-butyl acetate on NiY at 140°C; feed rates are 0.0177 ( ), 0.0292 ( ), 0.0806 ( ) and 0.156 ( ) gm. mole ester feed/ hr./gm. catalyst.

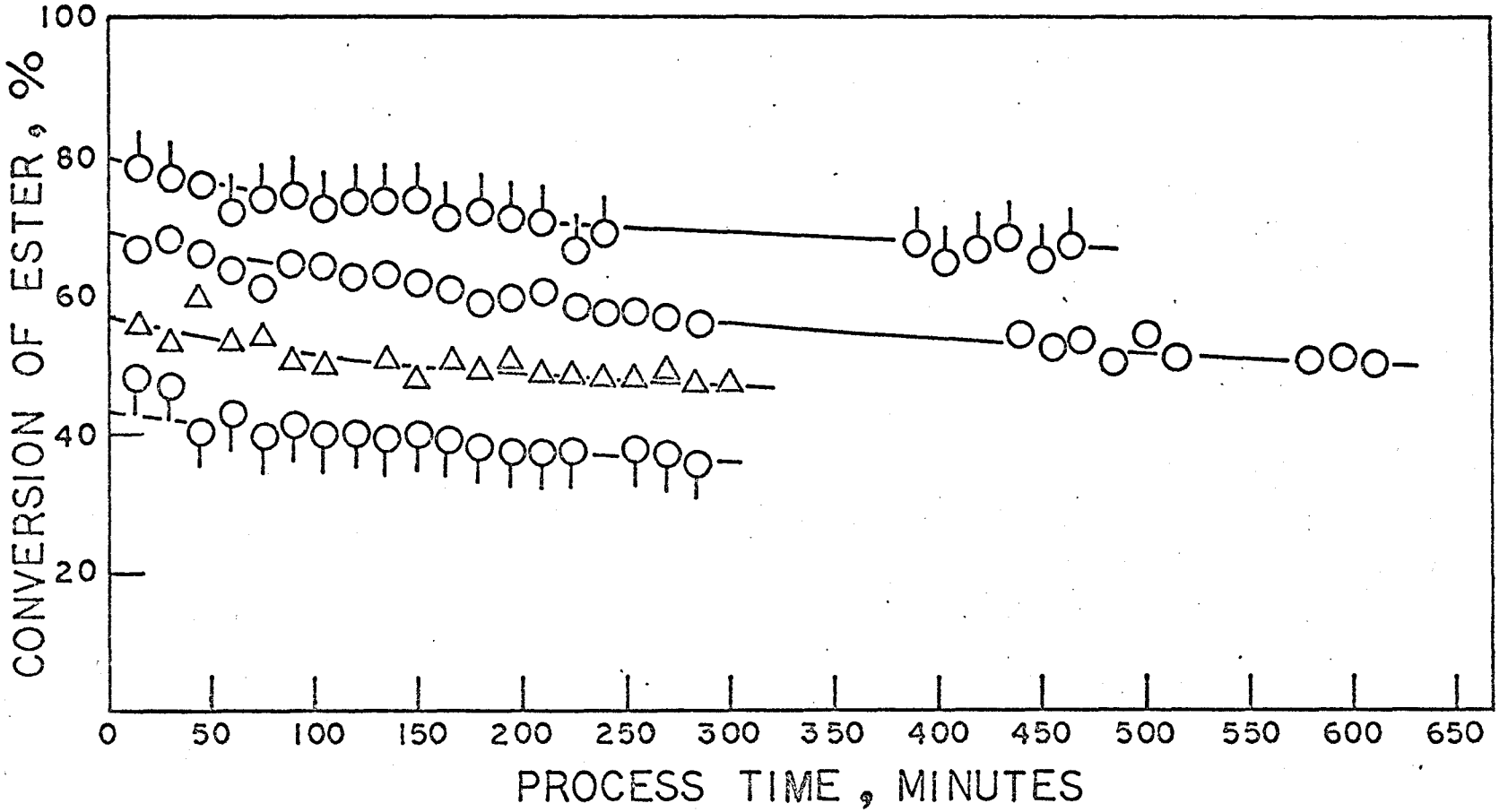

Fig. 6-6 The change of conversions with process time for the decomposition of sec-butyl acetate on NiY at 170°C; feed rates are 0.0149 ( ), 0.0315 ( ), 0.0610 ( ) and 0.134 ( ) gm. mole ester feed/hr./gm. catalyst.

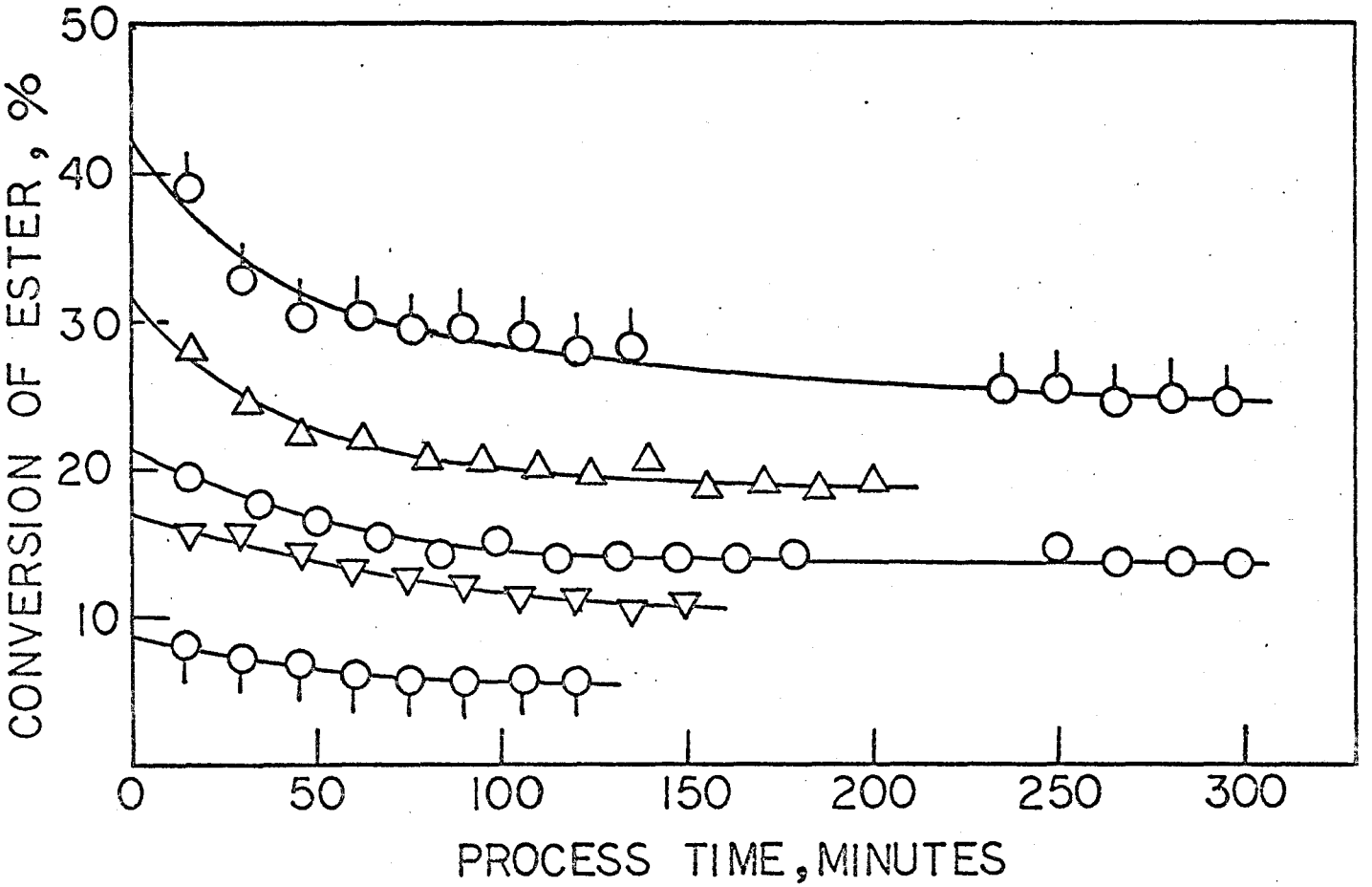

Fig. 6-7 Change of conversions with process time for the decomposition of sec-butyl acetate on silica-alumina at 140°C; feed rates are 0.0101 (○), 0.0187 (△), 0.0356 (○), 0.0526 (▽) and 0.204 (○) gm. mole ester feed/hr./gm. catalyst.

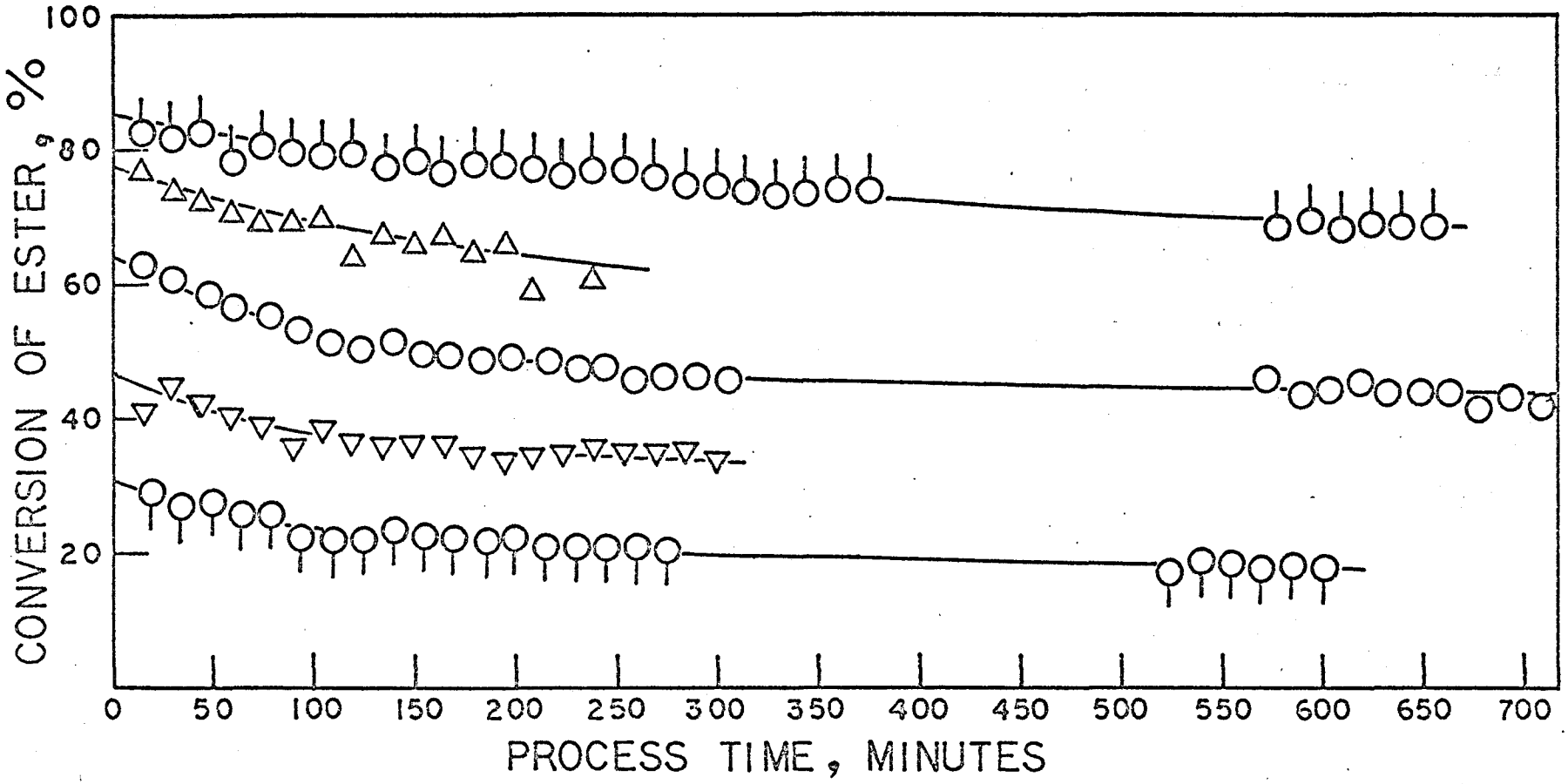

Fig. 6-8 Change of conversions with process time for the decomposition of sec-butyl acetate on silica-alumina at 170°C; feed rates are 0.0155 ( ), 0.0257 (△), 0.0427 (○), 0.0923 (▽) and 0.188 ( ) gm. mole ester feed/hr./gm. catalyst.

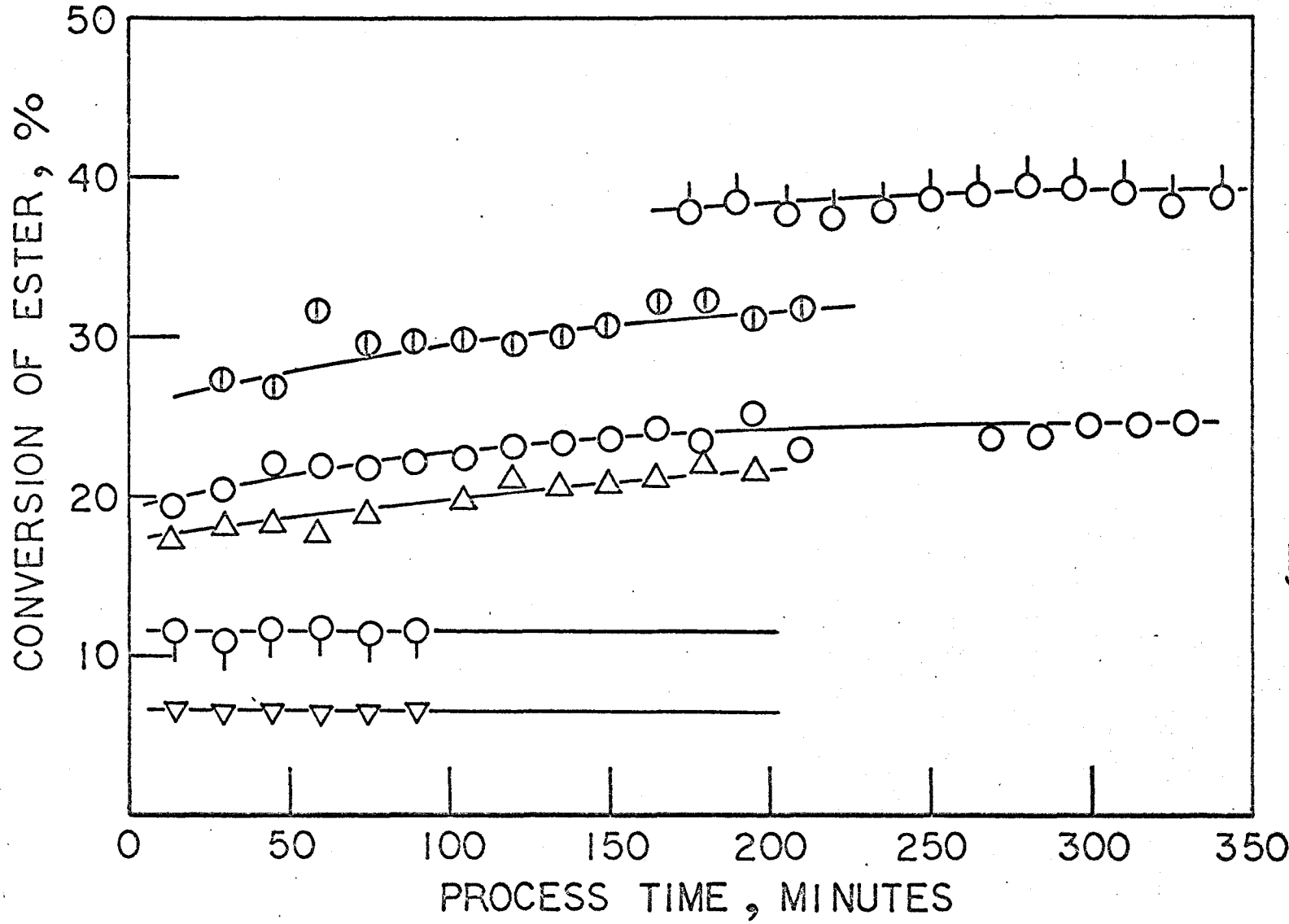

Fig. 6-9 Change of conversions with process time for the decomposition of sec-butyl acetate on AgY at 140°C, feed rates are 0.0178 (○), 0.0314 (◐), 0.0382 (○), 0.0690 (△), 0.172 (○) and 0.345 (▽) gm. mole ester feed/hr./gm. catalyst.

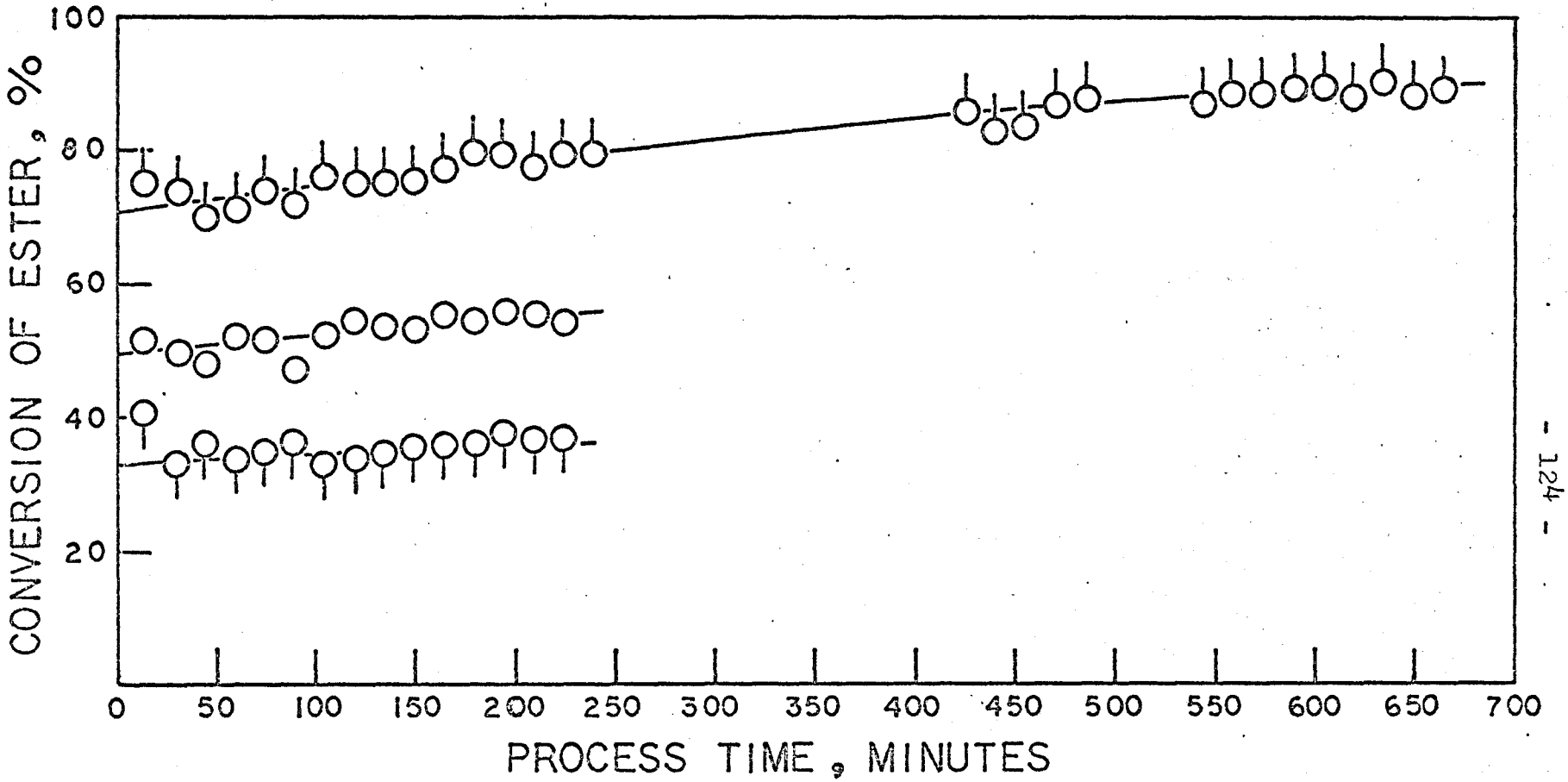

Fig. 6-10 Change of conversions with process time for the decomposition of sec-butyl acetate on AgY at 170°C; feed rates are 0.0389 ( ), 0.0707 ( ) and 0.193 ( ) gm. mole ester feed/hr./gm. catalyst.

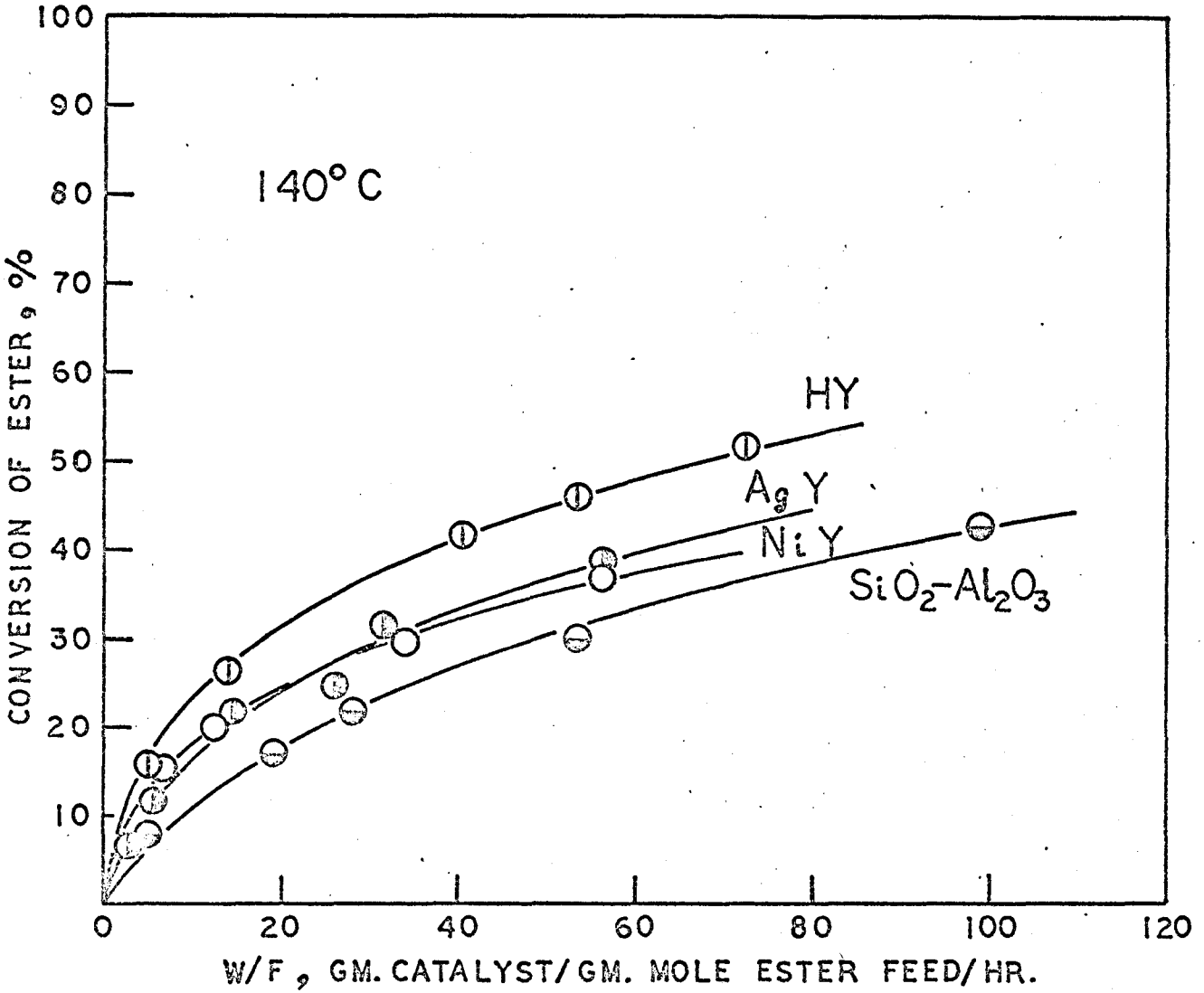

Fig. 6-11 Decomposition of sec-butyl acetate on HY (⊕), NiY (○), AgY (◑) and silica-alumina (⊖) at 140°C. The curves were obtained integrating the rate equation,

$$r = \frac{k/E\ P_e}{(P_e + (A/E)P_a)^2}.$$

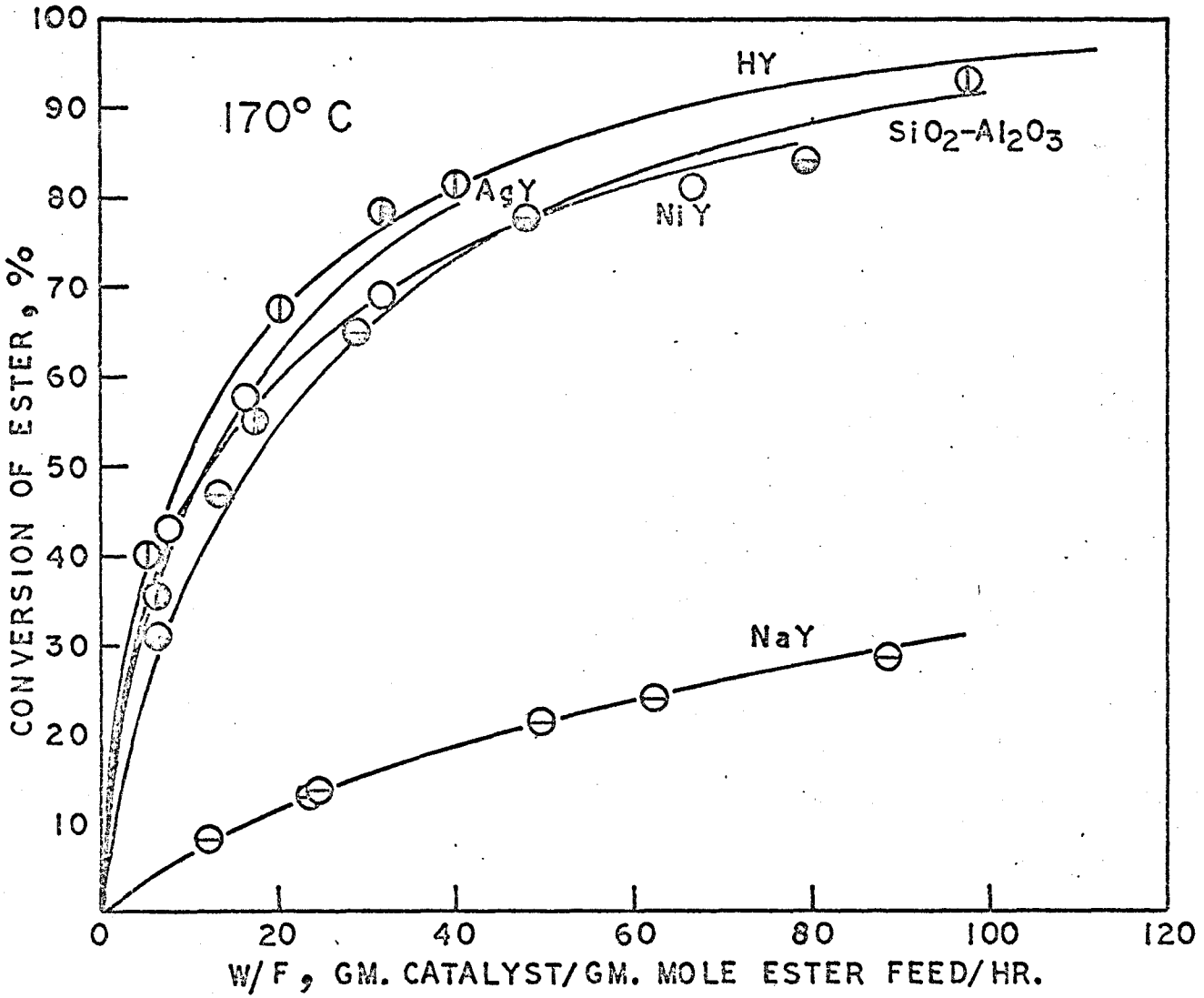

Fig. 6-12 Decomposition of sec-butyl acetate on HY (⊖), NiY (○), AgY (◑), NaY (⊖) and silica-alumina (⊖) at 170°C. The curves were obtained integrating the rate equation,

$$r = \frac{k/F\ P_e}{(P_e + (A/E)P_a)^2}.$$

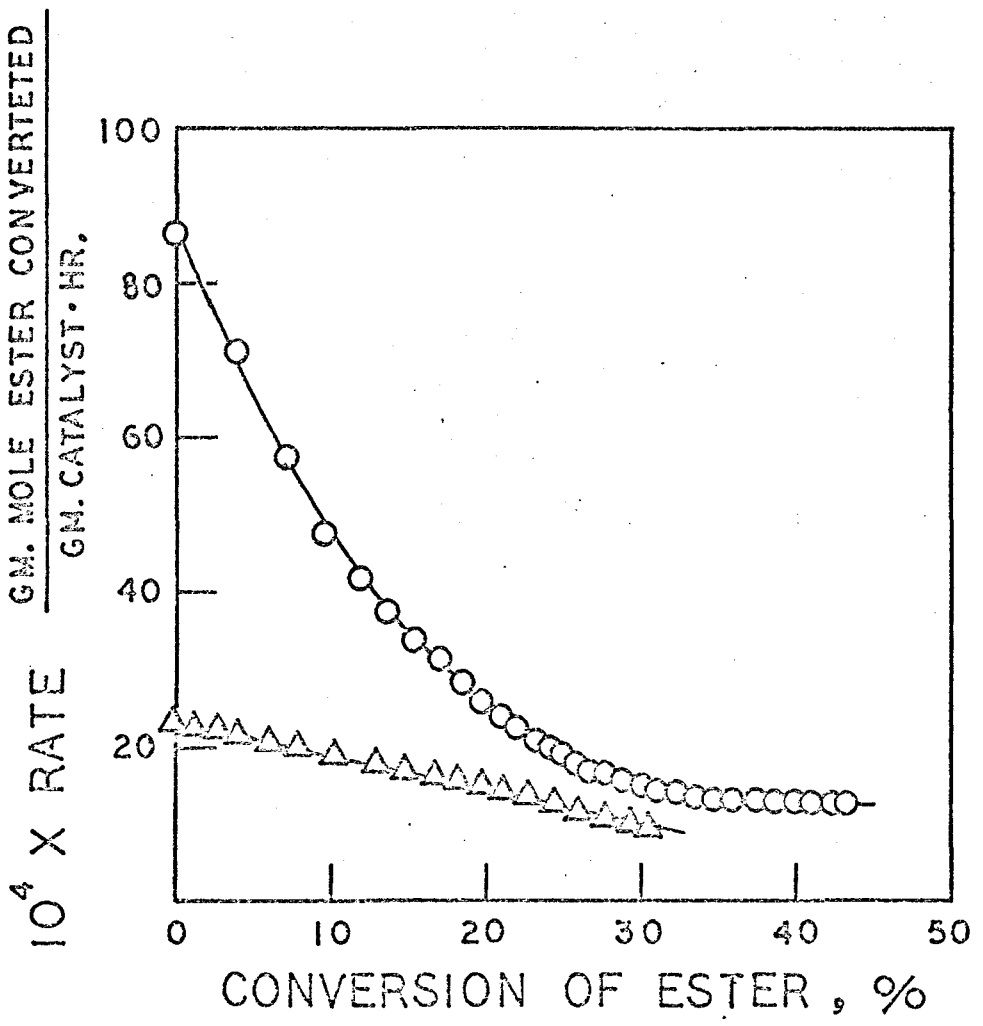

Fig. 6-13 Differential reaction rates for pure (O) and 81.87 mole % sec-butyl acetate (Δ) on NaY at 170°C.

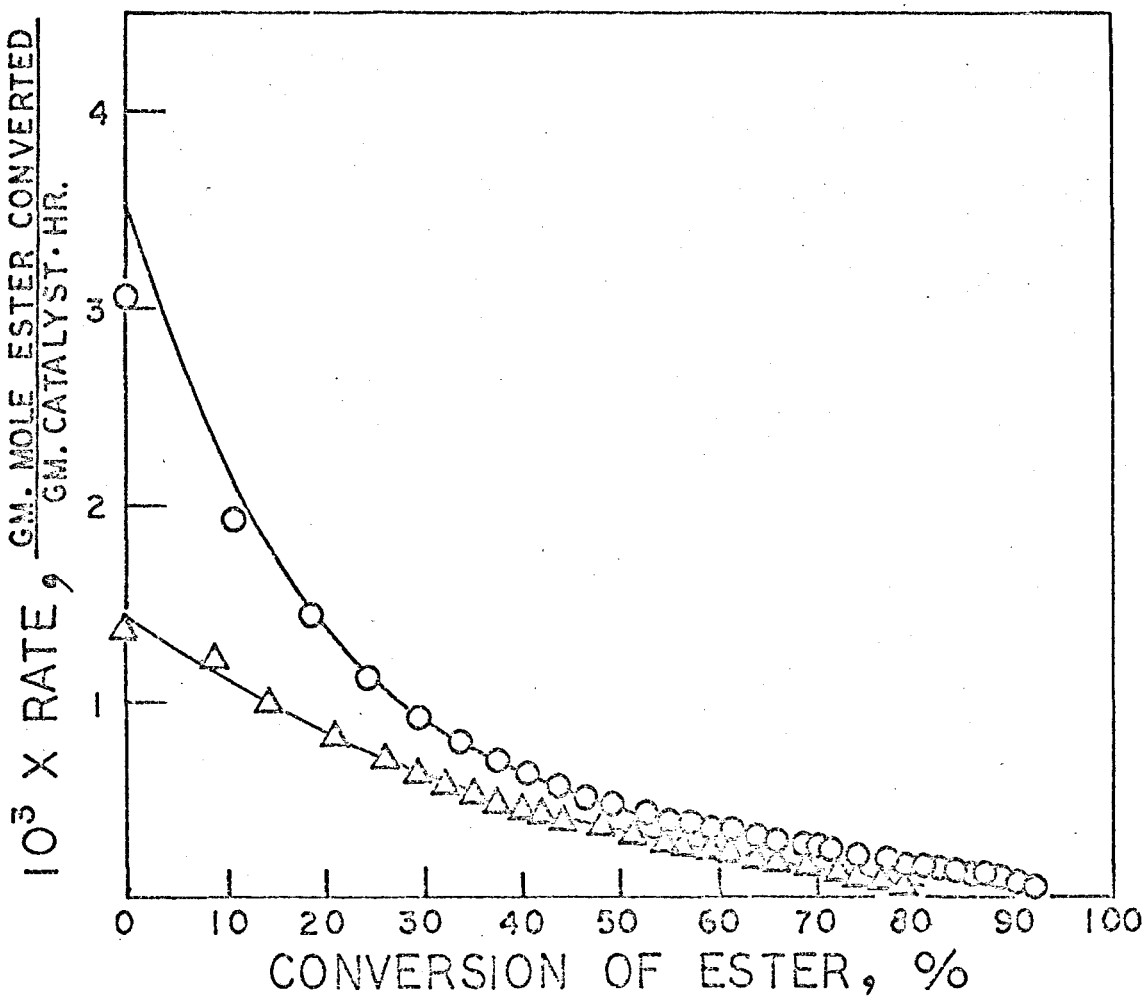

Fig. 6-14 Differential reaction rates for pure (O) and 81.87 mole % sec-butyl acetate (Δ) on NaY at 190°C.

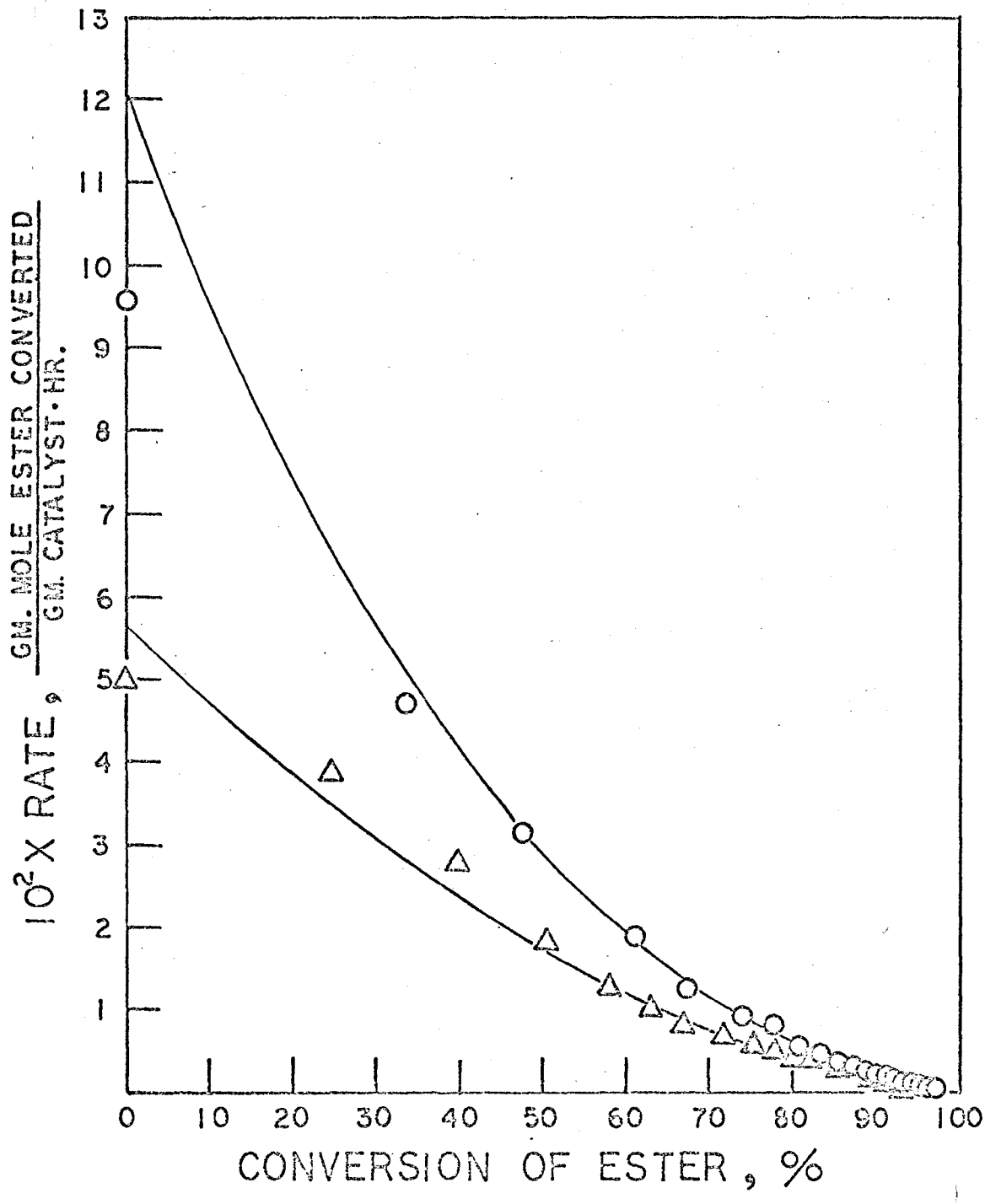

Fig. 6-15 Differential reaction rates for pure (O) and 81.87 mole % sec-butyl acetate (Δ) on NaY at 210°C.

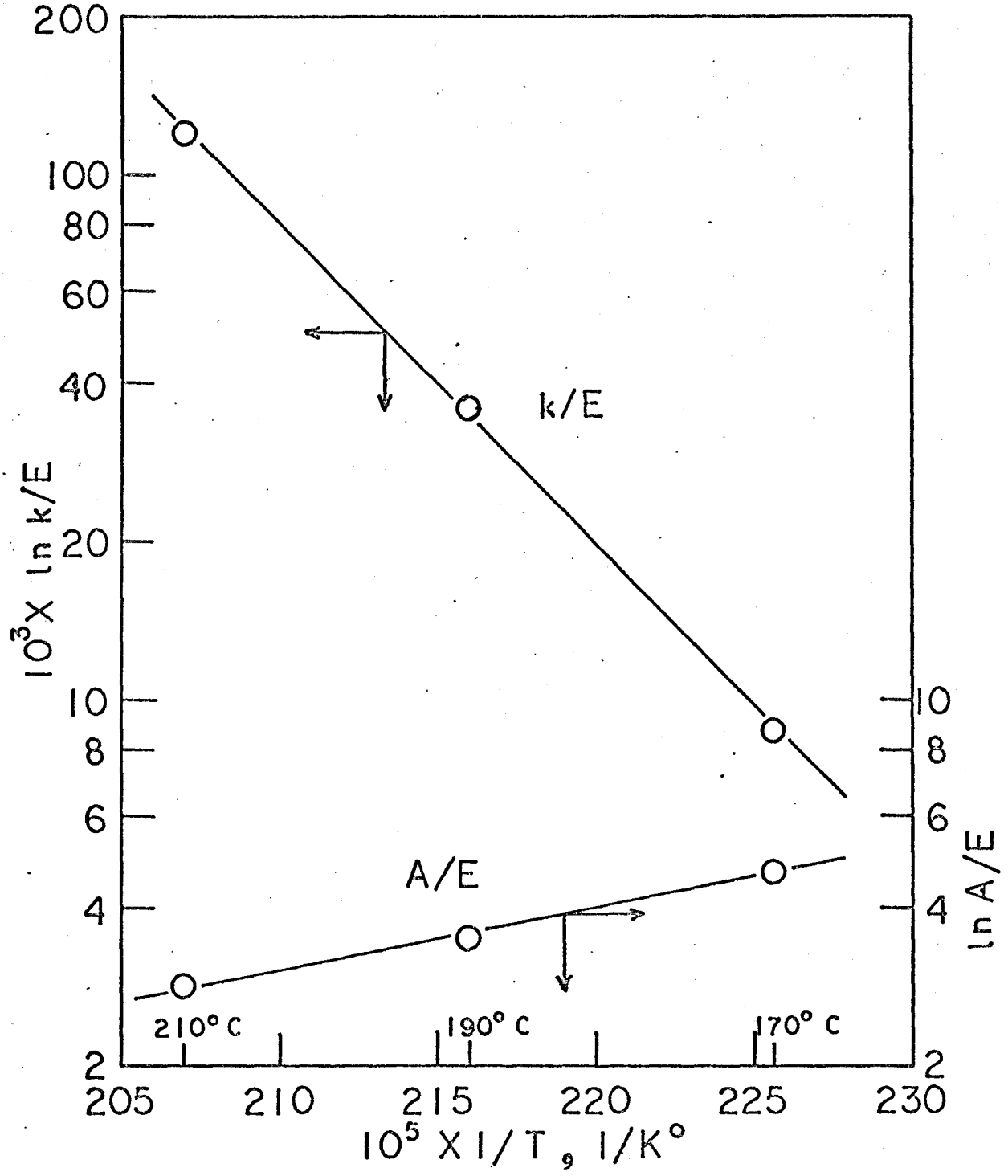

Fig. 6-16 Arrhenius plots of kinetic constants for the decomposition of sec-butyl acetate on NaY.

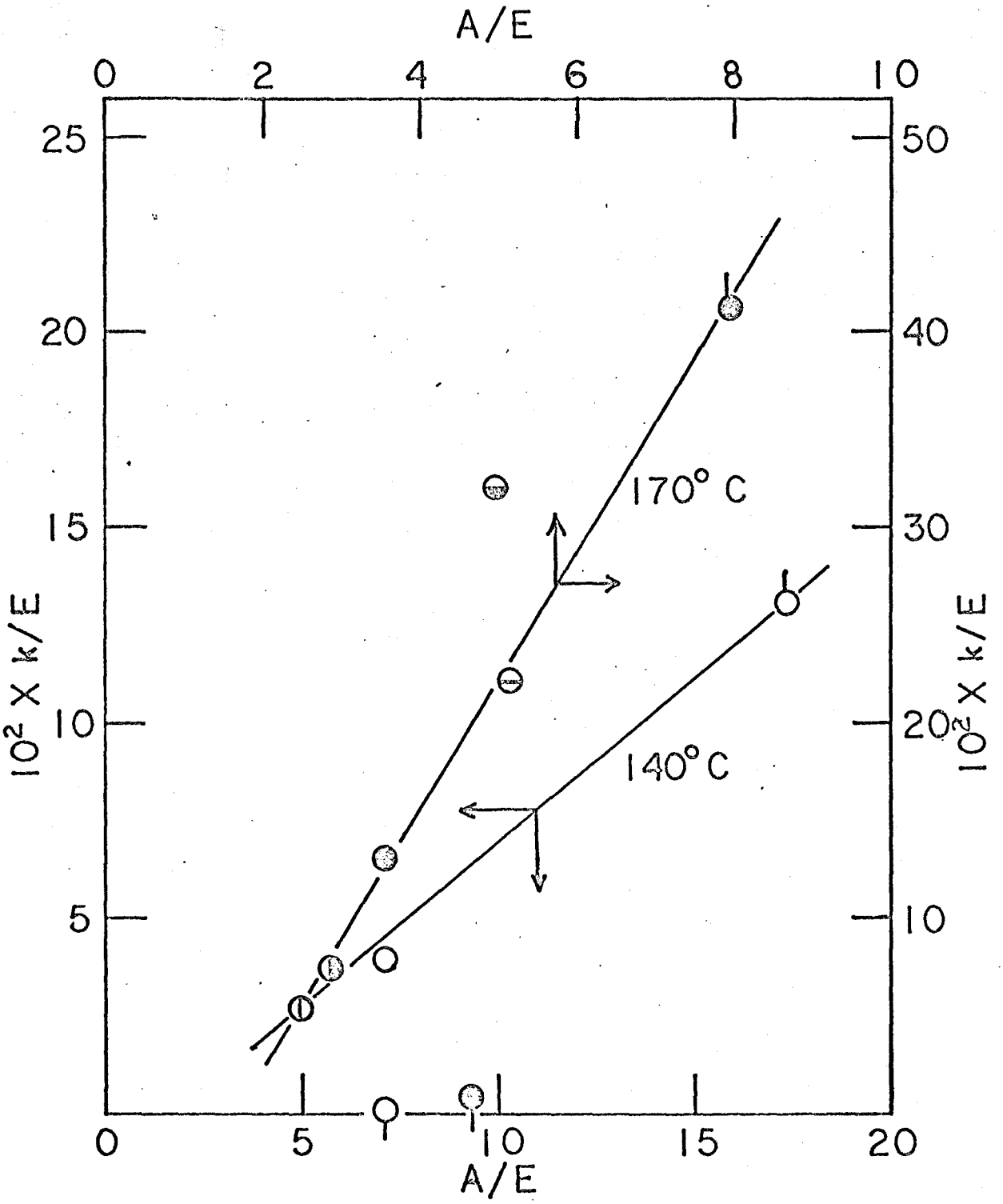

Fig. 6-17 Relation between k/E and A/E for NaY ( ), HY ( ), NiY ( ), AgY ( ) and silica-alumina ( ) at 140°C and for NaY ( ), HY ( ), NiY ( ), AgY ( ) and silica-alumina ( ) at 170°C.

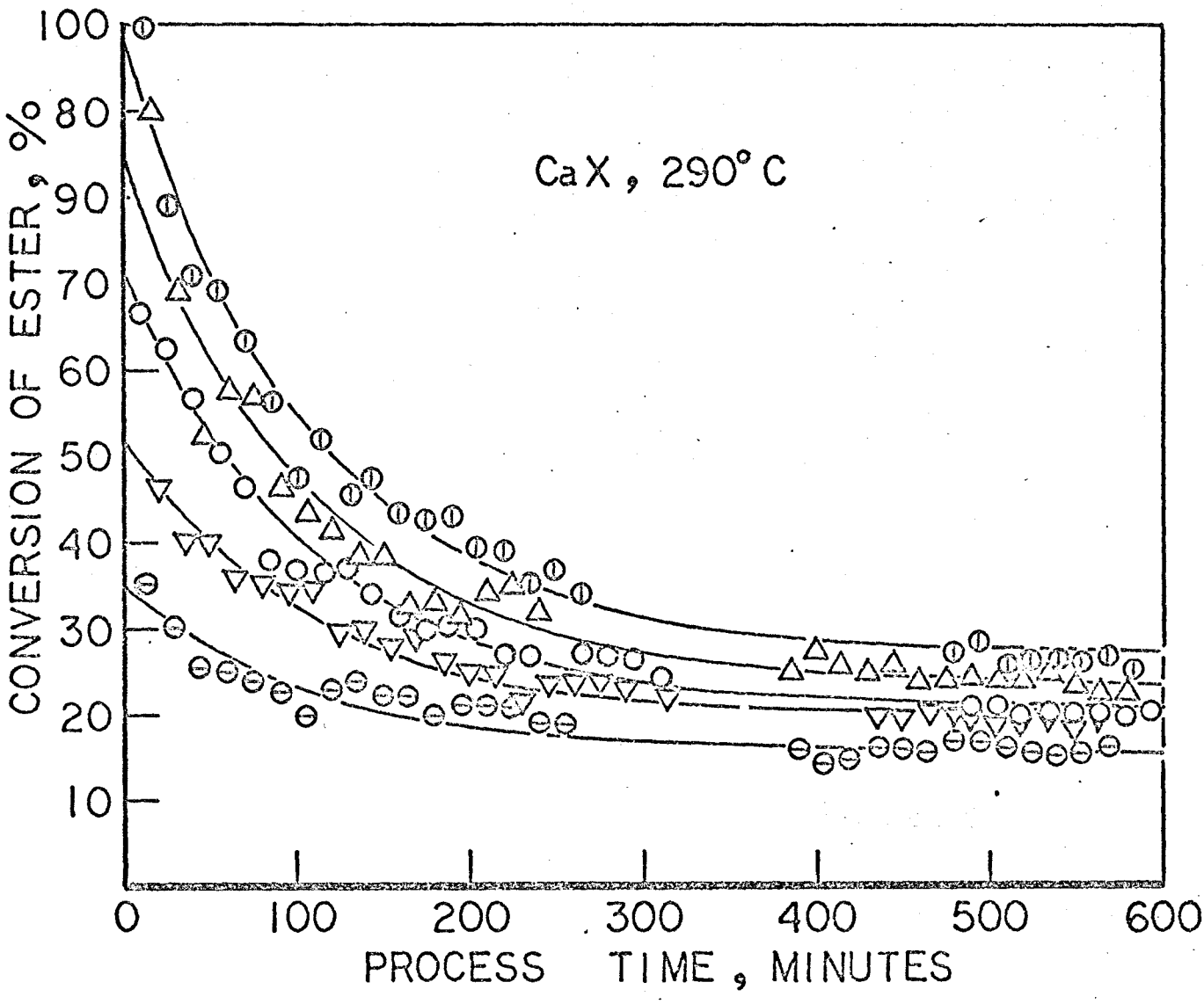

Fig. 7-1 Change of conversions with process time for the decomposition of n-butyl acetate on CaX at 290°C; feed rates are 0.00733 (Φ), 0.0115 (Δ), 0.0177 (O), 0.0442 (∇) and 0.111 (Θ) gm. mole ester feed/hr./gm. catalyst.

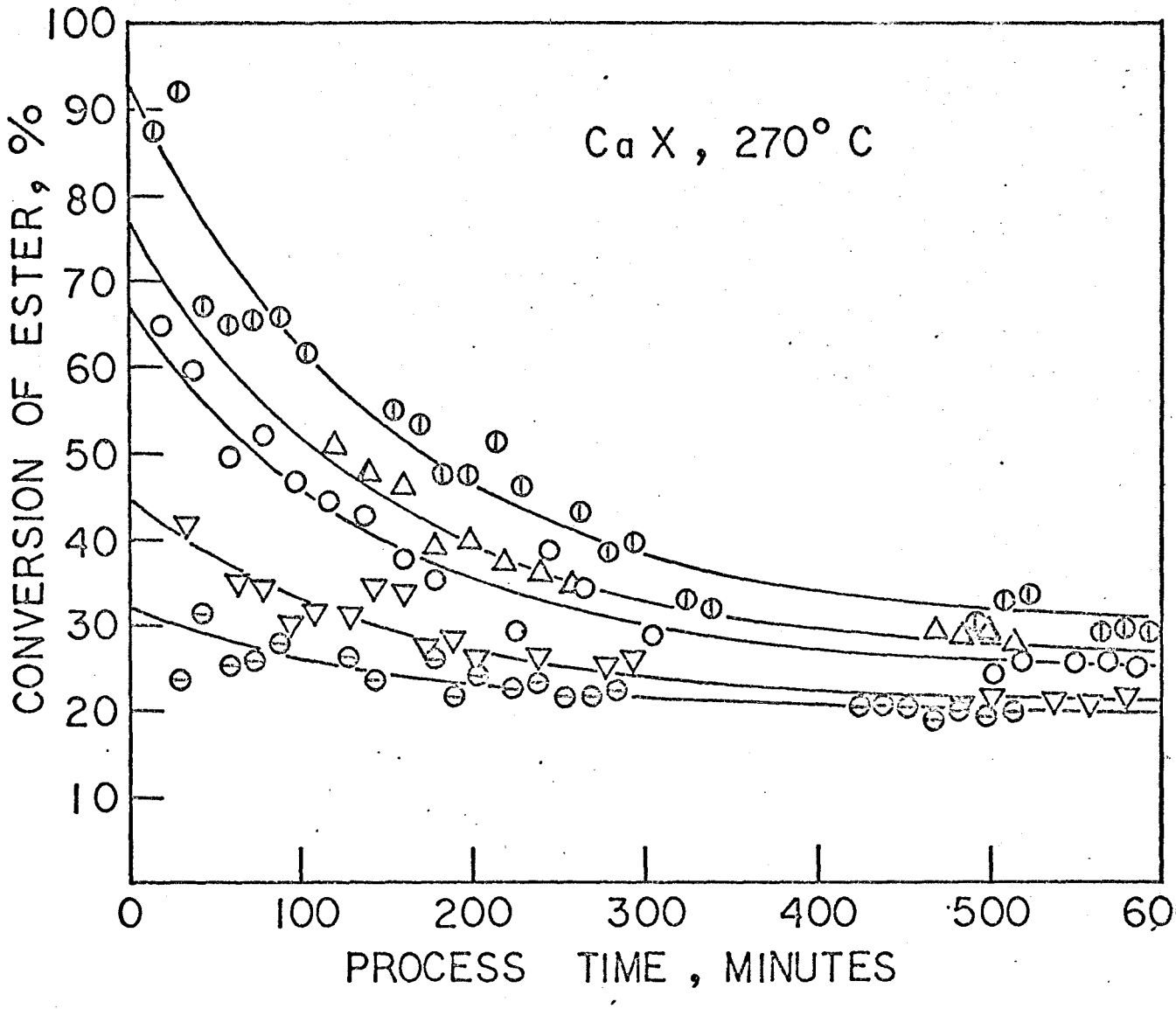

Fig. 7-2 Change of conversions with process time for the decomposition of n-butyl acetate on CaX at 270°C; feed rates are 0.00488 (Φ), 0.00993 (Δ), 0.0137 (O), 0.0254 (∇) and 0.0377 (Θ) gm. mole ester feed/hr./gm. catalyst.

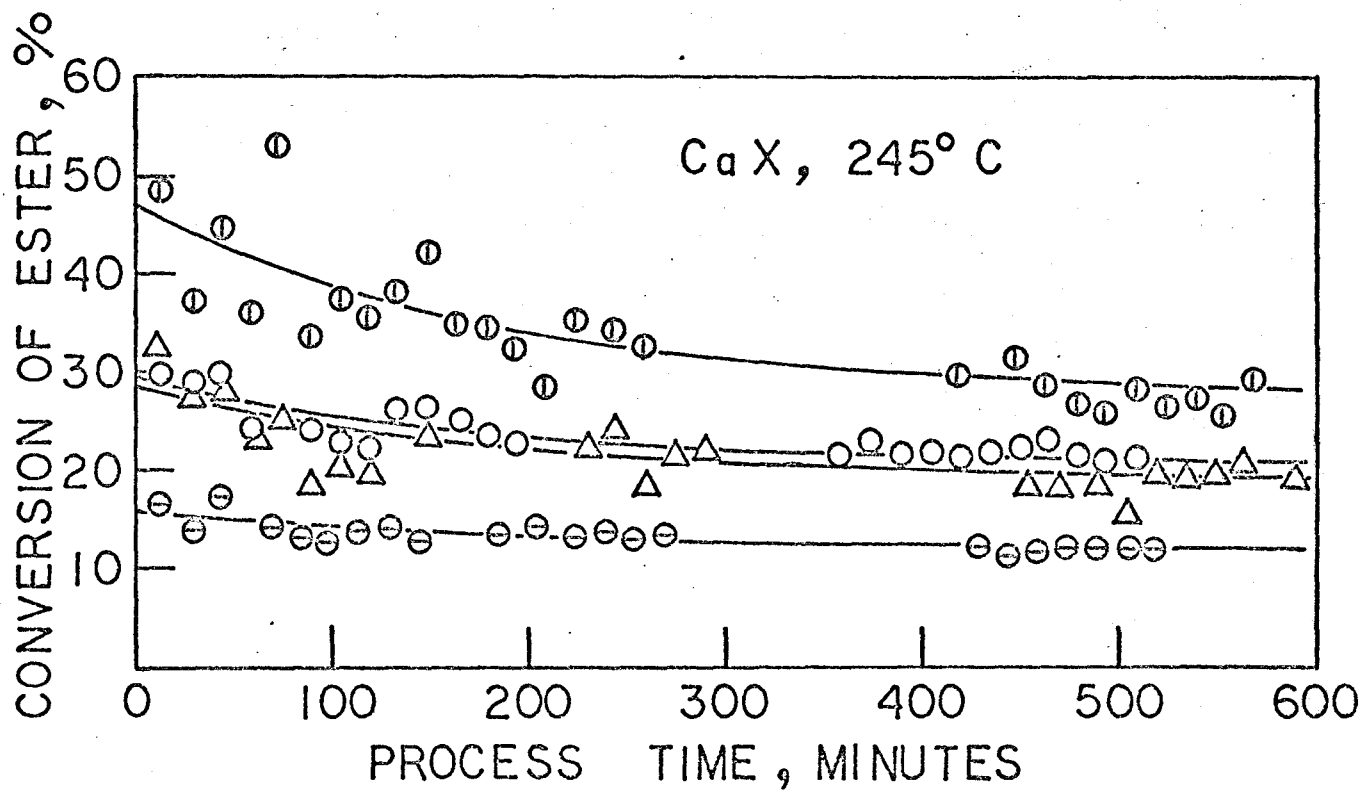

Fig. 7-3 Change of conversions with process time for the decomposition of n-butyl acetate on CaX at 245°C; feed rates are 0.00509 (Φ), 0.00949 (O), 0.0104 (Δ) and 0.0231 (Θ) gm. mole ester feed/ hr./gm. catalyst.

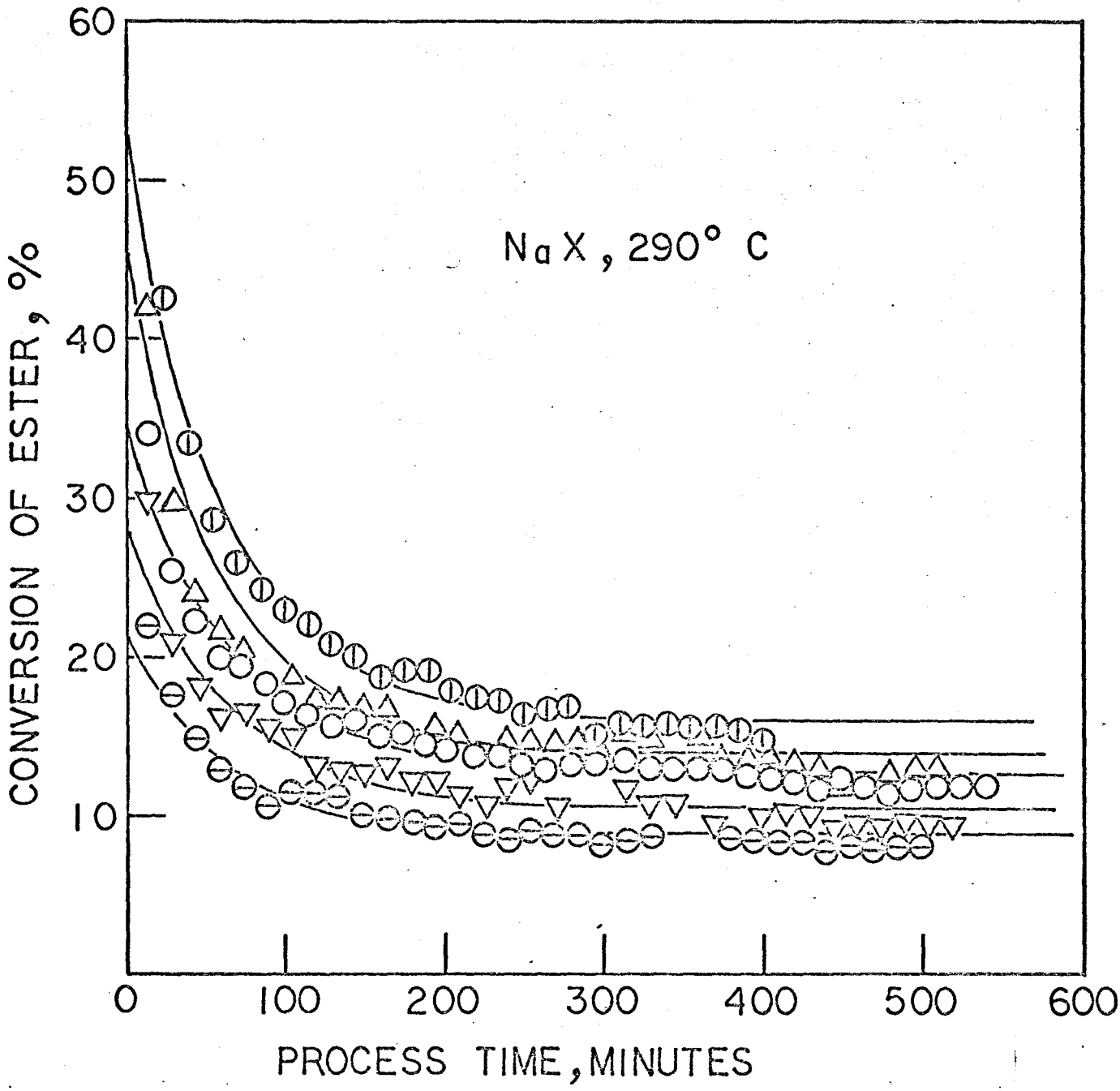

Fig. 7-4 Change of conversions with process time for the decomposition of n-butyl acetate on NaX at 290°C; feed rates are 0.00817 (Φ), 0.0109 (Δ), 0.0159 (O), 0.0241 (∇) and 0.0406 (Θ) gm. mole ester feed/hr./gm. catalyst.

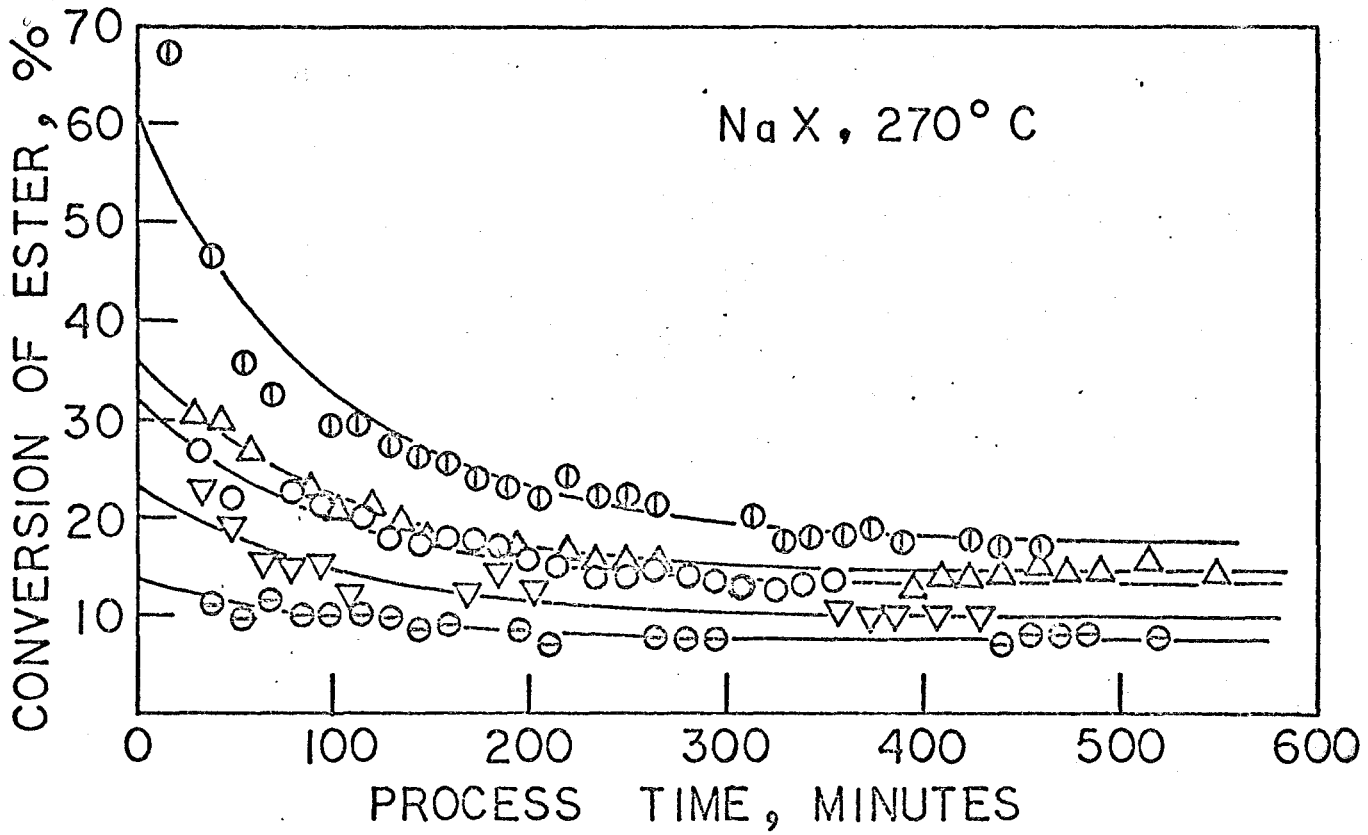

Fig. 7-5 Change of conversions with process time for the decomposition of n-butyl acetate on NaX at 270°C; feed rates are 0.00266 (Φ), 0.00458 (Δ), 0.00646 (O), 0.00955 (∇) and 0.0226 (Θ) gm. mole ester feed/hr./gm. catalyst.

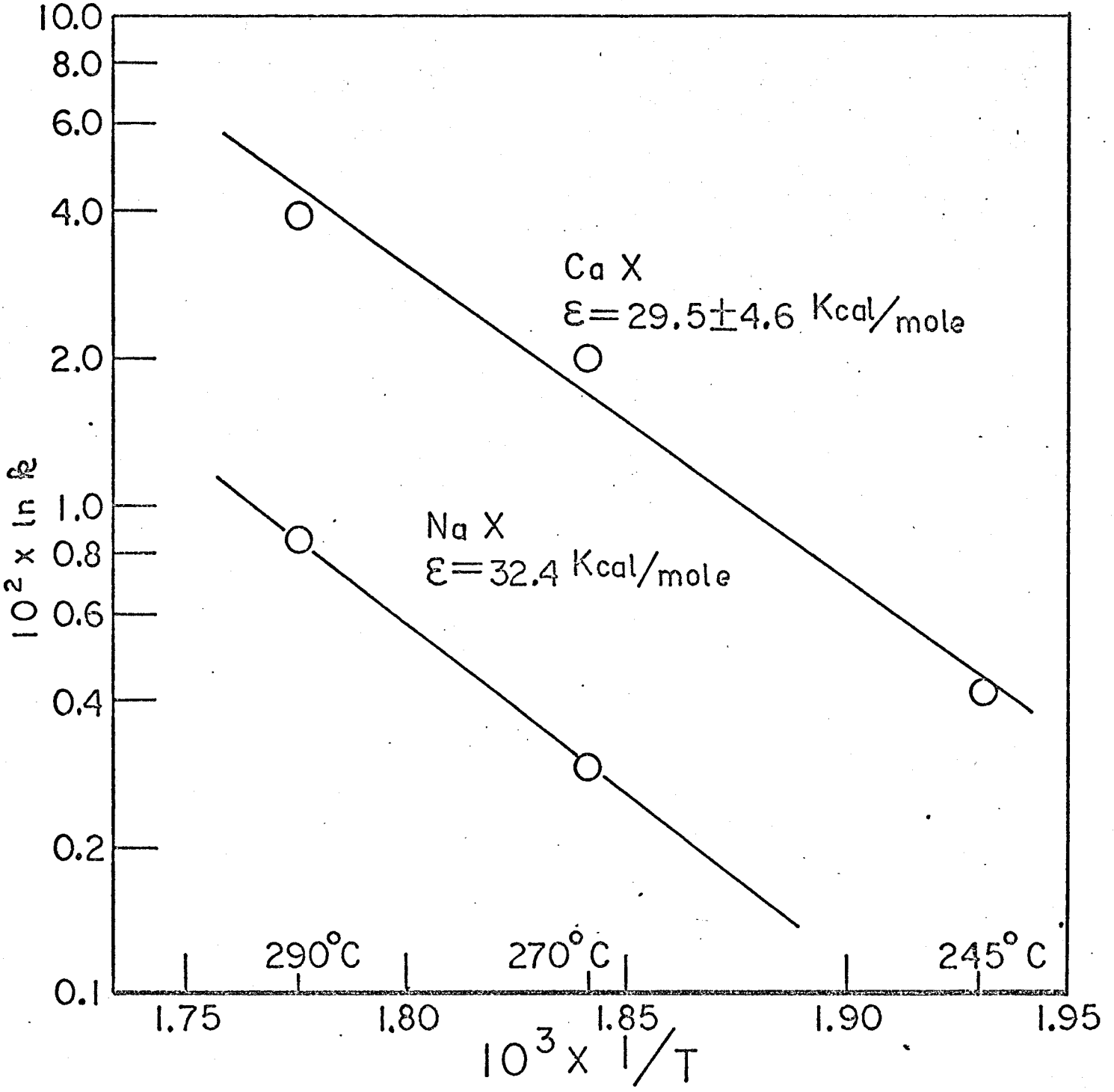

Fig. 7-6 Arrhenius plots of first-order rate constants for the decomposition of n-butyl acetate on NaX and CaX.

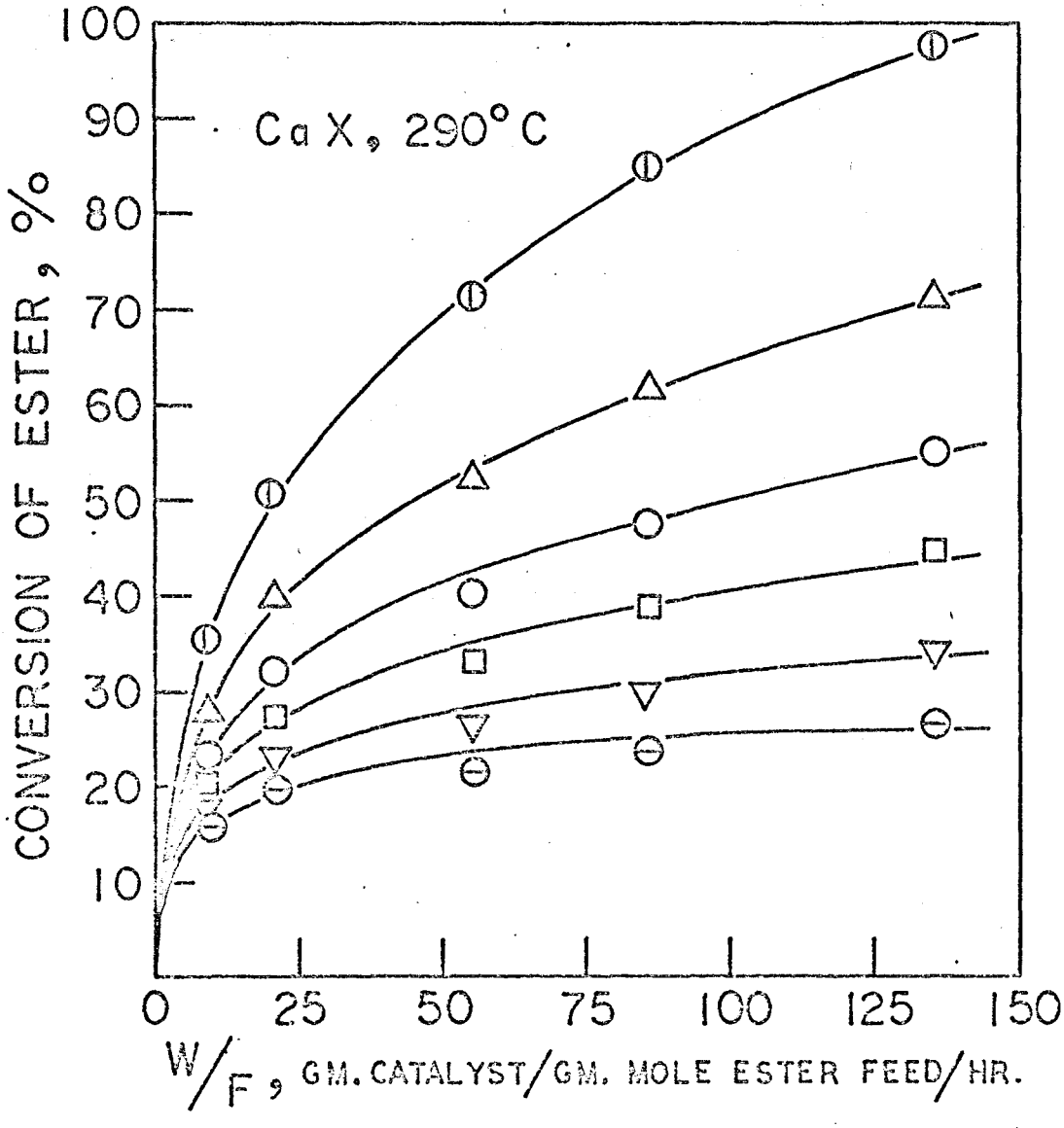

Fig. 7-7 Plots of conversion as a function of space time for constant process times for the decomposition of n-butyl acetate on CaX at 290°C. Process times are 0 (⏀), 50 (△), 100 (○), 150 (□), 250 (▽) and 500 (⊖) minutes.

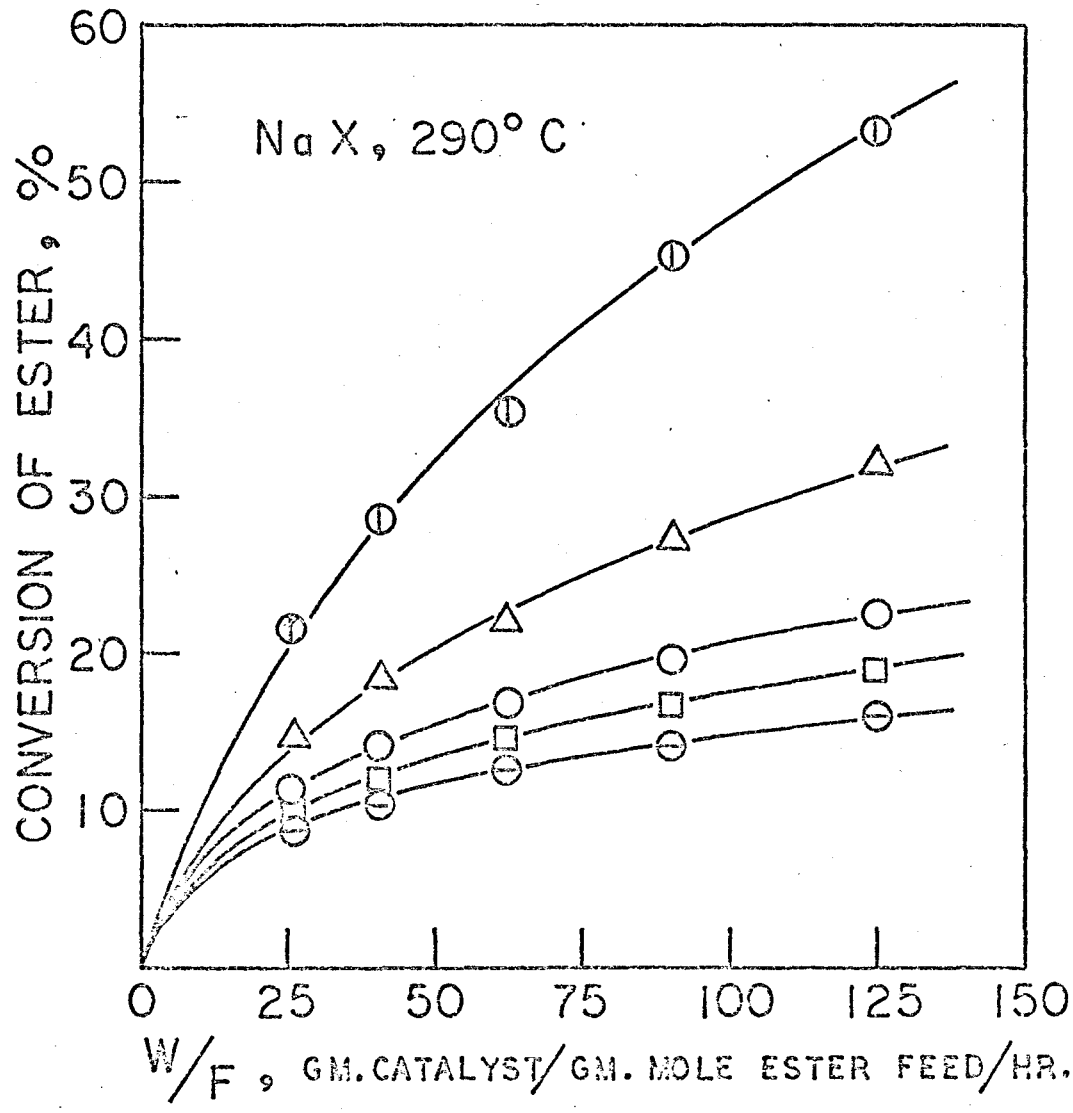

Fig. 7-8 Plots of conversion as a function of space time for constant process times for the decomposition of n-butyl acetate on NaX at 290°C. Process times are 0 (⏀), 50 (△), 100 (○), 150 (□) and 350 (⊖) minutes.

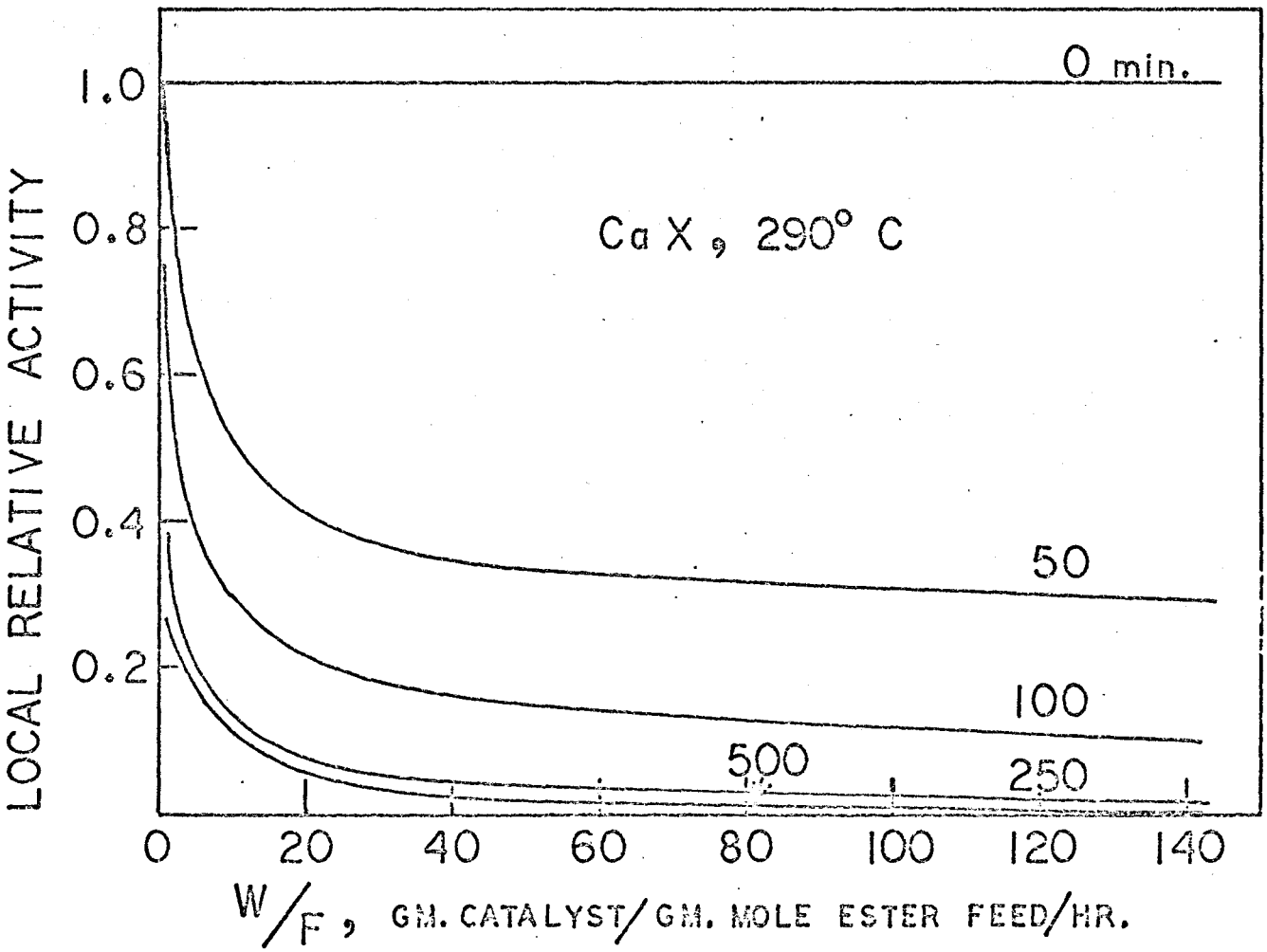

Fig. 7-9 Local relative activity as a function of space time for constant process times for the decomposition of n-butyl acetate on CaX at 290°C.

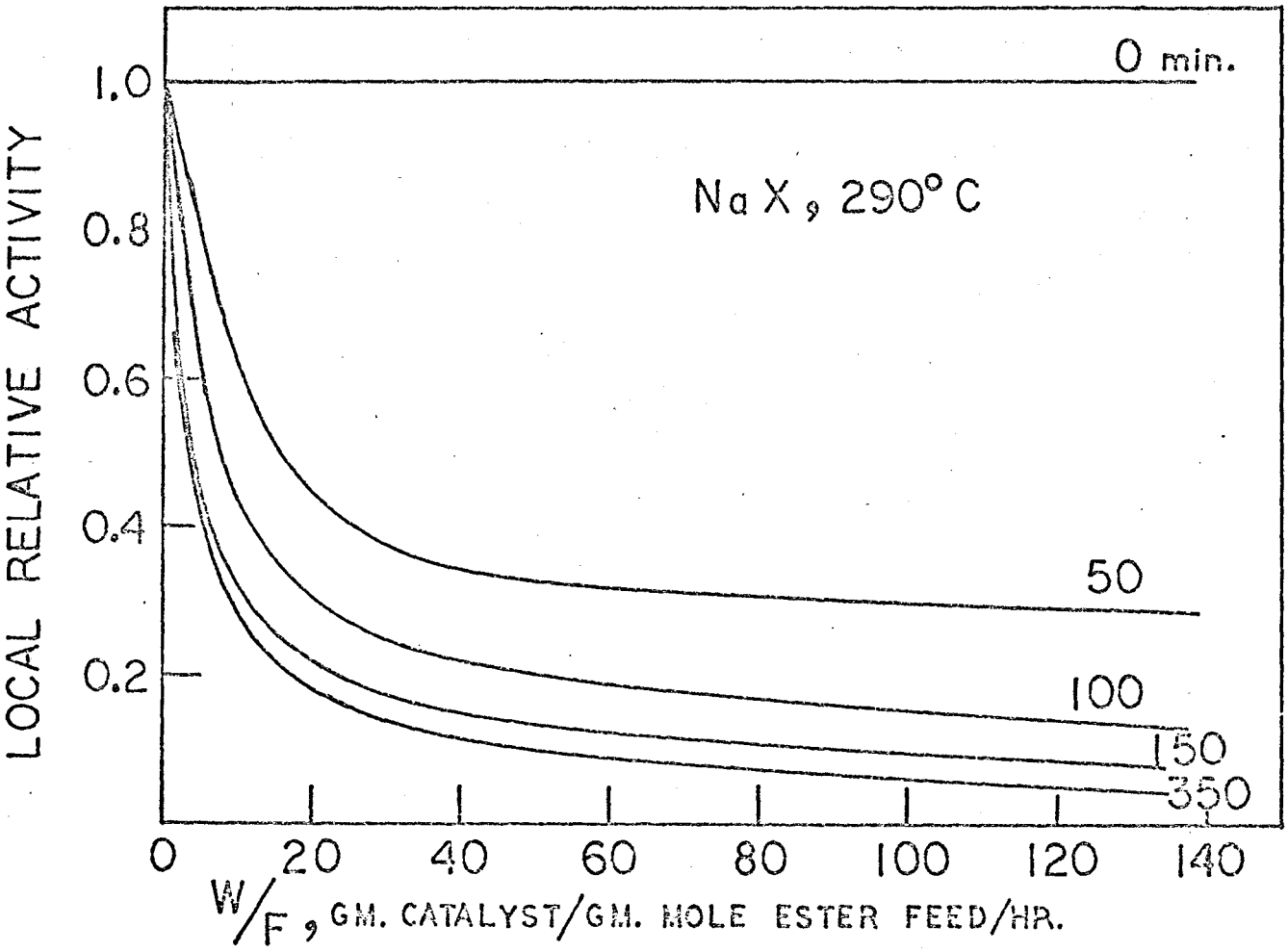

Fig. 7-10 Local relative activity as a function of space time for constant process times for the decomposition of n-butyl acetate on NaX at 290°C.

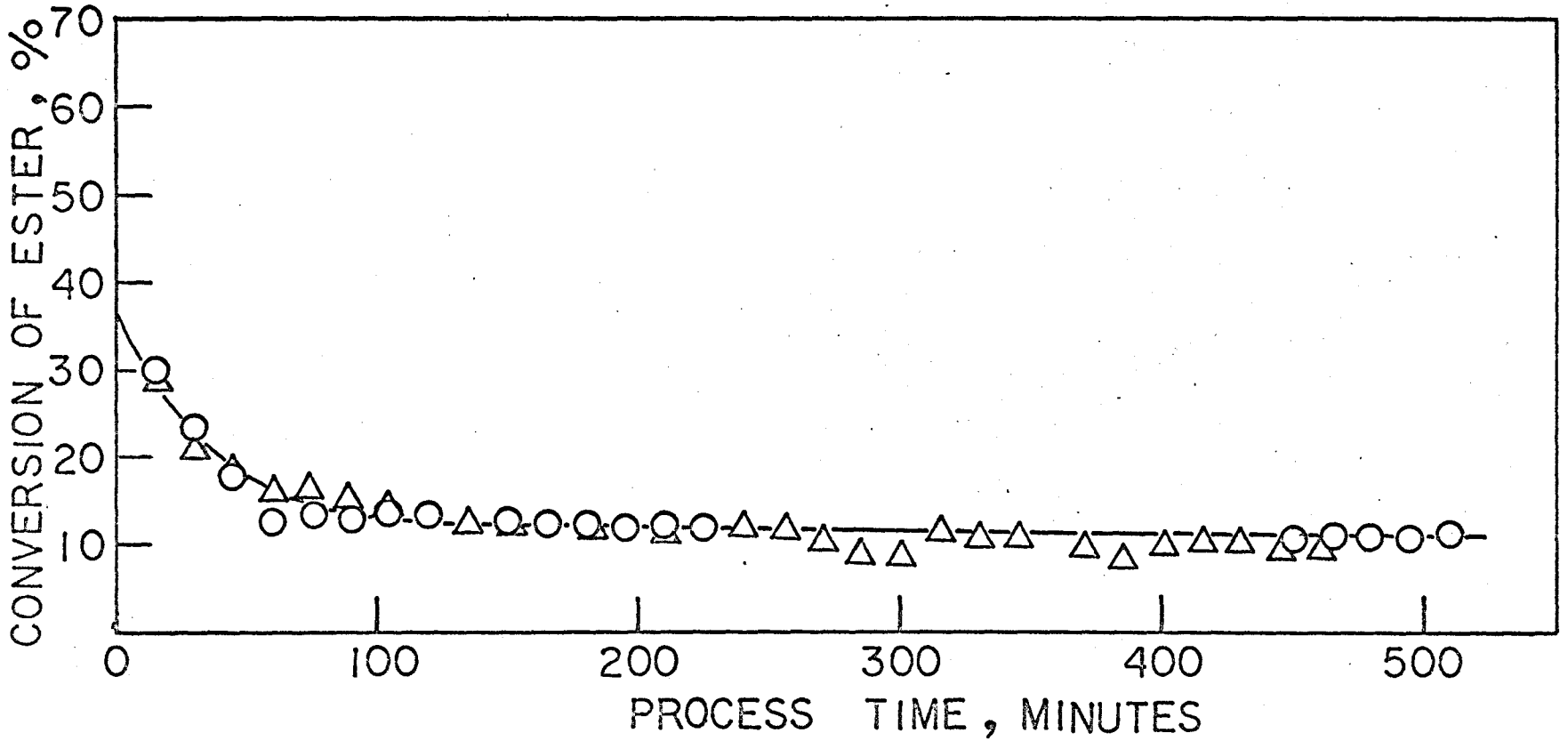

Fig. 7-11 Decomposition of n-butyl acetate on acetic acid treated NaX, Ac-NaX, (O) and fresh NaX (Δ) at 290°C.

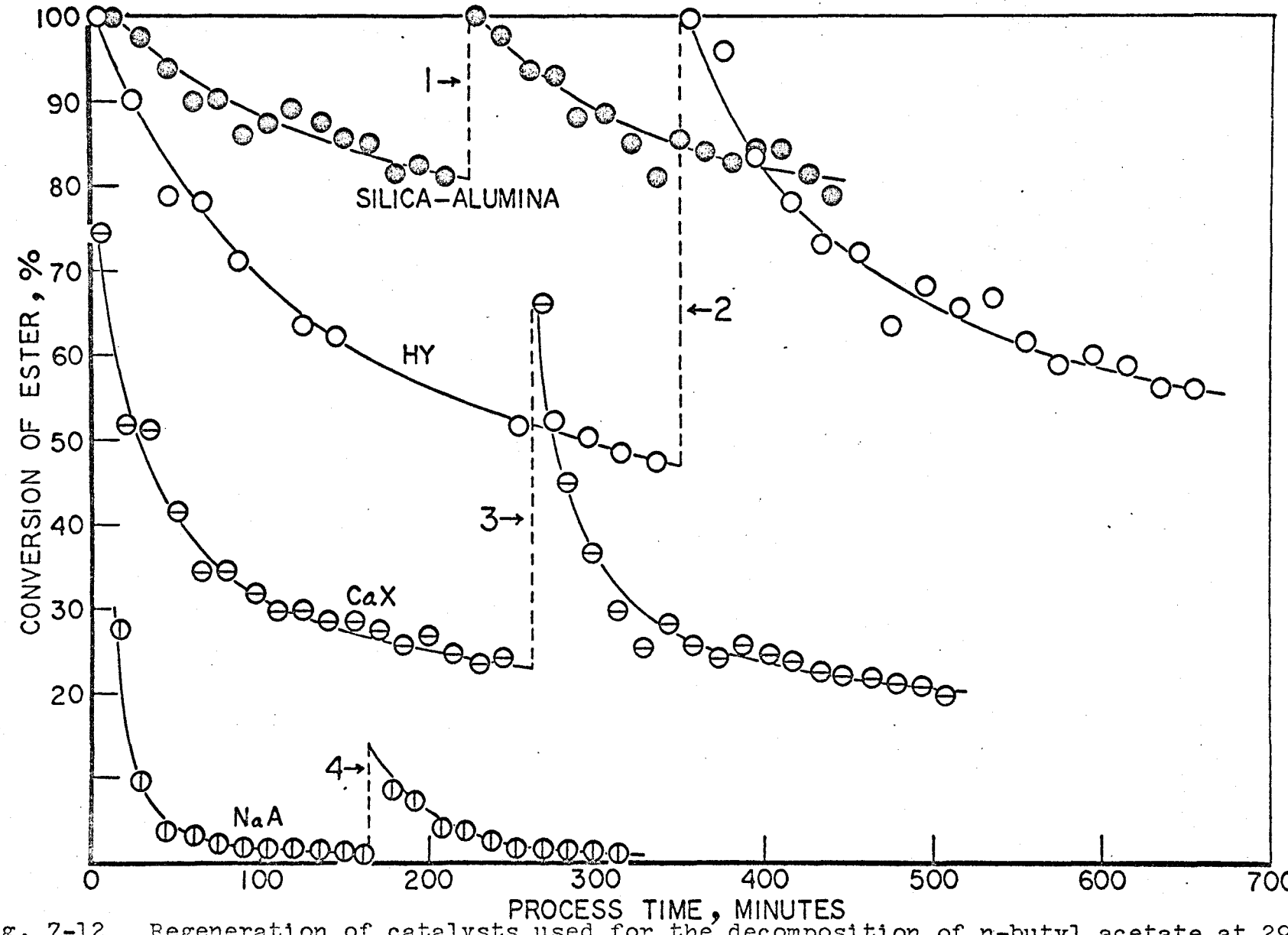

Fig. 7-12 Regeneration of catalysts used for the decomposition of n-butyl acetate at 290°C. All tests were done on one gram catalyst at feed rate 0.0341 gm. mole ester feed/hr. 1: Air was passed over the catalyst at 290°C for 19 hours. 2: Air was passed over the catalyst at 468°C for 16 hours. 3: Air was passed over the catalyst at 454°C for 16 hours. 4: Helium was passed over the catalyst at 290°C for 21.5 hours.

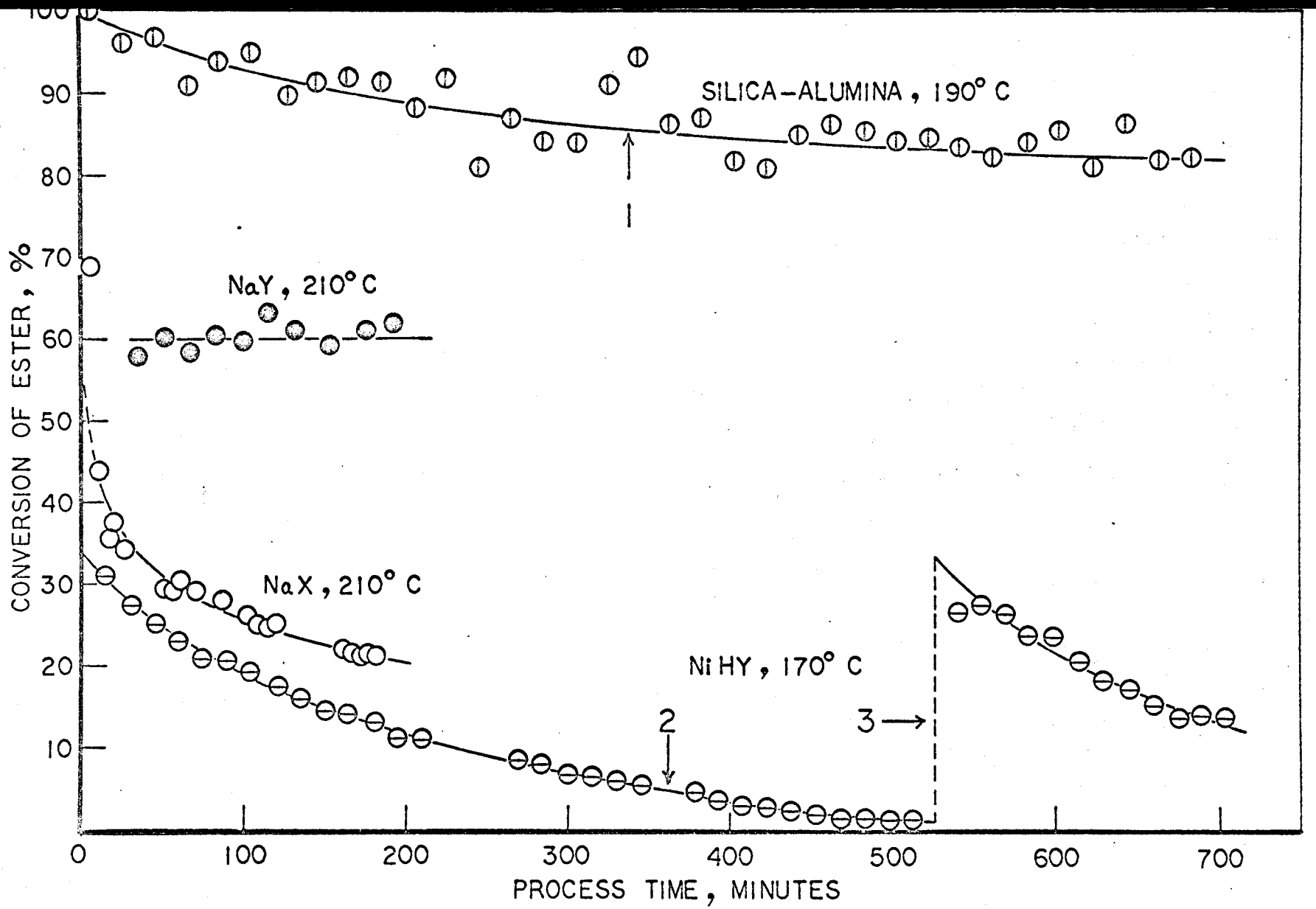

Fig. 7-13 Decomposition of sec-butyl acetate over silica-alumina (1.00 gm.), NaY (0.50 gm.), NaX (3.95 gm.) and NiHY (0.14 gm.) at feed rate 0.0338 gm. mole ester feed/hr. 1: Helium was passed over the catalyst at 190°C for 15 hours. 2: Helium was passed over the catalyst at 170°C for 17 hours. 3: Air was passed over the catalyst at 461°C for 8 hours.

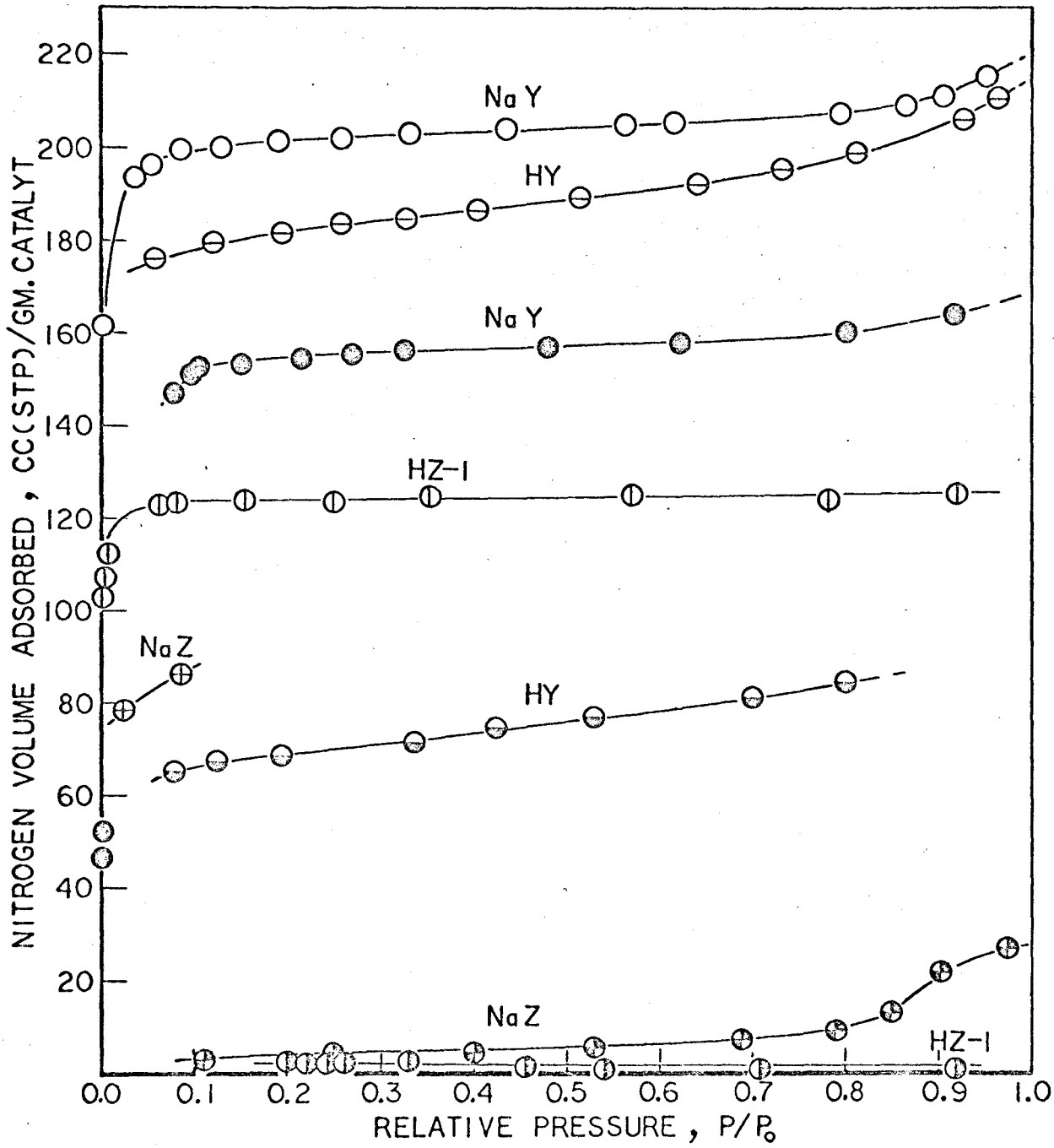

Fig. 7-14 Nitrogen adsorption isotherms on used catalysts at -195°C. Catalysts are before burning the deposit: NaY (⊙), HY (⊖), HZ-1 (◐) and NaZ (⊕), and after burning the deposit: NaY (O), HY (⊖), HZ-1 (◐) and NaZ (⊕).

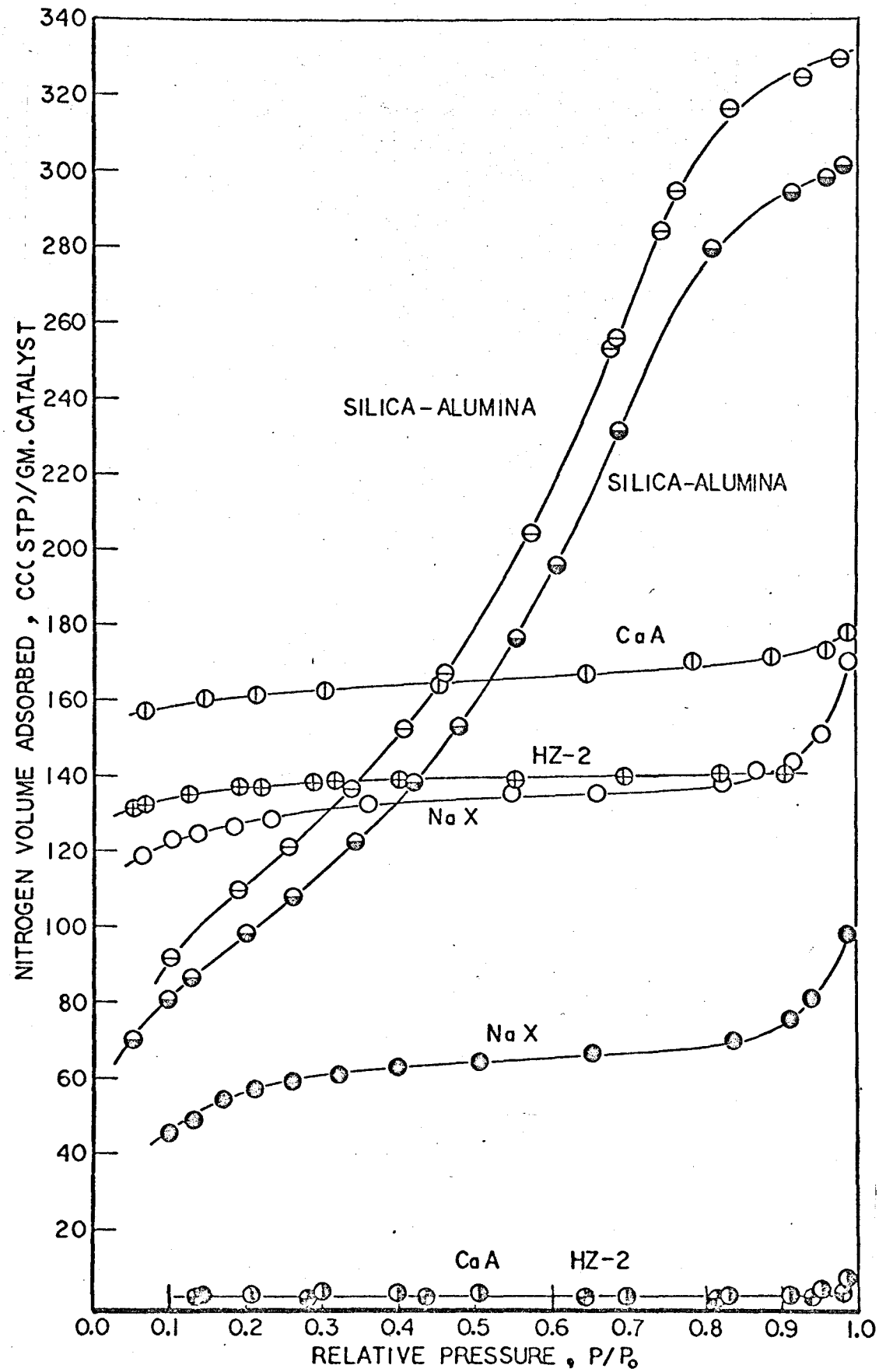

Fig. 7-15 Nitrogen adsorption isotherms on used catalysts at -195°C. Catalysts are before burning the deposit: silica-alumina (⊖), CaA (◐), HZ-2 (⊕) and NaX (◑), and after burning the deposit: silica-alumina (⊖), CaA (◐), HZ-2 (⊕), and NaX (○).

Table 2-1

Properties of Synthetic Zeolites (12)

Name	Composition	Symmetry and Cell Dimensions	Density[a] g/cm^2	Void Volume[b] cm^2/g	Aperture Size Å
NaA	$Na_{12}((AlO_2)_{12}(SiO_2)_{12})\cdot 27H_2O$	Cubic a=12.32 Å	1.33	0.30	4.2
NaX	$Na_{86}((AlO_2)_{86}(SiO_2)_{106})\cdot 264H_2O$	Cubic a=24.95 Å	1.29	0.36	8
NaY	$Na_{56}((AlO_2)_{56}(SiO_2)_{136})\cdot 264H_2O$	Cubic a=24.7 Å	1.30	0.35	8
Na mordenite	$Na_8((AlO_2)_8(SiO_2)_{40})\cdot 24H_2O$	Orthorhombic a=18.13 Å b=20.49 Å c= 7.52 Å	1.72	0.14	6.6

a) Calculated for dehydrated zeolite.

b) Based on amount of water contained per gram of dehydrated zeolite.

Table 2-2

Molecular Sieve Effects of Type A and X Zeolites (80)

Molecular sizes (13) in Å are given in brackets.

Adsorbed on NaA, CaA, CaX, and NaX	Adsorbed on CaA, CaX, and NaX, but not on NaA	Adsorbed on CaX and NaX, but not on NaA or CaA
Water (3.15)	n-Butanol and higher n-alcohols	i-Butane (5.58) and all i-paraffins
Methanol	n-Butene and higher n-olefins	Benzene (6.8) and all aromatics
Ammonia (3.8)	Propane (4.89) and higher n-paraffins up to at least C_{14}	Cyclohexane and all cyclics with at least 4-membered rings
Hydrogen sulfide	Cyclopropane (4.75)	Molecules larger than 5.0 but less than 9Å.
Sulfur dioxide	"Freon"-12 refrigerant	$(C_2F_5)_2NC_3H_7$
Carbon dioxide (2.8)		
Propylene (5.00)		
Ethylene (4.25)		
Ethane (4.2)		

Table 2-2 (Continued)

Molecular Sieve Effects of Type A and X Zeolites (80)

Adsorbed on NaX but not on NaA, CaA, CaX	Not adsorbed on NaA, CaA, CaX, or NaX
Di-n-propylamine	$(C_4F_9)_3N$
Di-n-butylamine	Molecules larger than 10Å.
Molecules larger than 9 but less than 10Å.	

Table 3-1

Ion-exchange of zeolites

Zeolites	Ion-exchange gm. atom %	Si/Al		Cation/Si	
HY*	69.5	2.47		0.119	(Na/Si)
NiY**	91.6	2.47		0.178	(Ni/Si)
NiHY**	85.4	2.47		0.167	(Ni/Si)
AgY**	108.8	2.47	***	0.435	(Ag/Si)
				1.04	(Ag/Al)
HZ*	93.9	5.82		0.0106	(Na/Si)
NaY				0.390	(Na/Si)
NaZ				0.174	(Na/Si)

* The percentage of decationization is calculated by sodium content.

** The percentage of nickel and silver ion-exchanged is based on original sodium content.

*** Silicon could not be analyzed accurately in the presence of silver; therefore the Ag/Al ratio was used for the calculation of ion-exchange level of AgY.

Sodium, nickel and silver content were analyzed by atomic absorption spectrophotometry.

Silicon and aluminum were analyzed by colorimetric spectrophotometry.

Table 4-1

Distribution of components in product mixtures for the decomposition of sec-butyl acetate

CATALYSTS	NaZ	NaX	CaX	Silica-Alumina
W, gm.	1.00	1.00	1.00	1.00
Temp., ^{o}C	290	290	290	190
t, min.	45	45	45	45
X, %	39.8	29.9	52.7	96.9
Mole ratios of components in product mixture.				
sec-Butyl Acetate	1.513	2.344	0.898	0.032
Acetic Acid	0.986	0.970	0.970	0.993
CH_4	nil	nil	nil	nil
CO_2	trace	trace	trace	trace
1-Butene	0.204	0.201	0.196	0.116
trans-2-Butene	0.331	0.420	0.355	0.411
cis-2-Butene	0.466	0.379	0.449	0.473
X1	nil	nil	nil	trace
trans-2-Pentene	nil	nil	trace	trace
cis-2-Pentene	nil	nil	trace	trace
X2	nil	nil	trace	trace

Table 4-1 (Continued)

Distribution of components in product mixtures for the decomposition of sec-butyl acetate

CATALYSTS	NaY	NaY	HY
W, gm.	1.00	1.28	1.00
Temp., °C	290	210	190
t, min.	45	40	45
X, %	100.0	80.8	98.8
Mole ratios of components in product mixture.			
sec-Butyl Acetate	nil	0.238	0.012
Acetic Acid	1.032	0.987	0.989
CH_4	trace	nil	nil
CO_2	trace	nil	trace
1-Butene	0.171	0.127	0.120
trans-2-Butene	0.465	0.468	0.431
cis-2-Butene	0.364	0.405	0.448
X1	nil	nil	trace
trans-2-Pentene	trace	nil	trace
cis-2-Pentene	nil	nil	trace
X2	trace	nil	trace

Table 4-2

Distribution of components in product mixtures for the reaction of 1- and cis-2-butene on CaX at 290°C

COMPONENTS	1-Butene Feed (mole %)	cis-2-Butene Feed (mole %)
Methane	trace	trace
Propane	0.1	nil
Propylene	1.8	0.1
n-Butane	0.6	0.2
1-Butene	22.0	22.1
Isobutene	0.1	trace
trans-2-Butene	44.1	38.5
cis-2-Butene	31.0	38.8
X1	trace	trace
trans-2-Pentene	0.2	0.1
cis-2-Pentene	trace	trace
X2	0.2	0.3

Table 4-3

CONVERSIONS OF sec-BUTYL ACETATE AT 190° and 290°C

Space velocity was 3.38×10^2 gm. moles ester/hr./gm. catalyst in all tests.

	PROCESS TIME, minutes				
CATALYSTS	15	25	50	100	200
	at 190°C				
HY	99.1%	99.0%	98.9%	98.0%	96.7%
Si/Al *	98.2	97.5	95.6	92.7	88.2
HZ	70.6	68.4	63.0	54.0	42.0
NaY	35.5	35.0	35.5	35.0	35.5
	at 290°C				
HZ	100.0	100.0	100.0	100.0	--
NaY	100.0	100.0	100.0	100.0	100.0
CaX	74.0	67.2	59.6	54.4	51.0
NaZ	62.8	58.5	50.9	42.0	37.0
NaX	48.0	39.5	29.4	23.0	19.5
CaA	36.8	32.0	26.0	22.0	20.0
NaA	12.0	9.0	6.1	4.5	3.5
KA	7.0	6.5	5.5	4.5	3.8

* silica-alumina

Table 4-4

Selectivity of n-Butenes in the Decomposition of sec-Butyl Acetate

Catalysts	Temperatures [°C]	Conversion of sec-Butyl Acetate [%]	1-Butene [%]	trans-2-Butene [%]	cis-2-Butene [%]	Cis-2-Butene / Trans-2-Butene
Silica-Alumina	140	0.0	7.4	42.6	50.0	1.17
		2.5 }a	7.5	42.5	50.0	1.18
		37.5 }a	9.0	41.5	49.5	1.19
	170	17.5 }a	10.0	40.6	49.4	1.22
		82.5 }a	10.0	41.5	48.5	1.17
	190	80.0	11.3	39.9	48.8	1.22
		97.5	11.3	41.3	47.4	1.15
		100.0	11.3	42.2	46.5	1.10
KA	290	5.0	19.0	39.0	42.0	1.08
NaA	290	0.0	23.0	35.8	41.2	1.15
		2.5	22.2	37.1	40.7	1.10
		10.0 }a	21.5	39.4	39.1	0.99
		75.0 }a	19.2	41.7	39.1	0.94
CaA	290	20.0 }a	20.0	34.6	45.4	1.31
		65.0 }a	18.8	36.1	45.1	1.25
NaZ	290	35.0 }a	19.8	34.1	46.1	1.35
		57.5 }a	19.8	32.1	48.1	1.50
HZ	190	0.0	11.5	39.0	49.5	1.27
		2.5	11.5	38.6	49.9	1.29
		5.0 }a	11.5	38.3	50.2	1.31
		70.0 }a	11.5	36.4	52.1	1.44
NaX	290	10.0	20.0	44.0	36.0	0.82
		20.0	20.0	41.5	38.5	0.93
		65.0	20.0	43.2	36.8	0.85
CaX	290	50.0 }a	19.0	36.6	44.4	1.21
		92.5 }a	19.0	38.0	43.0	1.21
NaY	140	0.0	14.0	50.5	35.5	0.70
		1.0	13.9	50.2	35.9	0.72
		2.5	13.6	49.4	37.0	0.75
		10.0	13.3	48.4	38.3	0.79
	170	0.0	13.2	46.3	40.5	0.87
		5.0 }a	13.2	46.3	40.5	0.87
		40.0 }a	13.2	46.3	40.5	0.87
	190	15.0 }a	13.5	46.4	40.1	0.86
		92.5 }a	13.5	46.4	40.1	0.86
	210	40.0	14.0	46.3	39.7	0.86
		97.5	14.0	46.3	39.7	0.86
HY	140	0.0	9.0	48.6	42.4	0.87
		2.5	9.0	48.3	42.7	0.88
		62.5	9.0	45.0	46.0	1.02
	170	12.5 }a	10.5	44.8	44.7	1.00
		90.0 }a	10.5	45.5	44.0	0.97
		94.0	10.5	46.5	43.0	0.92
NiY	140	0.0	8.0	49.4	42.6	0.86
		2.5	9.0	48.3	42.7	0.88
		5.0 }a	9.4	47.7	42.9	0.90
		35.0 }a	9.4	46.4	42.2	0.95
	170	12.5 }a	11.0	44.6	44.4	1.00
		75.0 }a	11.0	46.0	43.0	0.93

Table 4-4
(continued) Selectivity of n-Butenes in the Decomposition of sec-Butyl Acetate

Catalysts	Temperatures [°C]	Conversion of sec-Butyl Acetate [%]	1-Butene [%]	trans-2-Butene [%]	cis-2-Butene [%]	Cis-2-Butene / Trans-2-Butene
NiHY	140	0.0	4.5	61.5	34.0	0.55
		1.0	6.1	57.0	36.9	0.65
		2.5	8.3	50.5	41.2	0.82
		37.5	9.2	48.7	42.1	0.86
NiHY	170	0.0	8.0	55.0	37.0	0.67
		1.0	8.8	53.5	37.7	0.70
		2.5	9.3	51.3	39.4	0.77
		5.0 } a	9.7	48.7	41.6	0.85
		55.0 } a	10.0	47.5	42.5	0.89
AgY	140	0.0	9.7	57.3	33.0	0.58
		2.5	9.7	53.6	36.7	0.68
		5.0 } a	9.7	52.7	37.6	0.71
		40.0 } a	9.7	49.8	40.5	0.81
	170	35.0 } a	11.2	48.5	40.3	0.83
		90.0 } a	10.8	47.3	41.9	0.89
	Chemical Equilibrium (31)					
	140		8.0	55.1	36.9	0.67
	170		10.0	53.6	36.4	0.68
	190		11.5	52.4	36.1	0.69
	210		13.0	51.1	35.9	0.70
	290		18.5	46.5	35.0	0.75

a The change of n-butene selectivity was monotonic.

Table 5-1

Distribution of components in product mixtures for the decomposition of n-butyl acetate at 290°C

All tests were carried out using one gram of catalyst at feed rate of 0.0341 gram mole ester per hour.

CATALYSTS	HY	NaY	CaX	NaX
t, min.	45	45	35	35
X, %	78.7	64.1	51.3	17.5
Mole ratios of components in the product mixture.				
n-Butyl Acetate	0.271	0.560	0.949	4.71
Acetic Acid	1.005	0.995	0.931	0.913
CH_4	trace	trace	trace	nil
CO_2	trace	trace	trace	trace
Propylene	trace	nil	nil	nil
n-Butane	trace	nil	nil	nil
1-Butene	0.248	0.342	0.381	0.748
trans-2-Butene	0.419	0.360	0.328	0.137
cis-2-Butene	0.333	0.298	0.291	0.115
Isobutene	trace	nil	trace	nil
X1	trace	nil	trace	nil
trans-2-Pentene	trace	trace	trace	nil
cis-2-Pentene	trace	nil	trace	nil
X2	trace	trace	trace	nil

Table 5-1 (Continued)

Distribution of components in product mixtures for the decomposition of n-butyl acetate at 290°C

All tests were carried out using one gram of catalyst at feed rate of 0.0341 gram mole ester per hour.

CATALYSTS	HZ	NaZ	Silica-Alumina
t, min.	45	45	45
X, %	28.4	6.8	94.1
Mole ratios of components in the product mixture.			
n-Butyl Acetate	2.52	13.7	0.073
Acetic Acid	0.992	0.968	1.012
CH_4	nil	nil	trace
CO_2	trace	trace	trace
Propylene	nil	nil	trace
n-Butane	nil	nil	trace
1-Butene	0.235	0.383	0.206
trans-2-Butene	0.438	0.317	0.460
cis-2-Butene	0.327	0.301	0.334
Isobutene	nil	nil	trace
X1	nil	nil	trace
trans-2-Pentene	trace	nil	trace
cis-2-Pentene	nil	nil	trace
X2	trace	nil	trace

Table 5-2

Conversion of n-butyl acetate at 290°C

Space velocity was 3.41×10^{-2} (gm. moles ester feed/hr./gm. catalyst) in all tests.

CATALYSTS	Process Time, minutes 15	25	50	100	200
Silica-Alumina	99.8%	97.5%	93.2%	87.3%	82.2%
HY	94.2	89.5	80.0	67.3	55.4
NaY	79.0	77.8	75.0	69.8	62.3
CaX	63.0	53.0	40.2	31.2	25.5
HZ	57.0	42.0	29.4	22.1	17.9
CaA	27.0	12.0	6.0	4.5	4.1
NaX	23.0	19.0	15.0	11.6	9.7
NaA	19.0	9.0	4.0	1.5	1.0[a]
NaZ	13.0	9.5	6.2	5.3	4.1
γ-Alumina	9.2	8.5	7.1	6.0	5.8[a]
KA	<1.0	<1.0	<1.0	<1.0	---
α-Alumina	<1.0	<1.0	<1.0	<1.0	---
Silica Gel	<1.0	<1.0	<1.0	<1.0	---
Active Carbon	<1.0	<1.0	<1.0	<1.0	---

a Process times are 150 minutes.

Table 6-1

Possible rate equations, kinetic constants and standard deviations for the decomposition of sec-butyl acetate on NaY

	Temp. °C	kF	A	s
(a)	170	8.68×10^{-3}	7.90	1.23×10^{-2}
$r = \frac{kFP_e}{1+AP_a}$	190	3.60×10^{-2}	4.33	2.99×10^{-2}
	210	1.20×10^{-1}	2.55	2.30×10^{-2}
		k	A/E	
(b)	170	8.68×10^{-3}	9.60	0.95×10^{-2}
$r = \frac{kP_e}{P_e+(A/E)P_a}$	190	3.60×10^{-2}	6.20	2.41×10^{-2}
	210	1.20×10^{-1}	4.30	2.21×10^{-2}
		kF	A	
(c)	170	8.68×10^{-3}	3.04	0.82×10^{-2}
$r = \frac{kFP_e}{(1+AP_a)^2}$	190	3.60×10^{-2}	1.75	2.22×10^{-2}
	210	1.20×10^{-1}	1.06	2.92×10^{-2}
		k/E	A/E	
(d)	170	8.68×10^{-3}	4.70	0.88×10^{-2}
$r = \frac{k/E\ P_e}{(P_e+(A/E)P_a)^2}$	190	3.60×10^{-2}	3.52	3.39×10^{-2}
	210	1.20×10^{-2}	2.84	2.75×10^{-2}

Table 6-2

Kinetic constants and standard deviations for the decomposition of sec-butyl acetate on HY, NiY, AgY, NaY and silica-alumina

Catalysts	Temp. °C	k/F	A/F	s	$\varepsilon + Q_e$ Kcal/mole	$Q_a - Q_e$ Kcal/mole
HY	140	1.11×10^{-1}	10.36	0.663×10^{-2}	10.3	8.9
	170	2.60×10^{-1}	4.96	1.330×10^{-2}		
NiY	140	1.31×10^{-1}	17.29	0.523×10^{-2}	13.9	9.4
	170	4.11×10^{-1}	7.94	1.696×10^{-2}		
AgY	140	3.88×10^{-2}	7.17	1.536×10^{-2}	15.1	8.6
	170	1.35×10^{-1}	3.52	3.803×10^{-2}		
Silica-Alumina	140	1.69×10^{-2}	4.94	0.730×10^{-2}	18.0	6.7
	170	7.48×10^{-2}	2.85	2.412×10^{-2}		
NaY	140	1.25×10^{-3} a)	7.19 a)	--	28.0	5.4
	170	8.68×10^{-3}	4.70	0.884×10^{-2}		

a) The extrapolated values by the Arrhenius plot shown in Figure 6-16.

Table 7-1

Correlation of conversions with $X = C_1 e^{-pt} + C_2$ for the decomposition of n-butyl acetate on CaX and NaX

Catalyst, CaX
Temp., 290°C
$P = 9.14 \times 10^{-3}$

W/F	C_1	C_2	s*
9.0	0.196	0.158	0.019
22.6	0.323	0.199	0.015
56.5	0.501	0.210	0.021
87.0	0.615	0.236	0.037
136.4	0.709	0.273	0.032

Catalyst, CaX
Temp., 270°C
$P = 6.30 \times 10^{-3}$

W/F	C_1	C_2	s
26.5	0.126	0.196	0.014
39.4	0.244	0.207	0.019
72.8	0.432	0.243	0.030
100.7	0.517	0.258	0.015
204.9	0.642	0.296	0.051

Table 7-1 (Continued)

Correlation of conversions with $X = C_1 e^{-pt} + C_2$ for the decomposition of n-butyl acetate on CaX and NaX

Catalyst, CaX
Temp., 245°C
$P = 5.50 \times 10^{-3}$

W/F	C_1	C_2	s
43.3	0.043	0.120	0.010
91.4	0.100	0.190	0.032
105.4	0.088	0.206	0.014
196.6	0.197	0.276	0.041

Table 7-1 (Continued)

Correlation of conversions with $X = C_1 e^{-pt} + C_2$ for the decomposition of n-butyl acetate on CaX and NaX

Catalyst, NaX
Temp., 290°C
$P = 1.70 \times 10^{-2}$

W/F	C_1	C_2	s
26.4	0.130	0.087	0.006
41.5	0.181	0.105	0.009
63.1	0.222	0.128	0.008
91.7	0.318	0.139	0.006
122.5	0.372	0.160	0.010

Catalyst, NaX
Temp., 270°C
$P = 1.03 \times 10^{-2}$

W/F	C_1	C_2	s
44.2	0.066	0.075	0.006
104.7	0.138	0.098	0.008
154.9	0.191	0.130	0.011
218.5	0.224	0.143	0.008
375.5	0.435	0.175	0.012

* Standard deviation defined by $s = \sqrt{\frac{\sum_{i=1}^{N} (X_i - C_1 e^{-pt} - C_2)^2}{N}}$

Table 7-2 First-order rate constants and standard deviations for the decomposition of n-butyl acetate on CaX and NaX

Catalysts	Temperatures	Rate Constants	Standard Deviations
NaX	290°C	8.48×10^{-3}	1.93×10^{-2}
NaX	270°C	2.92×10^{-3}	2.92×10^{-2}
CaX	290°C	3.95×10^{-2}	5.30×10^{-2}
CaX	270°C	2.02×10^{-2}	2.42×10^{-2}
CaX	245°C	4.10×10^{-3}	1.10×10^{-2}

Table 7-3

X-ray diffraction analysis of used catalysts

Interplanar spacings and the degree of crystallinity lost.

Interplanar Spacing, d (Å)				
CaA[a]	NaX[b]	Ac-NaX[c]	HY[d]	HZ[e]
11.79 (L)	14.07 (L)	14.07 (L)	14.63 (L)	8.93 (N)
4.06 (S)	8.71 (L)	8.71 (L)	8.42 (L)	6.48 (N)
3.66 (N)	5.69 (S)	5.69 (L)	5.90 (N)	4.48 (N)
3.26 (S)	4.39 (N)	4.39 (S)	4.66 (N)	3.93 (N)
2.96 (N)	3.79 (S)	3.79 (S)	4.27 (N)	3.44 (N)
2.60 (S)	3.32 (N)	3.32 (S)	3.71 (N)	3.36 (N)
2.04 (L)	2.88 (N)	2.88 (S)	3.25 (N)	3.21 (N)
1.73 (S)	2.78 (S)	2.78 (L)	2.81 (N)	2.97 (N)
	2.65 (S)	2.65 (L)		

L: The peak area decreased more than 60%.

S: The peak area decreased between 20 to 60%.

N: The peak area decreased less than 20%.

The catalysts are used for

(a) the decomposition of n-butyl acetate at 290°C for 210 min.

(b) the decomposition of n-butyl acetate at 290°C for 260 min.

(c) the decomposition of n-butyl acetate at 290°C for 530 min.

(d) the decomposition of sec-butyl acetate at 190°C for 610 min.

(e) the decomposition of sec-butyl acetate at 190°C for 400 min.

Table 7-4

Pore volumes of used catalysts

Catalysts	Pore Volume, cc./gm. cat.		Change in Pore Volume on Regeneration, V_l*, cc./gm. cat.	Blocked Volume, %	Deposit, gm./gm. cat.	V_c**, cc./gm. cat.	$\frac{V_c}{V_l}$	Reaction Period, minutes
	Used	Regenerated						
HZ - 1	2.0	124.0	0.189	98.4	0.2012	0.112	0.59	145
HZ - 2	3.0	137.0	0.207	98.2	0.0594	0.033	0.16	310
NaZ	3.0	85.0	0.082	95.3	0.0272	0.015	0.18	265
HY	69.0	181.5	0.174	62.0	0.1367	0.076	0.44	285
NaY	154.0	202.0	0.074	23.8	0.1243	0.069	0.93	305
NaX	56.0	127.0	0.110	55.9	0.1011	0.056	0.51	340
CaA	3.0	161.0	0.244	98.1	0.1200	0.067	0.27	270
Silica-Alumina	300.0	330.0	0.046	9.1	0.0594	0.033	0.72	215

* calculated using liquid nitrogen density of 0.8081.

** calculated using carbon density of 1.8.

APPENDIX 1

CALIBRATION OF SYRINGE PUMP

The Harvard Infusion/Withdrawal Pump consists of a multi-speed transmission driving a glass syringe. Twelve pumping rates can be obtained by changing the position of the transmission gear. In the present study, the positions 8 to 11 were used. The ratio of speeds are 2.5 : 1.0 : 0.5 : 0.25 at positions 8, 9, 10 and 11, respectively. Positions 9 and 10 were most frequently used.

The feed rate of n-butyl acetate was calibrated using syringe I (20 cc.) and II (50 cc.) at position 9. The error limits of the feed rates by these syringes are within 1.2 % at a confidence limit of 95%. The feed rate of sec-butyl acetate was calibrated using syringe III (50 cc.) at positions 9 and 10. The analysis of variance shows that the ratio of pumping speed at position 9 to that at position 10 is 2.0 as it is designed.

The calibration was performed at room temperature (25°C). The ester was collected in a 50 cc. Erlenmeyer flask with a seal to prevent the loss of vapor. The period of collection was 5 to 10 hours.

(a) The calibration of n-butyl acetate feed rate by syringe I and II.

Table A-1-1

Calibration of n-butyl acetate feed rate by syringe I and II

Syringe	I	II
Feed rate, U_{ij}, gm./hr.	1.9846	3.9720
	1.9820	3.9558
	1.9736	3.9471
	1.9807	3.9571
Average, $U_{i.}$	1.9802	3.9580

The error limits of the feed rates were calculated by equation (A-1-1).

$$\text{error limit} = \pm ts \qquad \text{(A-1-1)}$$

Where t was the deviate of t distribution and s was the root of the mean-squared deviation given by equation (A-1-2).

$$s = \sqrt{\frac{\sum_{j=1}^{n} (U_{ij} - U_{i.})^2}{n - 1}} \qquad \text{(A-1-2)}$$

The s's of the feed rates by syringe I and II were 4.72×10^{-3} and 1.39×10^{-2} gm./hr., respectively. The value of t corresponding to 95% confidence and the degree of freedom 3 was 3.182. Therefore, the feed rates were:

for syringe I : $U = 1.9802 \pm 3.182 \times 4.72 \times 10^{-3}$

$= 1.9802 \pm 0.0155$ gm./hr.

for syringe II: $U = 3.9580 \pm 3.182 \times 1.39 \times 10^{-2}$

$= 3.9580 \pm 0.0442$ gm./hr.

Therefore, the errors were less than 1.2% of the mean feed rates.

(b) The calibration of sec-butyl acetate at positions 9 and 10 by syringe III.

Table A-1-2

Calibration of sec-butyl acetate feed rate at positions 9 and 10

Position	9	10
Feed rate, U_{ij}, mole/hr.	0.0340	0.0167
	0.0339	0.0166
	0.0343	0.0167
	0.0342	0.0167
Average, $U_{i.}$	0.0341	0.0167

The feed rates at position 10 were doubled and then the analysis of variance was performed. The results are shown in Table A-1-3. The observed value F_o is much smaller than the value of F-distribution at a confidence limit of 99%. Therefore, the ratio of pumping speed at position 9 to that at position 10 is 2.0 within the error.

Table A-1-3

Analysis of variance and expected mean squares

Source of Variance	Degree of Freedom	Sum of Square	Mean Square	Test Statistic, F_o
Between Positions	1	0.125×10^{-6}	0.125×10^{-6}	$\doteq 0.06$
Within Groups	6	12.75×10^{-6}	2.125×10^{-6}	
Total	7	12.875×10^{-6}		

APPENDIX 2

PREPARATION OF ION-EXCHANGED Y ZEOLITES

The ion-exchange of NaY was carried out using a one-liter round bottom flask. The flask was heated at 75°C in an oil bath. A condenser was attached to the flask and the outlet was covered by a sheet of aluminum foil to prevent loss of water.

The ammonium Y(NH_4Y) was obtained from NaY powder by ion-exchange with excess amount of 1.0 N aqueous solution of ammonium acetate at 75°C for two days followed by washing with distilled water. The hydrogen Y(HY) was made by thermal deamination of NH_4Y at 575°C in air for 4.5 hours. The silver Y(AgY) was prepared by ion-exchanging 30 gm. NaY powder with 784 gm. of 14.5 wt. % aqueous solution of silver nitrate at 75°C for two days. The nickel Y(NiY) was made by ion-exchanging 50 gm. NaY powder with 373 gm. of 19.7 wt. % aqueous solution of nickel II nitrate at 75°C for two days. The NiHY was prepared by ion-exchanging NH_4Y powder in the same manner as NiY. These ion-exchanged zeolites, AgY, NiY, NiHY, were washed with distilled water and calcined in air at 550°C for 5.5 hours.

The color of NH_4Y and HY was white, and that of NiY

and NiHY was light green for hydrated forms and purple after calcination. The color of AgY was gray.

APPENDIX 3

EXPERIMENTAL DATA FOR DECOMPOSITION OF sec-BUTYL ACETATE ON NaY

The decomposition of sec-butyl acetate over NaY was carried out at 170°, 190° and 210°C at atmospheric pressure. The feeds used were pure, 81.87 and 17.50 mole % ester, diluted by acetic acid. The 30 to 35 mesh particles of catalyst were used for experimental runs - 78, 83, 84, 118, 119, 126 and 127. The 70 to 80 mesh particles were used for experimental runs - 77, 81, 82, 120, 121, 128 and 129. The particle size used for other experimental runs was 30 to 80 mesh. The following tables show experimental run numbers, reaction temperatures, mole % of sec-butyl acetate in feed, weights of catalyst, feed rates of ester, space times, conversions of ester, averages of the conversions, and error limits of the average conversion at the confidence limit of 95%.

Table A-3-1

Decomposition of 100 mole % sec-butyl acetate on NaY at 170°C

RUNS	EXP-126	EXP-127	EXP-128	EXP-129
W, gm.	0.8385	0.8385	0.4068	0.4068
$F^{*1} \times 10^2$	3.375	1.688	3.375	1.688
W/F	24.8	49.7	12.1	24.1
X^{*2}	0.137	0.207	0.082	0.135
	0.139	0.216	0.091	0.131
	0.137	0.216	0.085	0.135
	0.134	0.215	0.082	0.136
	0.133	0.205	0.082	
	0.135	0.213	0.086	
			0.083	
$\bar{X}^{*3}$	0.138	0.212	0.084	0.134
DX^{*4}	0.0026	0.0055	0.0033	0.0041

*1 F , gm. mole ester feed/hr.

*2 X , gm. mole ester converted/gm. mole ester feed.

*3 $\bar{X}$, average of X.

*4 DX, error limit of $\bar{X}$ at confidence limit of 95%.

Table A-3-1 (Continued)

Decomposition of 100 mole % sec-butyl acetate on NaY at 170°C

RUNS	EXP-130	EXP-131	EXP-132	EXP-133
W, gm.	2.1048	2.1048	2.9947	2.9947
F $x10^2$	3.375	1.688	3.375	1.688
W/F	62.4	124.7	88.7	177.4
X	0.255	0.341	0.283	0.386
	0.240	0.340	0.280	0.404
	0.226	0.338	0.283	0.398
	0.224	0.364	0.282	0.393
	0.245	0.365	0.287	0.395
	0.235	0.357		
	0.239	0.350		
	0.239	0.346		
	0.246			
$\bar{X}$	0.239	0.350	0.283	0.396
DX	0.0079	0.0096	0.0035	0.0091

Table A-3-2

Decomposition of 81.87 mole % sec-butyl acetate on NaY at 170°C

RUNS	EXP-98	EXP-99	EXP-100	EXP-101
W, gm.	0.3370	0.3370	0.3370	1.7212
F $\times 10^2$	3.143	1.572	0.786	3.143
W/F	10.7	21.4	42.9	54.8
X	0.023	0.045	0.084	0.107
	0.024	0.046	0.085	0.111
	0.025	0.047	0.084	0.117
	0.022	0.043	0.088	0.122
		0.043	0.078	0.111
				0.112
				0.115
$\bar{X}$	0.024	0.045	0.084	0.114
DX	0.0024	0.0025	0.0050	0.0049

Table A-3-2 (Continued)

Decomposition of 81.87 mole % sec-butyl acetate on NaY at 170°C

RUNS	EXP-102	EXP-103	EXP-104	EXP-105
W, gm.	1.7212	1.7212	2.4617	2.4617
F $x10^2$	1.572	0.786	3.143	1.572
W/F	10.9	219.0	78.3	156.6
X	0.204	0.324	0.151	0.239
	0.204	0.332	0.162	0.240
	0.209	0.329	0.161	0.240
	0.206	0.328	0.151	0.240
		0.318	0.161	0.250
			0.150	0.265
				0.255
				0.253
				0.267
$\bar{X}$	0.206	0.326	0.156	0.250
DX	0.0043	0.0075	0.0067	0.0092

Table A-3-3

Decomposition of 100 mole % sec-butyl acetate on NaY at 190°C

RUNS	EXP-77	EXP-78	EXP-79	EXP-80	EXP-81
W, gm.	1.0016	0.3902	2.5754	2.5754	4.6021
F $x10^2$	3.375	3.375	3.375	1.688	3.375
W/F	29.7	11.6	76.3	152.6	136.4
X	0.351	0.213	0.586	0.791	0.739
	0.354	0.225	0.592	0.813	0.737
	0.336	0.221	0.575	0.780	0.752
	0.346	0.218	0.601	0.812	0.756
	0.344	0.213	0.578	0.797	0.743
	0.347	0.230	0.616	0.797	0.739
	0.324	0.219	0.589	0.800	0.734
	0.357	0.237	0.590	0.811	0.764
	0.340	0.221	0.615		0.758
	0.361	0.225	0.592		0.765
	0.374	0.244			
	0.371	0.239			
	0.352	0.237			
		0.236			
$\bar{X}$	0.351	0.227	0.593	0.800	0.749
DX	0.0086	0.0061	0.0104	0.0103	0.0088

Table A-3-3 (Continued)

Decomposition of 100 mole % sec-butyl acetate on NaY at 190°C

RUNS	EXP-82	EXP-83	EXP-84	EXP-85
W, gm.	4.6021	1.9910	1.9910	1.9910
F $\times 10^2$	1.688	3.375	1.688	0.844
W/F	272.6	59.0	118.0	235.9
X	0.929	0.531	0.708	0.894
	0.904	0.524	0.699	0.898
	0.932	0.548	0.721	0.899
	0.923	0.547	0.722	0.902
	0.930	0.559	0.735	
	0.919	0.559	0.717	
	0.900	0.543	0.730	
	0.929	0.544		
	0.927			
$\overline{X}$	0.921	0.544	0.719	0.898
DX	0.0096	0.0109	0.0123	0.0061

Table A-3-4

Decomposition of 81.87 mole % sec-butyl acetate on NaY at 190°C

RUNS	EXP-86	EXP-87	EXP-88	EXP-89
W, gm.	0.3230	0.3230	0.3230	1.7792
F $x10^2$	3.143	1.572	0.786	3.143
W/F	10.3	20.5	41.1	56.6
X	0.165	0.259	0.395	0.463
	0.171	0.272	0.382	0.429
	0.182	0.276	0.397	0.437
	0.179	0.262	0.367	0.439
	0.170	0.275	0.368	0.468
	0.163	0.272	0.386	0.473
	0.167	0.267	0.391	0.467
	0.165		0.381	0.454
	0.163			0.445
	0.172			0.470
	0.159			
$\bar{X}$	0.169	0.269	0.383	0.455
DX	0.0049	0.0065	0.0101	0.0120

Table A-3-4 (Continued)

Decomposition of 81.87 mole % sec-butyl acetate on NaY at 190°C

RUNS	EXP-90	EXP-91	EXP-92	EXP-93
W, gm.	1.7792	1.7792	1.9783	1.9783
F $x10^2$	1.572	0.786	3.143	1.572
W/F	113.2	226.4	62.9	125.8
X	0.630	0.779	0.477	0.661
	0.623	0.773	0.487	0.653
	0.625	0.763	0.487	0.638
	0.640	0.784	0.483	0.660
	0.612	0.767	0.486	
	0.599		0.484	
$\bar{X}$	0.622	0.773	0.484	0.653
DX	0.0165	0.0119	0.0044	0.0195

Table A-3-4 (Continued)

Decomposition of 81.87 mole % sec-butyl acetate on NaY at 190°C

RUNS	EXP-94	EXP-95	EXP-96	EXP-97
W, gm.	1.9783	1.4222	1.4222	1.4222
F $x10^2$	0.786	3.143	1.572	0.786
W/F	251.7	45.2	90.5	180.9
X	0.766	0.410	0.549	0.722
	0.771	0.393	0.557	0.719
	0.774	0.394	0.555	0.718
	0.775	0.396	0.549	0.710
	0.795	0.397	0.550	0.711
	0.792	0.385	0.549	
	0.789	0.401		
	0.771			
$\bar{X}$	0.779	0.397	0.552	0.716
DX	0.0099	0.0077	0.0041	0.0073

Table A-3-5

Decomposition of 100 mole % sec-butyl acetate on NaY at 210°C

RUNS	EXP-118	EXP-119	EXP-120	EXP-121
W, gm.	0.2343	0.2343	0.5022	0.5022
F $x10^2$	3.375	1.688	3.375	1.688
W/F	6.9	13.9	14.9	29.8
X	0.426	0.609	0.600	0.752
	0.430	0.617	0.581	0.754
	0.432	0.617	0.605	0.767
	0.444	0.624	0.630	0.785
	0.436		0.611	
			0.609	
			0.619	
$\overline{X}$	0.434	0.617	0.608	0.765
DX	0.0095	0.0113	0.0154	0.0279

Table A-3-5 (Continued)

Decomposition of 100 mole % sec-butyl acetate on NaY at 210°C

RUNS	EXP-122	EXP-123	EXP-124	EXP-125
W, gm.	1.2828	1.2828	2.5047	2.5047
F $x10^2$	3.375	1.688	3.375	1.688
W/F	38.0	76.0	74.2	148.4
X	0.808	0.943	0.932	0.964
	0.816	0.940	0.928	0.969
	0.804	0.931	0.938	0.970
	0.813	0.943	0.946	0.982
	0.841	0.933	0.946	0.976
	0.828			0.974
	0.851			0.976
	0.842			
	0.827			
$\bar{X}$	0.826	0.938	0.938	0.973
DX	0.0135	0.0079	0.0113	0.0059

Table A-3-6

Decomposition of 81.87 mole % sec-butyl acetate on NaY at 210°C

RUNS	EXP-106	EXP-107	EXP-108	EXP-109
W, gm.	0.3187	0.3187	0.3187	0.8564
F $x10^2$	3.143	1.572	0.786	3.143
W/F	10.1	20.3	40.5	27.2
X	0.391	0.567	0.654	0.632
	0.387	0.562	0.671	0.662
	0.400	0.563	0.651	0.628
	0.416	0.561	0.663	0.612
	0.416		0.664	0.628
	0.419		0.660	0.634
	0.420			
$\bar{X}$	0.407	0.563	0.661	0.633
DX	0.0140	0.0048	0.0083	0.0183

Table A-3-6 (Continued)

Decomposition of 81.87 mole % sec-butyl acetate on NaY at 210°C

RUNS	EXP-110	EXP-111	EXP-112	EXP-113
W, gm.	0.8564	0.8564	1.0322	1.0322
F $x10^2$	1.572	0.786	3.43	1.572
W/F	54.5	109.0	32.8	65.7
X	0.758	0.867	0.727	0.772
	0.781	0.871	0.737	0.778
	0.778	0.868	0.754	0.795
	0.769	0.863	0.722	0.803
	0.781		0.722	0.816
			0.710	0.800
			0.711	0.786
			0.707	0.795
			0.721	0.823
			0.740	
			0.724	
			0.721	
			0.722	
$\bar{X}$	0.773	0.869	0.724	0.796
DX	0.0138	0.0032	0.0082	0.0135

Table A-3-6 (Continued)

Decomposition of 81.87 mole % sec-butyl acetate on NaY at 210°C

RUNS	EXP-114	EXP-115	EXP-116
W, gm.	2.5374	2.5374	3.6867
F $x10^2$	3.143	1.572	3.143
W/F	80.7	161.4	117.3
X	0.890	0.914	0.923
	0.901	0.904	0.920
	0.897	0.944	0.918
	0.911		0.921
	0.906		
$\overline{X}$	0.901	0.921	0.921
DX	0.0112	0.0633	0.0038

Table A-3-7

Decomposition of 17.50 mole % sec-butyl acetate at 210°C

RUNS	EXP-200	EXP-201	EXP-202	EXP-203
W, gm.	1.1232	2.2811	0.5082	1.7856
F $x10^2$	1.118	1.118	1.118	1.118
W/F	100.5	204.0	45.5	159.7
X	0.256	0.455	0.165	0.398
	0.293	0.425	0.141	0.367
	0.359	0.467	0.168	0.391
	0.225	0.461	0.159	0.385
	0.418	0.524	0.166	0.388
	0.201	0.518	0.145	0.371
	0.223	0.521	0.125	0.391
	0.269	0.500	0.125	
		0.481		
		0.465		
		0.461		
$\bar{X}$	0.281	0.480	0.149	0.384
DX	0.0664	0.0225	0.0160	0.0113

APPENDIX 4

GAS CHROMATOGRAPHIC ANALYSIS

A relative thermal response factor is independent from operational condition and individual sensing unit of the gas chromatograph (50). In this study, the relative thermal response factor of component i is the ratio of peak area of one gram mole of 1-butene to the peak area of one gram mole of i. For instance, the peak area of one gram mole sec-butyl acetate and 1-butene in an arbitrary unit are obtained as follows.

	sec-Butyl Acetate	1-Butene
	189.6	120.5
	184.4	122.0
	187.7	122.2
	189.2	121.6
	190.7	121.5
Average	188.3	121.6

Therefore, the relative thermal response factor of sec-butyl acetate is 121.6/188.3 ≒ 0.646.

The mole fraction of component i in the mixture of

N components can be calculated by equation (A-4-1).

$$\text{mole fraction of } i = \frac{R_i S_i}{\sum_{j=1}^{N} R_j S_j} \qquad \text{(A-4-1)}$$

Where, R_i is the relative thermal response factor of i and S_i is the peak area of i in the gas chromatographic analysis of the sample.

The error of gas chromatographic analysis is less than 1.5% at a confidence limit of 99%.

The relative thermal response factors used in this study are given in Table A-4-1. The approximate retention times of components after the injection of the sample are shown in Table A-4-1.

Table A-4-1

Retention times and relative thermal response factors

Components \ Column and Conditions	Retention Times, minutes Note I	Note II	Relative Thermal Response Factors
Butenes	0.8		--
Acetic acid	1.7		1.55
n-Butyl acetate	4.0		0.574
sec-Butyl acetate	3.3		0.646
Methane	5.0		2.25 *
Carbon dioxide	7.7		1.69 *
Propane	8.9		1.25 *
Propylene	9.4		1.29 *
n-Butane	10.6		0.953*
1-Butene	13.3	5.1	1.00
Isobutene	13.9		--
trans-2-Butene	14.8	5.9	1.00
cis-2-Butene	16.6	6.6	1.04
X1	21.9		--
trans-2-Pentene	22.7		--
cis-2-Pentene	24.3		--
X2	26.3		--
Pentane	--		0.771*

Table A-4-1 (Continued)

Retention times and relative thermal response factors

Note I 1/4" x 3' Porapak P at 190°C, 1/4" x 50' 18 wt. % Propylene Carbonate on Chromosorb P at 25°C and at helium flow 120 cc.(S.T.P.)/min.

Note II 1/4" x 20' 10 wt. % bis(2-(2-methoxy-ethoxy)ethyl) ether on Chromosorb P at helium flow 110 cc.(S.T.P.)/ min. at 25°C.

* Reference (67).

NOTATIONS

A	adsorption constant of acetic acid, atm.$^{-1}$ or preexponential factor of rate constant on p. 24.
B	adsorption constant of butenes, atm.$^{-1}$ or preexponential factor of rate constant on p. 24.
C, C'	constants in the Arrhenius equations (6-9) and (6-10).
C_1, C_2	constants in equation (7-1).
E	adsorption constant of ester, atm.$^{-1}$.
F	molar feed rate of ester, gm. mole ester feed/hr.
f	local relative activity.
g(X)	concentration term in reaction rate equation (7-5).
H	adsorption constant of n-hexene, atm.$^{-1}$.
K	chemical equilibrium constant in equation (2-1).
k	surface reaction rate constant in equation (6-1) and rate constant in equation (7-4).
k_c	reaction rate constant for the isomerization of 1-butene to cis-2-butene.
k_t	reaction rate constant for the isomerization of 1-butene to trans-2-butene.
N	total number of data.
P_i	partial pressure of component i, atm.

p first-order aging rate constant, $min.^{-1}$.

Q_a heat of adsorption of acetic acid, Kcal/ mole.

Q_e heat of adsorption of ester, Kcal/mole.

R gas constant.

R_i relative thermal response factor of component $\underline{i}$ in gas chromatographic analysis.

r reaction rate.

r_c isomerization rate of 1-butene to cis-2-butene.

r_o initial reaction rate.

r_t isomerization rate of 1-butene to trans-2-butene.

S_i peak area of component $\underline{i}$ in gas chromatographic analysis.

s standard deviation or object function for regression.

T temperature, ^oK.

t process time, minutes.

V_c volume occupied by carbon deposit per one gram catalyst, cc./gm. catalyst.

V_g difference of nitrogen volume adsorbed on one gram catalyst between before and after burning the catalyst, cc.(S.T.P.)/gm. catalyst.

V_l difference of volume occupied by liquid nitrogen per one gram catalyst between before and after burning the catalyst, cc./gm. catalyst.

W	weight of catalyst, grams
W/F	space time, gm. catalyst/gm. mole ester feed/hr.
X	conversion, % or mole fraction.
Y	calculated conversion in equation (7-3), mole fraction.
y	mole fraction of ester in feed.
Z	mole fraction of 1-butene in total butenes.
α	ratio of rate constant of isomerization of 1-butene to decomposition of n-butyl acetate in equation (5-6).
ε	activation energy, Kcal/ mole.
π	total pressure in equation (2-3), atm.
π_e	saturation pressure of n-hexyl acetate in equation (2-3), atm.

Subscripts

a	acetic acid
b	butenes
e	ester
h	n-hexene
i,j,k,l	indices

BIBLIOGRAPHY

1. Amenomiya, Y., and Cvetanović, R.J., Can. J. Chem. 40, 2130 (1962).

2. Anderson, R.B., I & EC, Anal. Ed. 156 (1946).

3. Andréu, P., Letterer, R., Low, W., Noller, H., and Schmitz, E., 3rd Intern. Congr. Catalysis, Amsterdam, 1964 (ed. Sachtler, W.M.H., Schuit, G.C.A., and Zwietering, P.) Vol. II, 857. North-Holland Publ. Co., Amsterdam (1965).

4. Bachman, G.B., Tanner, H.A., U.S. Patent 2,304,872 (1942).

5. Barrer, R.M., Trans. Faraday Soc. 40, 555 (1944).

6. Barrer, R.M., Trans. Faraday Soc. 45, 358 (1949).

7. Barrer, R.M., Bultitide, F.W., and Sutherland, J.W., Trans. Faraday Soc. 53, 1111 (1957).

8. Barrer, R.M., and Peterson, D.L., Proc. Roy. Soc. (London) 280A, 466 (1964).

9. Basila, M.R., Kantner, T.R., and Rhee, K.H., J. Phys. Chem., 68, 3197 (1964).

10. Benesi, H.A., J. Catal. 8, 368 (1967).

11. Benson, S.W., and Bose, A.N., J. Amer. Chem. Soc. 85, 1385 (1963).

12. Breck, D.W., J. Chem. Educ. 41, 678 (1964).

13. Breck, D.W., Eversole, W.G., Milton, R.M., Reed, T.B., and Thomas, T.L., J. Amer. Chem. Soc., 78, 5963 (1956).

14. Broussard, L., and Shoemaker, D.P., J. Amer. Chem. Soc., 82, 1041 (1960).

15. Bryant, D.E., and Kranich, W.L., J. Catal. 8, 8 (1967).

16. Butler, J.D., Poles, T.C., and Wood, B.T., J. Catal. 16, 239 (1970).

17. Chapman, J.H., U.S. Patent 2,584,969 (1952).

18. Cramer, R., and Lindsey, R.V., Jr., J. Amer. Chem. Soc. 88, 3534 (1966).

19. Dimitrov, C., and Leach, H., J. Catal. 14, 336 (1969).

20. Dzis'ko, V.A., Kolovertnova, M., Vinnikova, T.S., and Bulgakova, Yu. O., Kinet. i Katal. 7, 655 (1966).

21. Eberly, P.E., Jr., I & EC, Fundamentals 8, 25 (1969).

22. Eberly, P.E., Jr., J. Phys. Chem. 67, 2404 (1963).

23. Emovon, E.U., Maccoll, A., J. Chem. Soc., 335 (1962).

24. Foster, N.F., and Cvetanović, R.J., J. Amer. Chem. Soc., 82, 4274 (1960).

25. Frilette, V.J., and Rubin, M.K., J. Catal. 4, 310 (1965).

26. Frilette, V.J., Weisz, P.B., and Golden, R.L., J. Catal. 1, 301 (1962).

27. Froemsdorf, D.H., Collins, C.H., Hammond, G.S., and DePuy, C.H., J. Amer. Chem. Soc. 81, 643 (1959).

28. Golden, D.M., Egger, K.W., and Benson, S.W., J. Amer. Chem. Soc. 86, 5416 (1964).

29. Groeneweg, P., and Anderson, R.B., unpublished (1970).

30. Haag, W.O., and Pines, H., J. Org. Chem. 24, 877 (1959).

31. Halpern, J., 3rd Intern. Congr. Catalysis, Amsterdam, 1964 (ed. Sachtler, W.M.H., Schuit, G.C.A., and Zwietering, P.) Vol. 1, p. 146, North-Holland Publ. Co., Amsterdam (1965).

32. Hattori, H., and Shiba, T., J. Catal. 12, 111 (1968).

33. Hersh, C.K., Molecular Sieves, Reinhold, New York (1961) p. 53.

34. Ibid., p. 54.

35. Hershey, H.C., Zaken, J.L., and Simha, R., I & EC, Fundamentals 6, 413 (1967).

36. Hightower, J.W., and Hall, W.K., Chem. Eng. Progr. Symposium Series 63, (73) 122 (1967).

37. Holm, V.C.F., Bailey, G.C., and Clark, A., J. Phys. Chem. 63, 129 (1959).

38. Hunsford, R.C., and Ward, J.W., J. Catal. 13, 316 (1969).

39. Hurd, C.D., and Blunk, F.H., J. Amer. Chem. Soc., 60, 2419 (1938).

40. Landis, P.S., and Venuto, P.B., J. Catal. 6, 245 (1966).

41. Levenspiel, O., "Chemical Reaction Engineering". Wiley, New York, (1962) p. 453-457.

42. Lombardo, E.A., Sill, G.A., and Hall, W.K., 2nd. Intern. Conference on Molecular Sieve Zeolites, Worcester Polytechnic Institute and American Chemical Society, 1970, p.258.

43. Macarus, D.P., and Syverson, A., I & EC, Process Des. Develop. 5, 397 (1966).

44. Maccoll, A., and Ross, R.A., J. Amer. Chem. Soc. 87, 1169 (1965).

45. Maccoll, A., and Ross, R.A., J. Amer. Chem. Soc. 87, 4997 (1965).

46. Maccoll, A., and Thomas, P.J., Progress in Reaction Kinetics 4, 127 (1967).

47. Maihle, A., Chem. Ztg. 37, 778 (1913).

48. Mascou, L., and Lakeman, M., J. Catal. 16, 173 (1970).

49. Meier, W.M., Z. Krist., 115, 439 (1961).

50. Messner, A.E., Rosie, D.M., and Argabright, P.A., Anal. Chem. 31, 230 (1959).

51. Miale, J.N., Chen, N.Y., and Weisz, P.B., J. Catal. 6, 278 (1966).

52. Misono, M., Saito, Y., and Yoneda, Y., J. Catal. 9, 135 (1967).

53. Norton Company Catalogue, ZEOLON Synthetic Zeolites Technical Data Sheet.

54. Oblad, A.G., Milliken, T.H., and Mills, G.A., Advan. Catalysis 3, 199 (1951).

55. Obolentsev, R.D., Usov, Y.N., Voikovskaya, M.G., Dokl. Akad. Nauk., SSSR, 80, 889 (1951).

56. Ozaki, A., and Tsuchiya, S., J. Catal. 5, 537 (1966).

57. Parry, E.P., J. Catal. 2, 371 (1963).

58. Pettit, P.J., and Anderson, R.B., Can. J. Chem. Eng. 48, 196 (1970).

59. Pickert, P.E., Rabo, J.A., Dempsey, E., and Schomaker, V., Proc. 3rd Intern. Congr. Catalysis, Amsterdam, 1964, Vol. I, p. 714, Wiley, New York (1965).

60. Pines, H., and Haag, W.O., J. Org. Chem., 23, 328 (1958).

61. Pines, H., and Manassen, J., Advan. Catalysis 16, 49 (1966).

62. Pis'man, I.I., Kas'yanov, V.V., and Dalin, M.A., Kinet. i Katal. 6, 741 (1965).

63. Rálek, M., and Grubner, O., Proc. 3rd Intern. Congr. Catalysis, Amsterdam, 1964, Vol. II, p. 1302, Wiley, New York (1965).

64. Reed, T.B., and Breck, D.W., J. Amer. Chem. Soc., 78, 5972 (1956).

65. Romanovskii, B.V., Tkhoang, K.S., Topchieva, K.V., and Piguzova, L.I., Kinet. i Katal. 7, 841 (1966).

66. Rosenbrock, H.H., and Storey, C., "Computational Techniques for Chemical Engineer," Pergamon Press, Oxford (1966) p. 48.

67. Rosie, D.M., and Grob, R.L., Anal. Chem. 29, 1263 (1957).

68. Rudy, C.E., Jr., and Fugassi, P., J. Phys. Colloid Chem. 52, 357 (1948).

69. Sanyal, S.K., and Weller, S.W., I & EC, Process Des. Develop. 9, 135 (1970).

70. Sashihara, T.F., and Syverson, A., I & EC, Process Des. Develop. 5, 392 (1966).

71. Sato, M., Aonuma, T., and Shiba, T., Proc. 3rd Intern. Congr. Catalysis, Amsterdam, 1964, Vol. I, p. 17, Wiley, New York (1965).

72. Scheer, J.C., Kooyman, E.C., and Sixma, F.L.J., Rec. Trav. Chim. 82, 1123 (1963).

73. "Selected Values of Physical and Thermodynamic Properties of Hydrocarbons and Related Compounds," American Petroleum Institute, Carnegie Press, Pittsburg, Pa., (1953) p. 715, 737, 759.

74. Shephard, F.E., Rooney, J.J., and Kemball, C., J. Catal. 1, 379 (1962).

75. Shiba, T., Aonuma, T., Yoshida, K., Hattori, H., and Sato, M., Shokubai 6, 176 (1964).

76. Smith, W.B., and Watson, W.H., Jr., J. Amer. Chem. Soc. 84, 3174 (1962).

77. Tamele, M.W., Disc. Faraday Soc. 8, 270 (1950).

78. Thomas, J.M., and Thomas, W.J., "Introduction to the principles of heterogeneous catalysis," Academic Press, London (1967) p. 422-435.

79. Ibid., p. 458.

80. Thomas, T.L., and Mays, R.L., Physical Method in Chemical Analysis (W.G. Berl, ed.), Vol. 4, Academic Press, New York (1961) p. 45.

81. Tung, S.E., and McIninch, E., J. Catal. 10, 166 (1968).

82. Turkevich, J., Nozaki, F., and Stamires, D.N., Proc. 3rd Intern. Congr. Catalysis, Amsterdam, 1964, Vol. I, p. 586, Wiley, New York, (1965).

83. Union Carbide Co. Catalogue, Linde Molecular Sieve.

84. Uytterhoeven, J.B., Christner, L.G., and Hall, W.K., J. Phys. Chem. 69, 2117 (1965).

85. Venuto, P.B., Givens, E.N., Hamilton, L.A., and Landis, P.S., J. Catal. 6, 253 (1966).

86. Venuto, P.B., Hamilton, L.A., and Landis, P.S., J. Catal. 5, 484 (1966).

87. Venuto, P.B., Hamilton, L.A., Landis, P.S., and Weisz, J.J., J. Catal. 4, 81 (1966).

88. Venuto, P.B., and Landis, P.S., J. Catal. 6, 237 (1966).

89. Venuto, P.B., and Landis, P.S., Advan. Catalysis, 18, 259 (1968).

90. Voge, H.H., and May, N.C., J. Amer. Chem. Soc. 68, 550 (1946).

91. Walker, P.L., Jr., Austin, L.G., and Nandi, S.P., "Chemistry and Physics of Carbon," Vol. 2, p. 257-371, M. Dekker, New York, (1966).

92. Ward, J.W., J. Catal. 10, 34 (1968).

93. Ward, J.W., J. Catal. 11, 238 (1968).

94. Ward, J.W., J. Catal. 9, 225 (1967).

95. Ward, J.W., J. Catal. 11, 251 (1968).

96. Ward, J.W., and Hansford, R.C., J. Catal. 13, 154 (1969).

97. Warrick, E., and Fugassi, P., J. Phys. Colloid Chem. 52, 1314 (1948).

98. Weisz, P.B., and Frilette, V.J., J. Phys. Chem. 64, 382 (1960).

99. Weisz, P.B., Frilette, V.J., Maatman, R.W., and Mower, E.B., J. Catal. 1, 307 (1962).

100. Weisz, P.B., and Miale, J.N., J. Catal. 4, 527 (1965).

101. W.R. Grace & Co. Catalogue, Molecular Sieves.

102. Yashima, T., Ahmad, H., Yamazaki, K., Katsuta, M., and Hara, N., J. Catal. 16, 273 (1970).